NTNU
Norwegian University of
Science and Technology

Analysis and Design of Ship Collision Barriers on a Submerged Floating Tunnel subjected to Large Ship Collisions

Gisle Hoel Århus

Marine Technology
Submission date: June 2016
Supervisor: Jørgen Amdahl, IMT

Norwegian University of Science and Technology
Department of Marine Technology

NTNU – Trondheim
Norwegian University of
Science and Technology

Analysis and Design of Ship Collision Barriers on a Submerged Floating Tunnel subjected to Large Ship Collisions

Gisle Hoel Århus

Submission: June 2016

Master Thesis
Department of Marine Technology
Norwegian University of Science and Technology

Supervisor : Professor Jørgen Amdahl, IMT
Industrial contact :Reinertsen AS: Jorge Bermudez
Industrial contact : Hydro Aluminium: Ole Runar Myhr

Master Thesis 2016

for

Stud. Techn. Gisle Hoel Århus

Analysis and Design of Ship Collision Barriers on a Submerged Floating Tunnel subjected to Large Ship Collisions

Aim of study:

The aim of the Project and Master thesis work is to quantify the response of a new concept for mooring floating bridges and submerged floating tunnels (SFT). The transition piece between the floating bridge and the SFT is especially exposed to ship collisions. A new concept for energy absorption shall be investigated on the basis of data for ship traffic and the likelihood for collision.

Background:

The Norwegian Public Roads Administration (NPRA) is running the project Ferry free coastal route E39, where they in 2012 initiated a study to investigate the feasibility for crossings the wide fjords on the west coast of Norway, focussed on Sognefjorden. REINERTSEN AS contributed in this study and showed that crossing the Sognefjord is technically feasible.

At present, REINERTSEN is further developing this concept together with Dr.techn Olav Olsen AS, Snøhetta Oslo AS, Norsk Hydro ASA, SAPA Profiles AB and Deep Ocean AS. The artificial seabed is REINERTSENs patent (Figure 1).

This master thesis will focus on the ship collision barrier in the concept. The concept consists of a floating bridge with a submerged floating tunnel (SFT) at mid-span to allow ship traffic in and out of the fjord (Figure 2). At the border between the floating bridge and the SFT, there is need for a ship collision barrier to protect the SFT at shallow water depths before the SFT reaches a water depth where the ships can pass over without colliding with the SFT

The size and speed of the large ships and design load cases at drift and collision will be taken from the reports developed by Rambøll in conjunction with the feasibility study in 2012 (will be provided the candidate upon starting the project).

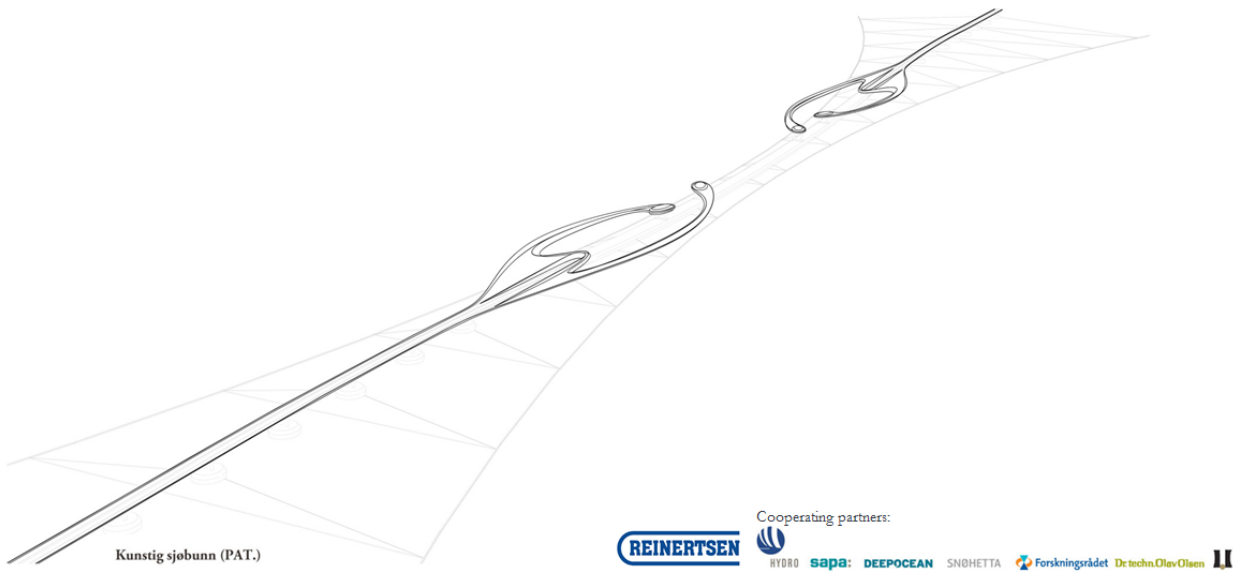

Figure 1: Concept with artificial seabed and mooring, floating bridge, submerged floating tunnel and collision barrier

The ship collision barrier needs to absorb and transfer the loads from the ship collision into the ship collision barriers itself (and down into the artificial seabed, respectively), without exceeding the allowances given in Håndbok N400 Bruprosjektering Eurokodeutgave issued by the NPRA (edition November 2011). Sizes and dimensions of the different components are detailed in the two project documents Last og Lastbeskrivelse, doc. No. 2401051-02-RE-020202 and Dimensjonering og materialbruk, doc. No. 2401051-02-RE-020203 which will be provided to the candidate upon starting the project.

The ship collision barrier is assumed to be made of steel and shall protect the SFT at water depths more shallow than 20m (refer Håndbok N400 Bruprosjektering 6.13 Rørbruer). The barrier will be considered a free floating structure in the water column (no moorings or fixed ends). The barrier will be a straight lined box of approx.. 380m length.

Scope of work

1. It has been proposed to fabricate the barrier in aluminium. Describe functional requirements related to the use of aluminium in a corrosive environment og with large demands for ductility and energy absorption. Fabrication aspects shall also be addressed. Select one or two alloys/ tempers as candidate material. for particular challenges related to the use of aluminium in the collision barrier. Characterize the material properties to be used in nonlinear analysis

2. Perform introductory analysis of stiffened panels subjected to lateral load and axial

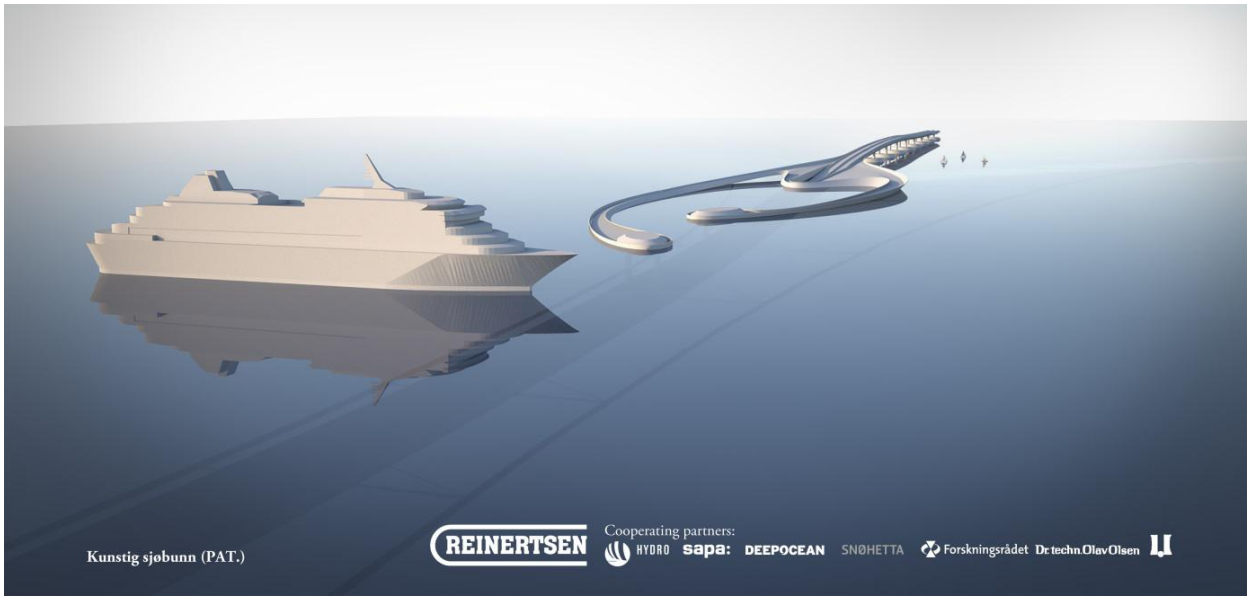

Figure 2: Collision barrier with floating bridge at rear and submerged floating tunnel with ship crossing in front

crushing. The heat affected zone (HAZ) shall be modelled with relevant material properties for alloy 6082 T and 5083 with temper 0 and H12. Hydro Aluminium will provide realistic values of engineering stressstrain curves for parent material and in the HAZ as well as HAZ width for actual material thicknesses. It is expected that the plates will have thicknesses in the range of 8-20 mm. It is proposed start with 12 mm plate thickness. Compare the results w.r.t. force-deformation, energy dissipation and extension of the yield zones.

3. Discuss various configurations of the barrier with respect to size, location, connection to the bridge, potential mooring to the artificial sea floor etc. How shall a weak link be designed?

4. Propose a detailed structural lay-out for the collision barrier including ballasting system. In addition to the local resistance to impact, the evaluation shall also include preliminary evaluations of the hydrostatic stability in damage condition. Special consideration should be given to how the local resistance to impact may be varied during nonlinear finite element analysis and how any ballast shall be modelled with respect to both local and global behaviour.

5. Discuss how the global motion of the barrier and the ship can be modelled for analysis in LS-DYNA. For the barrier this concerns added mass, viscous (drag) forces etc. For

ship a recently developed model for global ship motions shall be used. Modelling of the mooring/support of the barrier shall also be determined

6. For the selected barrier design and its variations perform nonlinear simulations of ship collisions with LS-DYNA for the various impact scenarios. The force-deformation (penetration) and energy dissipation in the ship bow and barrier shall be documented. Compare the results with those based on simplified methods. How is the collision force compared to code requirements ((Norsok N-004, Eurocode 1, Part 1.7, AASHTO Bridge Design Specifications)?

7. Establish a finite element mode for usfos analysis of the bridge and the artificial sea floor. Perform eigenvalue analysis of the bridge and compare the results with those obtained with alternative programs. To the extent data is available perform response analysis of the bridge subjected to extreme waves/wind

8. Perform collision response analysis of the bridge using force-deformation curves form LS-DYNA analyses.

9. Conclusion and recommendations for further work

Literature studies of specific topics relevant to the thesis work may be included.

The work scope may prove to be larger than initially anticipated. Subject to approval from the supervisor, topics may be deleted from the list above or reduced in extent.

In the thesis the candidate shall present his personal contribution to the resolution of problems within the scope of the thesis work.

Theories and conclusions should be based on mathematical derivations and/or logic reasoning identifying the various steps in the deduction.

The candidate should utilise the existing possibilities for obtaining relevant literature.

The thesis should be organised in a rational manner to give a clear exposition of results, assessments, and conclusions. The text should be brief and to the point, with a clear language. Telegraphic language should be avoided.

The thesis shall contain the following elements: A text defining the scope, preface, list of contents, summary, main body of thesis, conclusions with recommendations for further work,

list of symbols and acronyms, references and (optional) appendices. All figures, tables and equations shall be numerated.

The supervisor may require that the candidate, in an early stage of the work, presents a written plan for the completion of the work. The plan should include a budget for the use of computer and laboratory resources, which will be charged to the department. Overruns shall be reported to the supervisor.

The original contribution of the candidate and material taken from other sources shall be clearly defined. Work from other sources shall be properly referenced using an acknowledged referencing system.

Supervisor NTNU:
Prof. Jørgen Amdahl
Industrial contacts:
Reinertsen AS: Jorge Bermudez
Hydro Aluminium: Ole Runar Myhr

Deadline:, June 24 2016
Trondheim, January 25, 2016
Jørgen Amdahl

Preface

This is stud. techn Gisle Hoel rhus's final report in the specialisation subject at NTNU, fall 2015. This project thesis regards ship collision analysis and design. This thesis is a preparation for a master thesis on the same subject, spring 2016. The assignment is given as specialization subject at Marine technology, NTNU. The assignment is given by Prof. Jrgen Amdahl with Industrial contact Reinertsen AS, represented by Jorge Bermudez.

The thesis focus on literature review of design principles regarding ship collision, as an accidental action. Literature on ship collision forces as given in design codes is also reviewed. A design of the collision barrier is proposed and a analysis using decoupled methods based on energy consideration is preformed. The project thesis is written in cooperation with Reinertsen AS, and Jorge Bermudez has provided me with help in early stages of project thesis. Supervisor Professor Jrgen Amdhal has also been of great help during the work on the thesis, providing literature that has been vital in order to solve the assignment.

Trondheim, 18 desember 2015

Gisle Hoel rhus

Abstract

Reinertsen AS is developing a bridge crossing concept to cross the Sognefjord in Norway. The concept consist of floating bridge and submerged tunnel. The submerged tunnel is exposed to ship collisions from passing ship traffic. A protective ship collision barrier is used to protect the exposed part of the submerged tunnel. A design of the collision barrier is proposed.

The barrier is made in Aluminium. There are some special considerations one must take into account when using aluminium. Aluminium that is heat treated has a reduction in strength, referred to as reduction in heat affected zone. Different alloys react differently to heat treatments. Some have a large reduction in HAZ, while some are not affected at all. Two alloys are used and studied in this thesis. Alloy 5083 with temper O and H12, and allo 6082 with temper T6.

A Ramberg-Osgood material description is used to describe the material properties of Aluminium alloys in the Finite element analysis. A failure criteria is used based on design principles found in Eurocode 9. The failure criteria is only depending on yield stress of the alloy, which gives reason to doubt the goodness of the criteria, when strain failure for an aluminium alloy is depending on many other factors.

An analysis of a stiffened panel subjected to lateral and axial loading is done. The loading is in the form of a rigid sphere and rigid plate, moving with a constant velocity trough the plate. A comparison between the use of alloy 5083 O and alloy 5083 H12 is carried out. The effect of heat affected zone is also studied. The analysis showed that the impact stresses dominate more than the reduction in the HAZ regarding strain localisation and fracture pattern. There is a reduction in the resistance force capacity because of HAZ, both in axial and lateral direction.

A collision analysis of a model of a bow and barrier is carried out. The design of the ship model is based on the cruise ship MS Balmoral. The barrier design is based on local and global strength considerations. The barrier is modelled as a straigth rectangular cylinder, with clamped ends. A collision analysis using LSDYNA is carried out. The analysis consists of sending the bow trough the collision barrier. The analysis showed that the design of the barrier must be strengthened. The bow does receive little damage, and the barrier is to weak to protect the tunnel.

A model of the bridge concept is made in USFOS, with the intension to carry out a global collision -response analysis. This was not finished, due to time limitations.

Norsk sammendrag

Acknowledgment

I would like to thank the following persons for their great help on solving the assignments given in this thesis. Professor Jørgen Amdhal has provided me with literature, proving to be vital for me when solving the assignment at hand. He has also trough discussion, given me hints and motivation driving me further on, towards finding solutions of the assignment. Jorge Bermudez and Ole Runar Myhr has also been very helpful and has provided me with documents important for this thesis and also for my following master thesis in which I will start on January 2016.

G.H..

Contents

List of Figures

List of Tables

Nomenclature

Capital letters

Small letters

Greek letters

Abrivations

σ_y - Yield stress

y - Distance from neutral elastic axis to fiber

I - Second moment of area

M - Elastic bending section modulus

$_p$ - Plastic moment capacity

$_p$ - Plastic section modulus

P_{cr} - Critical load/ load capacity for beam

L - Length of beam. Length of barrier.

δW_e - external virtual work

δW_i - internal virtual work

δw - incremental lateral displacement

δq - incremental rotational displacement

K - Stifffness of a beam

E - Youngs modulus

A - Cross sectional area

l - half length of beam

α_0 -initial angle between horizontal line and beam in two bar system

r system degree of fredom, two bar problem

ϵ strain

h Height of two bar system.

R Applied load at center node in two bar system

∇ Change in length in beam element in two bar system

α -current angle between horizontal line and beam in two bar system

K_G - geometric stiffness of a beam in two bar system

K_o - additional stiffness due to axial load of a beam in two bar system

K_σ - Stifffness of a beam in two bar system

σ_T - True stress

ϵ_T - True strain

$\delta\sigma$ - incremental stress

$\delta\epsilon$ - incremental strain

$\Delta\sigma$ - incremental stress

$\Delta\epsilon$ - incremental strain

K_I -tangent stiffness

$\frac{d}{dr}$ differential operator with respect to r

K_I^{total} -total formulation of stiffness

$K_I^{updated}$ -updated formulation of stiffness

$Rint$ - incremental forces

$Rext$ - external forces

a - connectivity matrix

S - element nodal loads

n - iterative step number

x_n - iterative value in Newton -Raphson iterative method

$f(x_n)$ - non linear equation solved by Newton -Raphson iterative method

$f'(x_n)$ - first differentiate of value in Newton -Raphson iterative method

K -Stiffness matrix

C -Damping matrix

M -Mass matrix

R -External load vector

$\{r$ -vector of nodal displacement

$\dot{r}$ -vector of nodal velocity

$\ddot{r}$ -vector of nodal acceleartion

δt -time step

$\omega_{max}t$ -highest eigen frequency

$\lambda_c t$ -characteristic element length

X -Volume forces vector

T -Traction forces vector

V - volume

S -Surface area

$\mathbf{Q^{\cdot}c}$ -External concentrated forces vector

$\{q$ -displacement of nodal degree of fredom q

$\dot{q}$ - velocity of nodal degree of fredom q

$\ddot{q}$ - acceleartion of nodal degree of fredom q

$\bar{c}$ -modal damping

$\bar{k}$ - modal stiffness

$\bar{m}$ - modal mass

$\chi(x)$ -assumed modal shape function

$EI(x)$ -bending stiffness as a cunction of length

E_s - strain energy dissipation

m_s - mass of ship

a_s - added mass of ship

v_s - velocity of ship

m_i - mass of installation

a_i - added mass of installation

v_i - velocity of installation

$E_{s,s}$ - strain energy dissipation in ship

$E_{s,i}$ - strain energy dissipation in installation/barrier

$P(F > F_d)$ - Probability that impact force exceeds design force. Used to calculate design impact force

n - number of ships per time unit(traffic intensity)

T - period f time under consideration

p_a - probability that a collision is avoided by human intervention

$lambda(x)$ - probability of failure per unit traveling distance

$f_s(y)$ - distribution of initial ship position in y - direction

$v(x, y)$ - velocity of ship, given error at point (x,y)

k - stiffness of ship

P_s - Equivalent static impact force

m_s - mass of ship

f_y - yield stress

f_u - ultimate stress

ϵ_u - ultimate strain

ϵ_0 - conventional limit of elasticity

f_{ϵ_0} - stress corresponding to limit of elasticity

n - Ramgerg-Osgood exponent

- f_0 :Recorded value of yield stress for alloy.
- f_0 :Recorded value of ultimate stress for alloy.
- ϵ_u :residual strain corresponding to limit of elasticity
- ϵ_0 :residual strain corresponding to limit of elasticity
- b_{HAZ} :extent of heat affected zone
- t :plate thickness
- q :distributed load on barrier

K- added mass coefficient in surge motion

G-Centre of gravity

B-Centre of buoyancy

M-Meta centre

I-second moment of area of waterplane are of barrier(about longitudinal axis)

- Δ :volume displacement
- F_b :buoyancy forces on barrier
- F_b :gravity forces on barrier
- ρ_{sw} :density of sea water
- ρ_w :density of fresh water

L-length of barrier

B-Breadth of barrier

dr-draught of barrier

L-length of barrier

m˙barrier-mass of the barrier itself, only weigh of material

m˙ballast-mass of the ballast water in barrier

C˙ab-coefficient of added mass for barrier, in surge

C˙as-coefficient of added mass for barrier, in surge.

A- effective drag area

G-Centre of gravity

B-Centre of buoyancy

M-Meta centre

Chapter 1

Introduction

1.1 Background

Connecting Kristiansand and Trondheim with a continuous coastal route have been an ambition of the Norwegian government since 2012. Route E-39 crosses six counties and eight fjords. The Norwegian public roads administration has been studying different concepts on how to build bridges to cross these fjords at the west coast of Norway. Today the Sognefjord is crossed by use of a ferry. The Sognefjord is perhaps the most difficult fjord to cross due to its large width and depth.

Reinertsen AS has among others, contributed to a feasibility study, proving it is technically feasible to cross Sognefjorden. Reinertsen AS is developing a concept, providing a solution on how to cross this fjord. This solution is under further development with Dr.techn Olav Olsen AS, Snøhetta Oslo AS, Norsk Hydro ASA, SAPA Profiles AB and Deep Ocean AS.

1.2 Proposed Bridge concept

Reinertsen As' proposed crossing concept is a floating bridge and a floating, submerged tunnel. The floating submerged tunnel will connect to floating bridges at both ends, thus linking the north and south ends of E-39 at each side of the fjord. The submerged tunnel will allow ship traffic to cross in and out of the fjord. The floating bridges are moored to an artificial seabed. This seabed is Reinertsen's patent. Figure 1.1 shows the artificial seabed developed by Reinertsen AS

Figure 1.1: Artificial Seabed Concept A (*Picture provided by Reinertsen AS*)

The artificial seabed is defined by two pipelines spanning across the fjord. These pipelines are then connected with 13 crossbeams, see figure 1.2 . The submerged floating tunnel is protected by a ship collision barrier at the most exposed part which is where the tunnel is at more shallow water depths than 20 m.

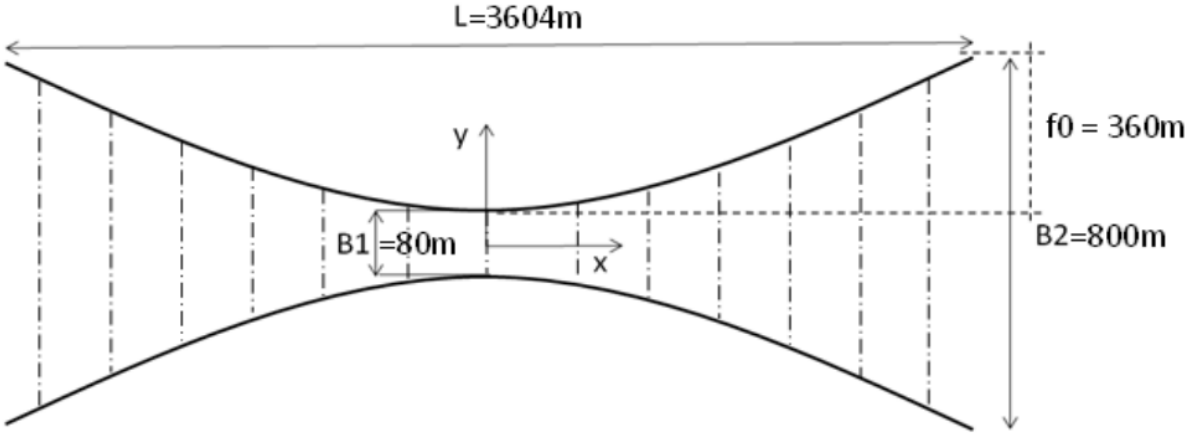

Figure 1.2: Artificial Seabed Concept B (*Picture provided by Reinertsen AS*)

1.3 Motivation

The probability of ship collisions are usually quite low, but the consequences are on the other hand, usually quite severe. The ship traffic in and out of the Sognefjord is of why accidents such as collisions may occur. If the submerged floating tunnel or the bridge were to be struck by a large ship, such as a cruise ship, the consequences could be very fatal. The collision barrier must be strong enough to prevent crucial damage to the submerged tunnel. However, the stability and safety of the ship should remain after the collision. Designing a ship barrier that holds all these abilities is very important. Thus making a good analysis model of the collision barrier is very important.

1.4 Objectives and Scope of work

The objective of this report is to analyse a collision between a cruise ship and a collision barrier. A design ship based on ship traffic in and out of the Sognefjord, was produced by Rambøl AS. A proposed design solution of the collision barrier is given in this thesis. Finite element analysis is done by the use of the finite element analysis program LS DYNA3D. A simulation of collision is also done in the finite element sofwtare USFOS. The third objective is to analyse the effect of heat affected zone in aluminium structures.

1.5 Structure of the Report

The rest of the report is organized as follows. Chapter 2 gives an overview of theory and methods used in order to solve the collision analysis and design of the collision barrier. Chapter 3 regards aluminium and its alloys. Fabrication aspects and special consireations are discussed. Chapter 4 is about the design of the barrier. Chapter 5 and 6 presents the modelling done in LS DYNA and USFOS. Chapter 7 presents the results obtained in the different analysis. Chapter 8 discusses the results and other important topics of the thesis. Finally chapter 9 gives conclusions and recommendations for further work

Chapter 2

Theory and methods

In this chapter theory and methods relevant for ship collisions will be discussed. Different methods for solving non-linear problems in structural analysis is covered to some extent. Design for ship collision is given by the Norsok Standards and presented. The background for the theoretical methods described in this chapter originates from work published by Professor Torgeir Moan, Professor Jrgen Amdahl, professor emeritus Ivar Langen and Norsok -Standard N004

2.1 Beam theory

A conventional analysis of a structure, often only assumes elastic response. Geometrically this means that deformations are small. Materially this means that stresses are in the elastic range. Plastic Beam theory is suitable for structural analysis when one assumes that one moves outside the elastic range, and into the plastic or elastoplastic range. Figure 2.1 below shows a representation of elastic and plastic range of a material, represented by a stress-strain curve. A typical behaviour for steel is the yield plateau that follows after the elastic limit.

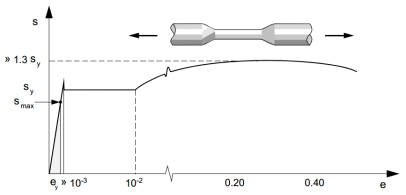

Figure 2.1: Stress strain curve for steel [Amdahl, 2005]

In elastic beam theory, yield is often given as design criteria for failure. For bending moments this is expressed as

$$\sigma_y = M\frac{y}{I} \tag{2.1}$$

σ_y - Yield stress

I-second moment of area

y - vertical distance from neutral axis to fiber

M - Bending moment

The first yield occurs at the outer fibers of the cross section, farthest from the neutral axis. Plastic beam theory takes it a little further. If loading persists after the first yield, more and more fiber will start to yield, until the entire cross section has yielded, and a plastic hinge forms. See figure 2.1 for an illustration of yield development in a cross section of a beam with loading as a bending moment.

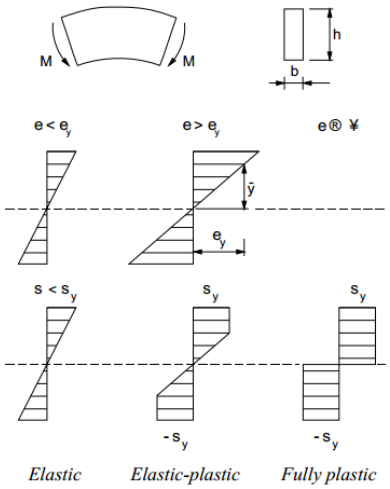

Figure 2.2: Development of plasticity in cross section[Amdahl, 2005]

For plastic beam theory a common value of design is the plastic bending moment or plastic section modulus. One can define the plastic bending capacity as

$$M_p = W_p\sigma_y \tag{2.2}$$

σ_y - Yield stress

M˙P-Plastic moment capacity

W˙p- Plastic section modulus

The plastic section modulus is a measure of how much bending a beam can take before the plastic hinge forms, and the beam becomes a mechanism. Figure 2.1 below illustrates how plastic hinge form for a fully clamped beam with lateral evenly distributed load. The hinges form at the clamped ends due to the maxima of bending moment in these positions. Consequently, the beam cannot bear more moment. Thus the beam acts as a pinned beam.

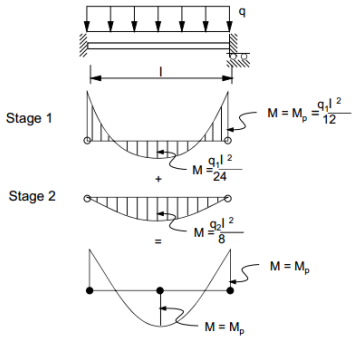

Figure 2.3: Formation of plastic hinge in clamped beam [Amdahl, 2005]

It is possible to determine a critical load for a structure based on plastic hinge theory, called plastic resistance capacity. By using a static and kinematic analysis, one can determine this load. For a pinned beam with a centric applied load, the critical load can be calculated assuming a formation of a hinge at the centre of the beam

$$P_{cr} = \frac{4Mp}{L} \tag{2.3}$$

Here P_{cr} denotes the maximum load the beam can take, L denotes the length of the beam itself, and the plastic moment capacity M_p is calculated based on the cross section geometry and material property of the beam.

To be able to find the critical load, one uses the principle of virtual work. By finding equilibrium between the external virtual work and the internal virtual work, one finds the expression of the critical loading. One must assume a plastic hinge mechanism as seen in figure 2.1

External virtual work can be expressed as [Amdahl, 2005]

$$\delta W_e = P_{cr}\delta w \tag{2.4}$$

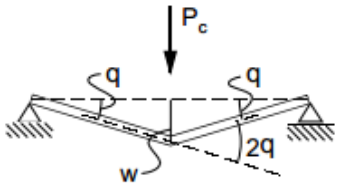

Figure 2.4: Mechanism in pinned beam [Amdahl, 2005]

Moreover, internal virtual work as

$$\delta W_i = M_p \delta q \tag{2.5}$$

Where

W_e - External virtual work

W_e - Internal virtual work

δq -Virtual rotation in hinge

δw - Virtual vertical deformation at hinge

P_{cr} - Critical load at beam

M˙P-Plastic moment capacity

Here the kinematics are crucial. By assuming a wrong mechanism, the kinematics are wrong, and one will calculate the wrong critical load. For a pinned beam, kinematics are quite simple, but for more complex structures, it is not always easy to guess the mechanism form. It is possible to predict an upper and a lower limit for the plastic resistance by following these theorems [Amdahl, 2005]

Upper bound theorem - All mechanisms kinematic admissible will result in a too large plastic resistance,-except the true one

Lower bound theorem -All static kinematic admissible will result in a too large plastic resistance,-except the true one

Uniqueness theorem - If the mechanism chosen is both static and kinematic admissible, the determined mechanism is correct.

The expression static and kinematic admissible refers to the load condition and displacement field of the structure at hand. The load condition can be said to be statically

admissible if static equilibrium between external action and internal forces or moments holds everywhere and the bending moments does not exceed the plastic moment anywhere. The displacement field can be said to be kinematic admissible if the geometric compatibility between virtual rotations and displacement exists everywhere and the plastic moment is equal to moment capacity in hinges.

[Amdahl, 2005]

2.2 Finite Element Method

In this section, basic theory and principles regarding finite element analysis is discussed. Finite element analysis is a very valuable and useful tool when considering complex marine engineering problems.

2.2.1 Nonlinear FEM Analysis

In accidental action problems, such as ship collisions, where displacements of the structure potentially can be large, structural nonlinear analysis must be applied. Both Geometrical and material nonlinear effects can affect the finite element analysis of a collision. The three principles of structural analysis are the principles of equilibrium, kinematic compatibility and stress-strain relationships, e.g., Hooke's laws. In conventional linear analysis, the assumptions are that of small displacement and that the material remains elastic and linear [Moan, 2003] When the displacement remains small, one can base the analysis on initial configuration or geometry. Thus a one have a linear relation between strains and displacement, e.g., the strain relies on the displacement gradient. In cases such as collisions, both material nonlinearity, and geometrical nonlinearity typically arise. The material undergoes significant deformation, and the relation between stresses and strains are no longer linear. This is often called plastic deformation, or permanent deformation. One can no longer base the analysis on the initial configuration as the structure deforms, and an updated geometric stiffness must be used to account for the change in the geometry of the structure. A third source of nonlinearity is from boundary conditions. Nonlinearity in boundary conditions occurs in contact problems, such as collisions. The computational time is logically often much larger for nonlinear analysis compared to a linear one. Computer technology is a growing science, however, and today one can use computers of large capacity to solve nonlinear problems relatively fast.

2.2.2 Nonlinear geometry

When a structure undergoes a deformation, as the structure deforms the geometry of the structure must be updated. To obtain correct stress and strain calculations, one must use the current displacement of the structure. When considering linear deformation patterns, there is no need to update or iterate the solution since the deformations are small. A simple example of two bar system consisting of a bar with angle subjected to a lateral point load is displayed in figure 2.2.2

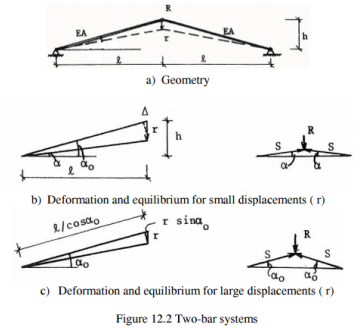

Figure 2.5: Two bar beam , kinematics [Moan, 2003]

With an assumption of small deflection, the stiffness may be expressed as [Moan, 2003]

$$K = \frac{2EA}{l} sin(\alpha_0)^2 cos(\alpha_0) \tag{2.6}$$

$$R = \frac{2EA}{l} sin(\alpha_0)^2 cos(\alpha_0) * r \tag{2.7}$$

$$S = EA\epsilon = \frac{EA}{l} sin(\alpha_0) cos(\alpha_0) * r \tag{2.8}$$

$$\epsilon = \frac{rsin(r\alpha_0)}{l/cos(\alpha_0)} = \frac{r}{l} sin(\alpha_0) cos(\alpha_0) \tag{2.9}$$

The equations above show the linear relation between load and deformation. However if we assume large deformations, this will not give correct results. Thus a nonlinear model must be made, including the change in geometry. The axial deformation, when considering large deformations is now, by geometric considerations

$$\Delta = \frac{l}{cos(\alpha_0}) - \frac{l}{cos(\alpha} \tag{2.10}$$

Further it can be shown, [Moan, 2003] , that the force-displacement relationship can be written as , using the true axial deformations above

$$R = \frac{2EA}{l}(\frac{h}{r} - 1)(\frac{l}{\sqrt{l^2 + (h-r)^2}} - \frac{l}{\sqrt{l^2 + h^2}})r \tag{2.11}$$

As can be seen, the stiffness is now not the same as when using the linear theory. It is now a function of r. This example illustrates the need of updating the stiffness with changing geometry.

$$R = K(r)r \tag{2.12}$$

Wherein

E - Youngs modulus

A - Cross section area of beam

K - Stiffness of beam system

R - Apllied load at center node

r - Lateral deformation at center node

S - Axial force in beam element

ϵ - Engineering strain in beam element

h - Height of original configuration see **??**

l - half span of original configuration see **??**

l - half span of original configuration see **??**

α - updated angle of system see **??**

α_0 - initial angle of system see **??**

Δ - Change in length of beam element

By assuming small angles α α_0 one can write

$$sin(\alpha) \approx \frac{h-r}{l} \tag{2.13}$$

$$cos(\alpha) \approx \frac{h-r}{l} \tag{2.14}$$

$$cos(\alpha) \approx \frac{h-r}{l} \tag{2.15}$$

Further assuming

$$\alpha \approx \frac{h}{l} \tag{2.16}$$

$$\frac{h}{l}^2 \ll 1 \tag{2.17}$$

The stiffness relation can now be written by two different parts, namely linear and nonlinear stiffness [Moan, 2003]

$$\begin{aligned} K(r) = \frac{2EA}{l}(\alpha_0)^2(1-\frac{h}{r})(1-\frac{r}{2h}) = \\ \frac{2EA}{l}(\alpha_0)^2 + \frac{EA}{l}(\alpha_0)^2(\frac{r}{h}-3)\frac{r}{h} = K_g + K_0 \end{aligned} \tag{2.18}$$

K_0 represent the linear stiffness and K_g the nonlinear geometric stiffness. Usually, a Lagrangian approach is used to describe the problem. If an analytical expression for the stiffness for a problem is unobtainable, it is useful to write it in differential form and solve incrementally. Solving incrementally can be very powerful with today's computer capacity. If one consider an initial axial force in the beams, S_0, the stiffness of the two bar system can be written [Moan, 2003]

$$K_I = K_G + K_0 + K_\sigma \tag{2.19}$$

Here K_σ is the additional stiffness due to the initial axialload S_0

$$K_\sigma = 2S_0\frac{h-r}{l} \tag{2.20}$$

K_σ represents the initial stiffness due to stresses in the beam, meaning the stresses from the previous increment.

2.2.3 Material Nonlinearity

Material nonlinearity occurs when the material no longer behaves linearly. Material testing shows that if the stress applied is large enough, when unloading, the strains of the specimen will be permanent, e.g., the strain is plastic. The difference between linear and nonlinear analysis is that in the linear analysis it is assumed that the material remains in the linear domain, and Hooke's laws are thus applicable. When dealing with nonlinear material behaviour, it is important to use true stress and strains. . True strain and stress are defined as

$$\sigma_T = \sigma(1+\epsilon) \tag{2.21}$$

$$\epsilon_T = ln(1 + \epsilon) \tag{2.22}$$

Here σ and ϵ denotes engineering strain and stress. Figure 2.2.3 and 2.2.3 show how elastic and plastic material behaviour differs for Aluminium and for steel, and fig 2.2.3 illustrates difference between engineering and true strains. As can bee seen for conventional steel, the typical yield plateau follows after the elastic limit, resulting in little change in stress as the strain increases. For aluminium, however, it does not have a yield plateau. The stress strain curve for aluminium is more curved, and the yield point is not as easily determined.

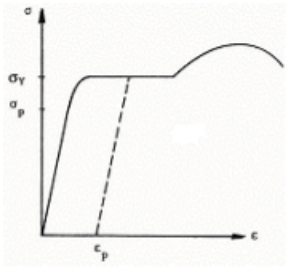

Figure 2.6: Stress strain curve for conventional steel [Moan, 2003]

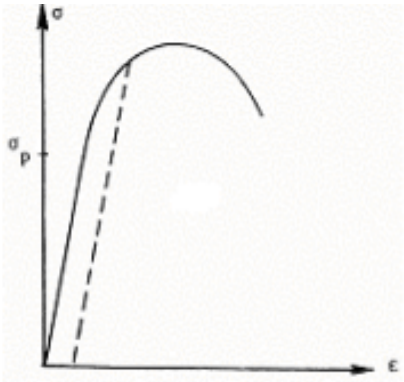

Figure 2.7: Stress strain curve for aluminium [Moan, 2003]

Hooke's law covers the elastic domain

$$\sigma = E\epsilon \tag{2.23}$$

Whereas a continuous analytical model can describe the plastic domain

$$\sigma = \sigma(\epsilon)$$

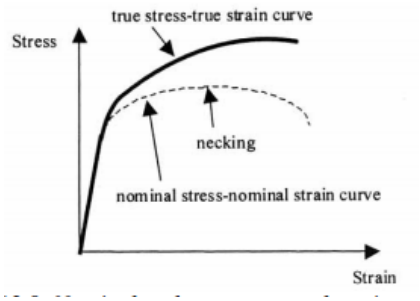

Figure 2.8: Stress strain curve. True stress vs nominal stress [Moan, 2003]

(2.24)

There are many different material models to describe plastic behaviour for different metals. Some simple examples are rigid plastic behaviour, elastic-plastic behaviour or piecewise plastic behaviour, see 2.2.3

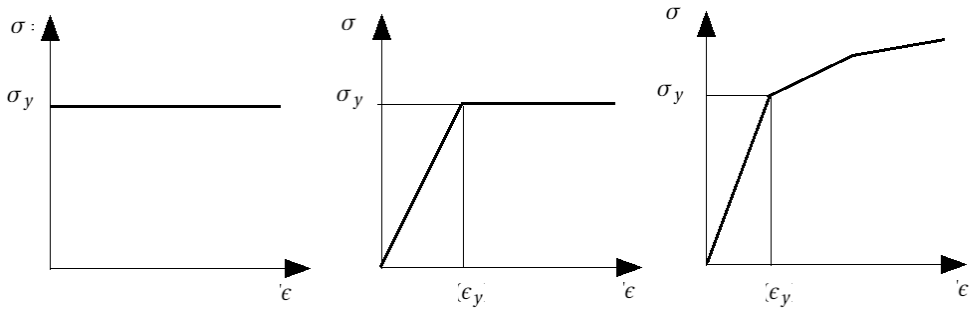

Figure 2.9: Rigid plastic vs elastic-plastic vs piecewise plastic behaviour

There are more powerful methdos to describe plastic behaviour. An example of a power law, Ramberg-Osgood model will be described more in detail in chapter 3.

One can summarise the rules for material nonlinearity as [Moan, 2003]

Yield Criterion - The yield criterion describes where the first yield in material begins.

Hardening rule - The hardening rule dictates the change in yield criterion based on the history of plastic flow.

Flow rule - The flow rule describes the relation between the incremental stress with the incremental strain.

Compared to an elastic-plastic material behaviour, where strain hardening occurs, it is necessary to continue to increase stress to deform the material 2.2.3, Whereas the elastic-plastic material, continues to deform at a constant value of stress at the yield stress. The flow rule relates the incremental stress $\delta\sigma$ to the incremental strain $\delta\epsilon$. In the elastic region this can be written

$$\delta\sigma = E\delta\epsilon \tag{2.25}$$

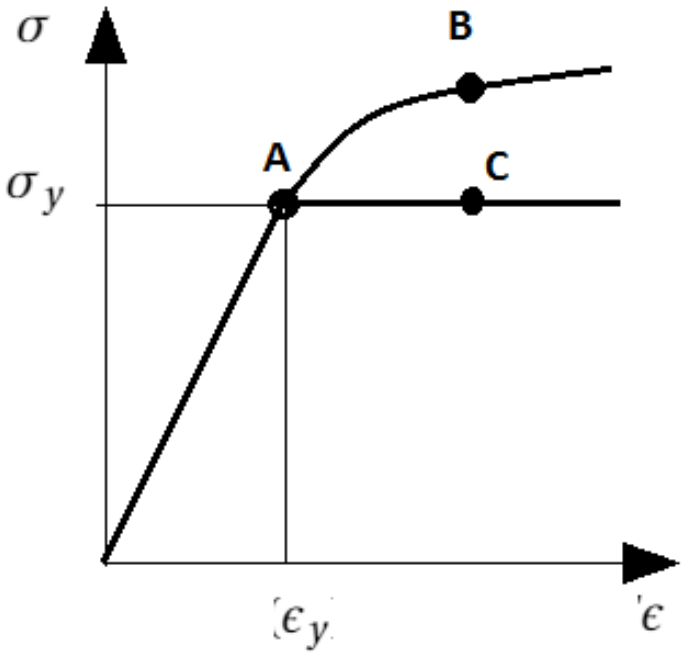

Figure 2.10: Stress strain curve . Hardening vs non hardening.

Two important ways of modelling strain hardening in material behaviour is called kinematic hardening and isotropic hardening. Isotropic hardening means that the model gets harder by each load cycle. If one loads a specimen above yield into the plastic domain, then to unload it, and reload it again, one would find one need more load to reach the same deformation. For isotropic hardening the hardening effects and increase of yield point the same in tension and compression, whereas kinematic hardening the yield point is lower in compression [Moan, 2003], as can be seen in fig 2.2.3

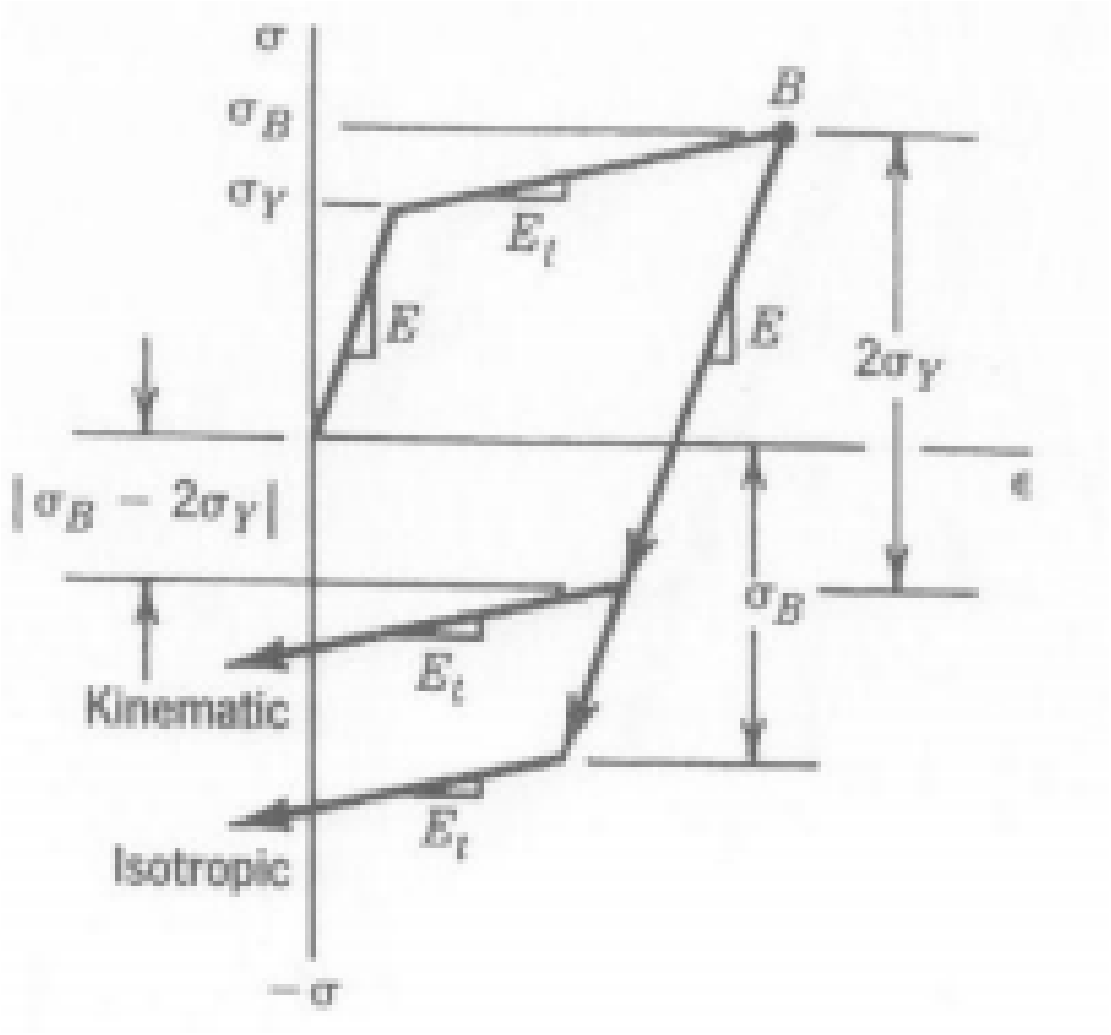

Figure 2.11: Kinematic hardening vs isotropic hardening [Moan, 2003]

2.2.4 Formulations

The most common formulations for describing a change in fluids and solids are the Lagrangian and the Eulerian approaches. The Lagrangian approach often called the material description because it focuses on what happens at a material particle. The formulation is independent of initial configuration and time, and thus it is a common approach to using in solid mechanics since the initial configuration is often known a priori. The Eulerian approach is often called the spatial formulation. This because it focuses on a space in a given time. This formulation is more used in hydrodynamics.

The Lagrangian formulation can be solved using different methods. Total Lagrangian

formulation stress and strain measures are taken accordingly to the initial configuration, while the updated formulation measure strain and stress in an updated configuration. The updated configuration continuously updates from the deformed configuration. When a formulation updates the configuration, following a stepwise increase in loading and referring each element of the structure by a local coordinate system is called a co-rotational system. The local coordinate system will rotate when the structure is deformed, and the updated configuration follows this deformation. The goal is to establish a system of equation in the form

$$\Delta R = K_I \Delta r \tag{2.26}$$

moreover, in incremental form

$$\mathbf{d}R = K_I \mathbf{d}r \tag{2.27}$$

$\Delta\ R$ - Incremental external load acting on structure

$K_I\ \Delta\ r$ - Incremental internal reaction forces in structure item[] K_I - Incremental stiffness matrix. Also called tangent stiffness

If one have an expression for the stiffness, as in the two bar example, the tangent stiffness may be expressed as

$$K_I = \frac{d}{dr}(K(r)r) \tag{2.28}$$

One can use different solution techniques to solve the system of equation **??** above. The stiffness matrix K_I can vary on wether u use total or updated formulation. For example the stiffness matrices for the two bar formulation above can be expressed by the updated formulation and the total formulation by [Moan, 2003]

$$K_I^{total} = K_0 + K_G + K_\sigma \tag{2.29}$$

$$K_I^{updated} = K_0 + K_\sigma \tag{2.30}$$

In most modern computer software the updated Lagrangian formulation is preferred because the total Lagrangian formulation often becomes very complex for large deformations because it refers to a global reference system. While the updated Lagrange formulation uses a local reference system, the governing equations often are more straightforward. The need to storage information for every iteration also becomes less for the

updated, since it only needs information from the previous iteration, while the total Lagrangian need information from the initial configuration.

2.2.5 Solution techniques

There are many different solution techniques to solve a non-linear problem. [Moan, 2003] presents three main categories

Iterative methods

Incremental methods

Combined methods

Governing incremental equations for non-linear problems can be expressed as [Moan, 2003], based on total equilibrium between internal and external forces

$$R_{int} = R_{ext} \tag{2.31}$$

The internal stiffness can be expressed as

$$R_{int} = \Sigma(a^i)^T S^i \tag{2.32}$$

Hence the two equation to be solved, where the external load $\mathbf{R^{\cdot}ext}$ is given, the displacement $\mathbf{r}$ is the unknown

$$\mathbf{d}R = K_I \mathbf{d}r \tag{2.33}$$

$$R_{ext} = \Sigma(a^i)^T S^i \tag{2.34}$$

I will present some examples of each.

Load incremental methods

One can iterate to a solution of a given non-linear problem by load iteration. A famous load incremental method is the Euler-Cauchy method. Figure 2.2.5 below shows how load increment method works. For a given

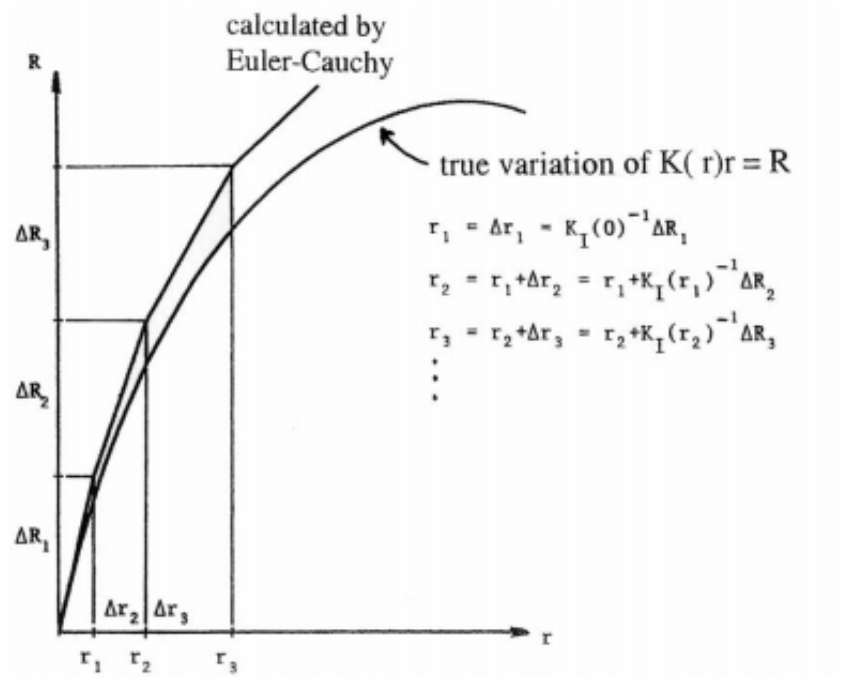

Figure 2.12: Euler-Cauchy solution method[Moan, 2003]

This method increases the external load stepwise, and the displacement Δr is calculated using equation **??**. The total displacement calculated by summarising each displacement at every step, before moving on to the next load step. Calculation of the tangent stiffness based on known displacement and stress configuration from the previous step [Moan, 2003].The Euler-Cauchy method needs to be corrected due to the fact it does not fulfil total equilibrium at each load step [Moan, 2003]. This is illustrated in the deviation between the calculated pushover curve by Euler-Cauchy method, and the true pushover curve.

Iterative methods

A very popular, and perhaps the most widely used iterative method is called the Newton -Raphson method. This method is based on the Newton-Raphson method of finding roots of a nonlinear equation by use of the differential expression of the nonlinear equation. This numerical method is quite computational efficient and is therefore quite popular in numerical analysis.

$$x_{n+1} = x_n - \frac{f^{'}(x_n)}{f_(x_n)} \tag{2.35}$$

n -iteration step number n

X˙n - x value at iteration step number n

$f(x_n)$- Non-linear equation with respect to x value at iteration step n

$f^{'}(x_n)$- First differentiate of Non-linear equation with respect to x value at iteration step n

Equation **??** can be written as an iterative formula, in the same manner as Newton -Raphson equation above, as

$$r_{n+1} = r_n - K_I^{-1}(r_n)(R_{int} - R) \tag{2.36}$$

Figure **??** below, illustrates the basic process of the Newton-Raphson method for a one-dimensional case. However, one of the disadvantages of this method is the time-consumption to calculate the stiffness and displacement at each step. One can modify the method by not to update the stiffness at each step, but use the tangent stiffness from last load step, instead of an iterative step.

Using the Newton-Raphson method, one usually iterates until a satisfying criterion. This criterion is acchieved when the vector norm of the difference between the displacement at iteration n+1 and displacement at n, is smaller than a given value. One can use vector norms based on energy or force as well.

2.2.6 Combined iterative and incremental Methods

Combined methods include both incremental load method and iterative methods into a more powerful method. One can combine iterative methods such as Newton -Raphson method with load incremental Euler-Cauchy methods to get a powerful method to solving pushover curves. Using this force-based formulation is only a good solution if the pushover curve is monotonically increasing. If not, one should combine with displacement -based formulations to iterate over a maximum point.

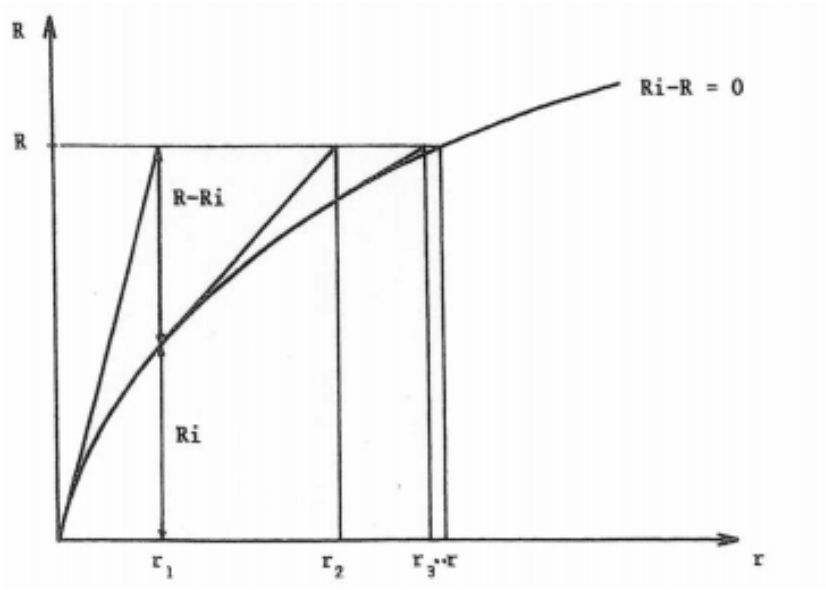

Figure 2.13: Newton-Raphson solution technique [Moan, 2003]

2.2.7 Central Difference Method -Direct integration

To solve static non-linear problems, one can use a finite-difference method on a dynamic equilibrium equation for the system. The equation

$$\mathbf{Kr} = \mathbf{R}(t) \tag{2.37}$$

can be solved by applying finite difference method to the equation

$$\mathbf{M}\ddot{r} + \mathbf{C}\dot{r} + \mathbf{Kr} = \mathbf{R}(t) \tag{2.38}$$

How this works is by replacing the velocity and acceleration by differences of displacement at various time steps. One can differ between explicit and implicit finite difference methods. The method is said to be explicit if the displacement at the current time step is calculated based on displacement, velocity and acceleration of the previous time step. Mathematically this can be written [Moan, 2003]

$$r_{ni+1} = f(r_i, \dot{r_i}, \ddot{r_i}, r_{i-1}, \dot{r_{i-1}}, \ddot{r_{i-1}}, ..) \tag{2.39}$$

The method is implicit if the displacement at the new time step is calculated based on velocity and acceleration at the new step, but also the history of the old steps. Mathematically this can be expressed [Moan, 2003]

$$r_{i+1} = f(\dot{r_{i+1}}, \ddot{r_{i+1}}, r_i, \dot{r_i}, \ddot{r_i}..) \tag{2.40}$$

The solver in LSDYNA3D is an explicit method. The method is called the central difference theorem. The central difference theorem assumes that Taylor series expansion can describe the displacement at the new step time step $(t+\Delta t)$ as well as the previous one $(t-\Delta t)$ [Moan, 2003]

$$r_{i+1} = r_0(t) + \Delta t \dot{r_{i+1}} + \frac{\Delta t^2}{2}\ddot{r_{i+1}} + \frac{\Delta t^3}{6}\dddot{r_{i+1}}... \tag{2.41}$$

And

$$r_{i-1} = r_0(t) - \Delta t \dot{r_{i+1}} + \frac{\Delta t^2}{2}\ddot{r_{i+1}} - \frac{\Delta t^3}{6}\dddot{r_{i+1}}... \tag{2.42}$$

Where

$$r_0(t) = r_i \tag{2.43}$$

One can consider the third order terms as negligible. Subtracting the second equation by the first and by rearranging the velocity and acceleration at current time step, one can show, see [Moan, 2003] that the dynamic equation can be written as

$$(\frac{1}{\Delta t^2}\mathbf{M} + \frac{1}{2\Delta t}\mathbf{C})r_{i+1} = R_i(t) - \mathbf{K}R_i(t) + \frac{1}{\Delta t^2}\mathbf{M}(2r_i - r_{i-1}) + \frac{1}{2\Delta t}\mathbf{C}r_{i-1} \tag{2.44}$$

The main advantages of an explicit method such as the central difference method are that it does not need to invert the tangent stiffness matrix, and it does reduce the need for computer memory capacity [Moan, 2003] The equation **??** is conditionally stable only if the time step satisfies the following

$$\Delta t < \frac{2}{\omega_{max}} \tag{2.45}$$

Where ω_{max} is the highest eigenfrequency found by eigenvalue evaluation of the system.The highest eigenvalue obtainable is depending on the acoustic wave speed and the

characteristic element length. In a dynamic analysis, one must make sure that information does not propagate over more than one element each time step [Moan, 2003]. This characteristic element length can be defined as

$$\Delta t = \frac{\lambda_e}{c} \tag{2.46}$$

2.3 Dynamic Analysis

Theory regarding oscillation of complicated structures, induced by irregular time dependent loads is covered by Ivar Langen and Ragnar Sigbjrnsen in **??**. *The need of dynamic analysis of structures has increased gradually as structural engineering has made new and complicated structures located in a very harsh environment in the northern sea. Some basic theory on how to solve dynamic analysis is treated in this section*

2.3.1 Basic principle of describing a dynamic problem-Virtual work

To solve a dynamic equation, describing a structure exposed to external forces, one can use the principle of virtual work. The traditional physical understanding of energy is that it cannot be created or removed, only transformed into different forms, and transported between the various objects. This principle is also valid in the principle of virtual work . The external virtual work must thus equal the internal virtual work at all times. Described with mathematics this implies, [**?**]

$$\int_V \delta \mathbf{u}^T \ \mathbf{X} \ \mathbf{dV} + \int_{S_0} \delta \ \mathbf{u}^T \mathbf{T} \ \mathbf{dS} \ + \delta \mathbf{r}^T \mathbf{Q}_c = \int_V \delta \epsilon^T \sigma \mathbf{dV} \tag{2.47}$$

The expression on the left-hand side represents the external virtual work on a system or structure, while the right-hand side represents the internal virtual work in the structure. The vectors $\mathbf{X}$,$\mathbf{T}$,$\mathbf{u}$,ϵ and σ Represents volume forces, surface tractions, displacement vector, strain vector and stress vector [**?**] respectively. V denotes the volume of the system exposed to the loads, S_0 denotes surface where surface traction works, $\delta\epsilon$ denotes virtual strain, δr denotes virtual rotations and δu virtual displacements This is one way of describing a dynamic problem. One can use this principle further to find the dynamic equation of equilibrium for an oscillating structure, such as a beam, as long as the assumed displacement field is kinematic compatible.

By the use of d'Alemberts principle, see [**?**] one can find the dynamic equation of equilibrium for a beam

$$\bar{m}\ddot{q} + \bar{c}\dot{q} + \bar{k}q = \bar{Q(t)} \tag{2.48}$$

Where the assumed oscilation form is

$$w = \phi(x)q(t) \tag{2.49}$$

The modal mass, stiffness and damping is denoted

$$\bar{m} = \int_0^l \rho(x)(\phi(x))^2 dx \tag{2.50}$$

$$\bar{c} = \int_0^l c(x)(\phi(x))^2 dx \tag{2.51}$$

$$\bar{k} = \int_0^l EI(x)(\frac{\delta^2}{\delta x^2}\phi(x))^2 dx \tag{2.52}$$

$$\bar{Q} = \int_0^l p(x,t)(\phi(x))dx \tag{2.53}$$

Where $\rho(x)$, c(x), EI(x) and p(x,t) denotes respectively the mass, damping and bending stiffness of the beam, as funciton of x and p(x,t) as the load acting along the beam as a function of time.

2.4 Ship collision theory

There are different approaches one can choose to analyse a ship collision event. This thesis is solved using a decoupled method , based on energy considerations. One can use other approaches, such as complete ship-barrier fluid interaction analysis. In this chapter different theory used in decoupled approach of analysing ship collisions will be discussed and presented.

2.5 General

The dynamics of a ship collision can be described by using the principles of conservation of momentum and energy. A ship moving with a given velocity has kinetic energy. This energy must be absorbed. Depending on how the configuration of the barrier. The collision energy will be absorbed when the barrier deforms , as strain energy. Friction will also absorb some energy, as drag acting on the submerged bodies, if the bodies are allowed to move after impact.

Mechanics and material properties of the vessels involved in the collision will determine the response of the vessels after collision. There will always be some damage of both vessels at a collision. Depending on the strength of the ship and the barrier the damage will be distrubited accordingly. Circumstances surrounding the structures will determine how much of the kinetic energy of the ship that will be absorbed as strain energy and friction, and how much remains as kinetic energy afterwards.

2.6 Design standards on Ship Collisions

2.6.1 Design classifications

The Norsok Standards contain guidelines for design principles of a ship collision. It distinguishes between three distributions of strain energy dissipation (Norsok)

- Strength Design
- Ductility Design
- Shared Energy Design

See figure **??** for a illustrative description of strain energy dissipation given by the standard. If the installation is only damaged slightly with minor deformations it implies a strength design. The hull of ship dissipates most of the energy. If however the installation undergoes large deformations this implies a ductile design of the installation. An event where both ship and installation dissipates significant energy implies shared energy design. The complexity of the collision analysis increases considerably if both ship and installation is deformed significantly ([Norsok, 2004]).

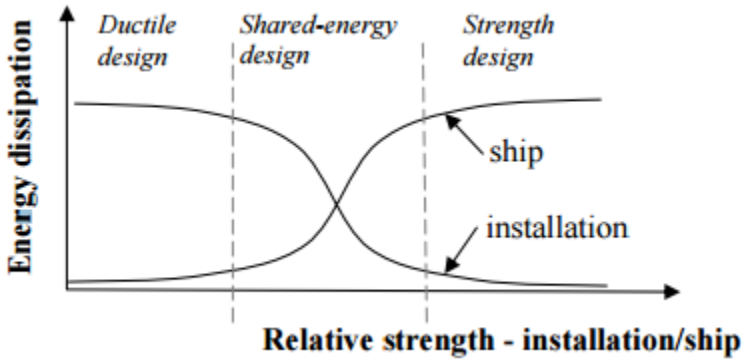

Figure 2.14: Strain energy dissipation types.Source;([Norsok, 2004]
)

Strain dissipation models

Using the laws of conservation of momentum and kinetic energy, Norsok standard N-004 articulates a formula for calculating the strain energy dissipation. The rest of the collision energy will be absorbed in the stiffness and damping of the system. Which for the barrier is mooring forces and drag forces. The formulas below provide an estimation of how much the installation must absorb after impact.
For fixed installations([Norsok, 2004]);

$$E_s = \frac{1}{2}(m_s + a_s)\vec{v_s}^2 \tag{2.54}$$

For compliant installations

$$E_s = \frac{1}{2}(m_s + a_s)\vec{v_s}^2 \frac{(1 - \frac{v_i}{v_s})^2}{1 + \frac{m_s + a_s}{m_i + a_i}} \tag{2.55}$$

m_s - mass of ship

a_s - added mass of ship

v_s - velocity of ship

m_i - mass of installation

a_i - added mass of installation

v_i - velocity of installation

An installation can be assumed fixed if the duration of impact is long compared to the natural period of the installation. Installation can be assumed compliant if impact is short compared to natural period ([Norsok, 2004]).

2.6.2 Dissipation of strain energy

A force - deformation curve can describe the energy dissipated by the structures in a collision. The energy dissipated in a collision, is the area under this curve. The total energy dissipated as strain energy is the sum of the areas under force-deformation curves of both ship and barrier. A regular figure of a force - deformation curve is given in figure **??**.

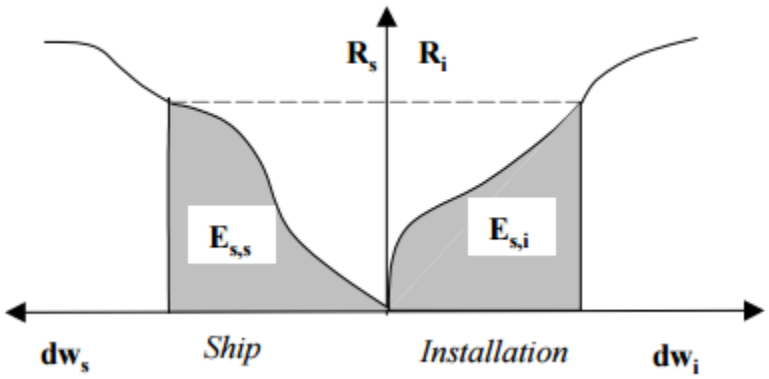

Figure 2.15: Force and deformation curve.(Soure: [Norsok, 2004])

The total strain energy dissipated may be written as

$$E_s = E_{s,s} + E_{s,i} \tag{2.56}$$

Numerical simulations can be used to find the force- deformation relation. Load levels are usually not know a priory a collision, therefore a incremental method is generally needed ([Norsok, 2004]). There are difficulties using non-linear finite element simulations. It is important to make a model that is able to capture important geometrical and material non linearity. Using a rigid model for either the ship will over estimate the strength of the rigid structure. Both structures will in reality deform. Using helpful documents such as DNV-GL RPC 208, may help in making a good finite element model one can use in collision simulation and analysis.

Chapter 3

Aluminium in structural engineering

Aluminium is a popular material to use in engineering, particular in aircraft engineering. Even from back to when Zeppelin aircraft was filling the sky, aluminium has been widely used. High speed vessels are also benefited by use of aluminium, due to its light weight, which is very important for high velocity vessels. When regarding civil engineering steel is a conventional material and it is often desired due to its excellent strength and ductility properties. A concern regarding marine engineering, is corrosion. Aluminium has very good properties regarding corrosion. In this chapter benefits and weakness of Aluminium will be discussed. Material properties will be compared to properties steel. Material models used in finite element method will also be described

3.1 Classification of Aluminium alloys

The classification of aluminium alloys can be given in two separate ways [**?**]

1. The Numerical designation
2. The Alpha Numerical designation

There can be some variation in how alloys are classified, some countries differ from other. The numerical designation gives the chemical composition, followed by the alpha numerical designation giving the manufacturing process. The numerical designation is derived from American aluminium nomenclature and is also commonly used in European countires. An overview of the numerical designation is given below.

Numerical Designation of Aluminium Alloys

Class ID	Main alloying element
1xxx	Aluminium considered pure (more than 99 percent)
2xxx	Cobber
3xxx	Manganese
4xxx	Silicon
5xxx	Magnesium
6xxx	Magnesium and Silicon
7xxx	Zinc
8xxx	Other elements
9xxx	Unused Series

Table 3.1: Numerical designation of aluminium alloys

The fabrication stage designation describes how the alloy is manufactered. The following series was first proposed by the Aluminium Association [Mazzolani, 1994]. The fabrication stage designation, sometimes referred to as the alloys temper, is seperated into five main groups:

- F rough stage of fabrication
- O annealed stage of fabrication
- H work hardened stage of fabrication
- W tempered non stabilised stage
- T heat treated stage

The stages H and T, are also subdivided by respective three and twelve stage. Each sub stage has a special way of treating the alloy , giving it desired properties.

3.1.1 General properties of aluminium

Choosing Aluminium as material is considered a good option when lightness is required. Aircraft and high speed vessel that needs to be light often prefer Aluminium. Aluminium is also quite soft. Youngs modulus of Aluminium is about one third that of steel. This section gives a brief overview of important properties of aluminium and compares them to steel.

Physical properties of aluminium

Below is a table comparing average physical properties of steel and aluminium.

	Physical properties of Aluminium Alloys vs Steel		
Physical Property	Aluminium	Conventional Steel	Stainless steel
Density $[kg/m^3]$	2700	7850	7900
Youngs modulus $[Nmm^{-2}]$	68500	206000	206000
Melting Point$[^{\circ}C]$	658	1450-1530	1450
Thermal expansion coefficient$[^{\circ}C^{-1}]$	24*10^-6	12*10^-6	17.3*10^-6
Thermal conductivity $[calcm^{-1}s^{-1}{}^{\circ}C^{-1}]$	0.52	0.062	0.035

Table 3.2: Physical properties of aluminium

The density of Aluminium is much lower than steel. Steel is almost three times heavier.Aluminium is originally quite ductile($\epsilon_t \cong 40 percent$), but not very strong ($f_{0.2}$) $\cong$ $20Nmm^{-2}$) **??**. One can however treat the material in order to obtain 5 times higher strength. This usually decrease the ductility. Ductility can be somewhat maintained, by use of other materials , e.g making alloys, with magnesium or manganeese as mentioned above.

Steel has a much higher Youngs modulus, making it much rougher than Aluminium. Aluminium is more flexible than steel, which in some cases can be an advantage. When considering the barrier, this could be beneficial , because the more the barrier deforms, the more energy it will absorb as strain energy.

After a collision, the costs of repairing the ship is more likely to be higher than to replace the damaged section of the barrier.

Mechanical properties of aluminium

Below is a table comparing some mechanical properties of steel and aluminium.

	Mechanical properties of Aluminium Alloys vs Steel			
Mechanical Property	AlMg4.5Mn	AlMgSi1	Fe360	Fe510
Yield stress(tension) f˙y $[Nmm^{-2}]$	140	260	235	350
Ultimate stress(tension) f˙T $[Nmm^{-2}]$	280	320	360	510
Ultimate strain(tension) f˙T [ ]	10-25 percent	10-25 percent	25-35 percent	25-35 percent

Table 3.3: Mechanical properties of aluminium

Aluminium does not behave the same way as conventional steel after it starts to yield. Where mild steel has a quite clear yield point, aluminium as well as high strength steel has a more curved behaviour after yield, where conventional steel has the so-called yield plateau. Since there is no easy way to define the yield point, often a 0.2 percent proof stress is chosen as yield stress for engineering purposes. The lower Young's modulus

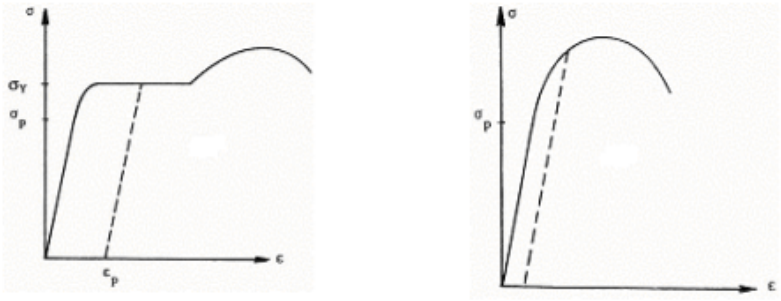

Figure 3.1: Stress strain curve for conventional steel vs aluminium [Moan, 2003]

of aluminium makes it more prone to deformation and instability than steel. However mentioned, deformation can be advantageous for a collision barrier.

3.1.2 Aluminium in marine environment-Collision Barrier

Aluminium has high corrosive resistance properties. Due to the Aluminium Oxide film forming on the structures surface when aluminium is in contact with air or other oxygen-containing fluid, it is protected against further corrosion. The aluminium alloy 5083 is a common alloy used in plates in the marine industry. Temper O and H are both of interest. The 5000 series have excellent corrosive properties. They are not as strong as the 6000 series, but they can be cold worked, to increase the strength. It was decided in discussion with Supervisor Jørgen Amdahl that alloy 5083 was to be used and that I investigated the difference between temper O and H12.

The 6000 series has good strength abilities due to its heat treatment; the strength is increased. These alloys are particular suited for extrusion making them suitable for stiffeners. Alloy 6082 is the strongest in the series, making it the most preferable. Because the barrier is filled with ballast water, and sea water being a reasonable choice, the inside of the barrier must be corrosive resistance as well. The 6000 series are, and thus the stiffeners inside the barrier will be protected against corrosion. It was decided to use alloy 6082 with temper T6 in the stiffeners of the barrier.

Sea water contains chlorine particles. The chlorine can break down some of the aluminium oxide film. If this happens, additional corrosion protection is needed. Eurocode 9 part 1.1 has a classification system focusing on the durability of different alloys, in which one can use as a design criterion. See Appendix B. Using this criterion; one can see what type of extra protection an alloy needs, given environment. For alloy 5083 and 6082, found in sea water, protection depends on any special consideration of the structure. Eurocode 9 refers to EN 1090 guideline as a guideline for special considerations.

3.1.3 Plastic collapse and fracture consideration for aluminium

In conventional plastic hinge theory, the plastic collapse capacity is solely depending on the cross sections plastic section modulus. This is not applicable for structures built by Aluminium. For general elastic limit state the plastic capacity in bending for a cross section

$$M_p = \sigma_y W_p \tag{3.1}$$

Due to the fact that the region below yield is perfectly elastic,one can calculate stresses as

$$\sigma = \frac{M}{I} y \tag{3.2}$$

Because aluminium has no specific yield point, unlike conventional steel, the conventional plastic hinge theory should be modified for use in aluminium structures. Mazzolani proposes a solution to this [Mazzolani, 1994]

$$\sigma = \frac{M}{\Psi I} y \tag{3.3}$$

The numerical value of Ψ can be found in the ECCS recommendations, and it is based on French specifications found in [Mazzolani, 1994] There are developed other alternative methods to other than the classical plastic method, but not further discussed here, see [Mazzolani, 1994].

3.2 Different material models usable for aluminium

To describe a chosen aluminium alloy with a stress-strain curve, one can do a specimen test. There are however several different material models that one can use

to describe the mechanical properties of aluminium. Both Bahre **??** and Mazzolani [Mazzolani, 1994] describes proposed analytical models in the form

$$\sigma = \sigma(\epsilon) \tag{3.4}$$

Both models are based on separating the stress-strain curve into three regions

- Region 1: Elastic region
- Region 2: Inelastic region
- Region 3: Work Hardening region

Fig 3.2 shows how the stress-strain curve is separated into the three regions. The methods described by Bahre and Mazzolani must be continuous between each region. Thus coincident points at the region limits must be defined. It is very difficult to produce a law on the form $\sigma = \sigma(\epsilon)$ to fit every different alloy, but it can be a good estimate. The methods are based on experimentally observed values of yield at 0.1 and 0.2 percent, as well as Young's modulus for the specific alloy under examination. The equations are quite complex and will not be described here, but they are found in [Mazzolani, 1994]

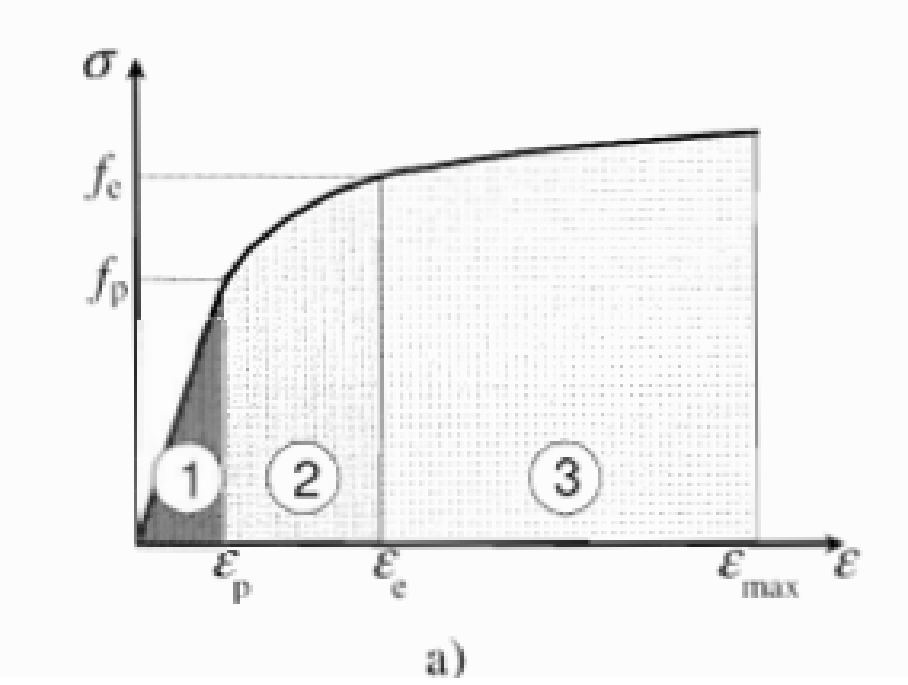

Figure 3.2: Stress strain curve for steel [Eurocode, 2006]

The Ramberg-Osgood Law propose an analytical model of stress-strain curves, on the form

$$\epsilon = \epsilon(\sigma) \tag{3.5}$$

It is described as [Eurocode, 2006]

$$\epsilon = \frac{\sigma}{E} + \epsilon_{0,e}(\frac{\sigma}{f_e})^n \tag{3.6}$$

where

- E: Youngs modulus
- ϵ_0: conventional limit of elasticity
- f_{ϵ_0} :residual strain corresponding to limit of elasticity
- n: Ramberg -Osgood exponent, describing the level of hardening. Must be defined by use of experiments

By use of extensive tests, the Eurocode 9 propose an analytical expression one can use for aluminium alloys, as long as the following parameters are known

- f_0 :Recorded value of yield stress for alloy.
- f_0 :Recorded value of ultimate stress for alloy.
- $f\epsilon_u$:residual strain corresponding to limit of elasticity
- f_{ϵ_0} :residual strain corresponding to limit of elasticity

The Ramberg-Osgood law can then be described, in plastic range:

$$\epsilon = \frac{\sigma}{E} + 0.002(\frac{\sigma}{f_0})^n \tag{3.7}$$

where

$$n = n_p = \frac{ln(0.002/\epsilon_u)}{ln(f_0/f_u)} \tag{3.8}$$

The figure below shows how a Ramberg-Osgood representation of a material behaviour looks like for alloy 5083 temper O. The Ramberg-Osgood material law is good at describing work hardening and the inelastic region. It does not, however, describe the reduction in strength, near the fracture point. By the use of the Ramberg-Osgood law, and experimental values for ultimate strength and yield strength, the material description of the alloys 5083 and 6082 is complete. The only thing missing is the value of strain at failure. Eurocode 9 part 1.1 gives a very simplified estimation for how to evaluate the ultimate strain value. It is given by the condition

$$\epsilon_u = 0.3 - 0.22\frac{f_y}{400Nmm^{-2}} \forall f_y \in [0, 400Nmm^{-2}] \tag{3.9}$$

$$\epsilon_u = 0.08 \forall f_y \in [400Nmm^{-2}, \infty\rangle \tag{3.10}$$

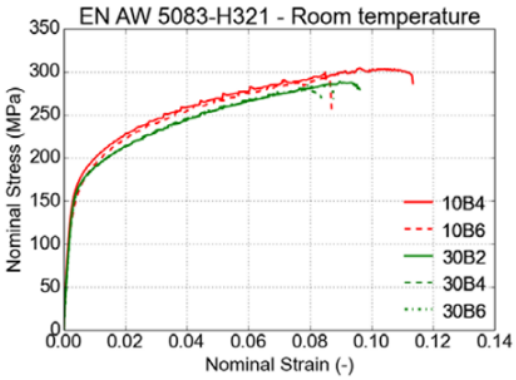

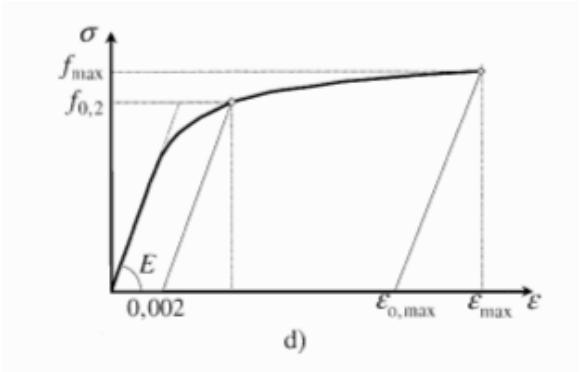

figureleft: meassured stress-strain values , 5083 H12, provided by Norsk Hydro. Right(typical Ramberg-Osgood curve. [Eurocode, 2004]

3.3 Welds and heat affected zone

Large structures, such as barrier is too large and complicated to be extruded or rolled, and must be welded together by smaller pieces, such as plates and stiffeners. Welding offers some complications when the material welded is aluminium. When an alloy is cold worked, to increase the strength and later heat treated, such as welding, it returns to the same state it was in before it was cold worked. What happens is that the alloy is increasing strength by cold working, and then reducing it again because of the heat treatment. The area in which the reduction in strength of the alloy is called the heat affected zone. One can age the structure after it is welded to regain some of the reduced strength in the heat affected zone.

Some typical properties that reduce in welds or heat affected zones are the elastic limit and ultimate strength. Ultimate elongation can also be reduced for some alloys; this greatly reduces the ductility for the alloy. Ageing can increase the ductility to some extent, varying between 10 percent and 80 percent of original value [Mazzolani, 1994]

The effect of heat affected zones must be considered when doing structural analysis using aluminium. Both butt welds and fillet welds have a reduction of strength due to heat affected zones, compared to the base material. Mechanically properties decrease gradually from near the weld, to a minimum at the weld centre see figure **??**

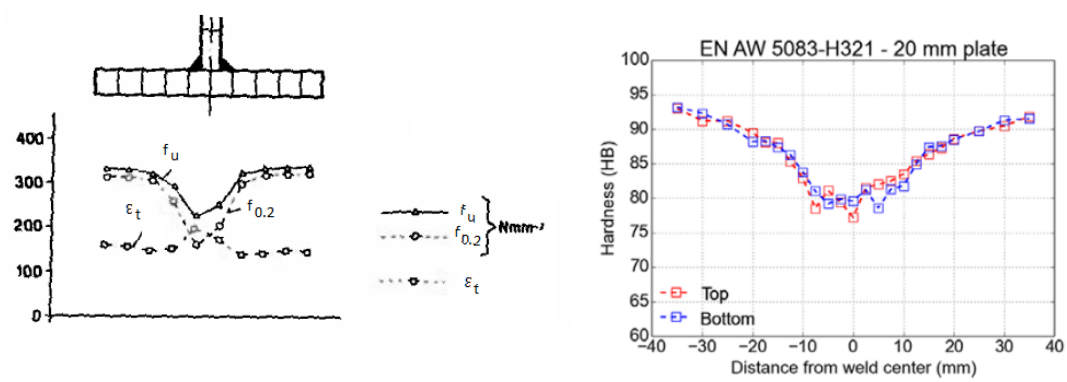

figureleft: Typical effect of heat treatment in welds, [Mazzolani, 1994]. Rigth:Picture provided by Norsk Hydro, meassured hardness abilities for a 5083H312 plate.

For comparison supervisor Ole Runar Myhr provided curves for a 20 mm thick plate with temper 5083 H312. As can be seen, the hardness decrease in the same manner shown in **??**. The zone where this effect of strength reduction occurs is characterised by a zone width, b_{HAZ}. This width sometimes referred to as extent of HAZ ,describes where there is a variation of strength, compared to the parent material. The width of the HAZ depends on many different parameters and welding procedure. Meaning voltage and weld velocity, as well as the thickness of joints. The values of the extent of heat affected zones found in Eurocode 9 are meant to be conservative, meaning the extent of the HAZ for the particular thickness is, in fact, smaller in reality. In the Eurcodes the following design criteria for a given plate thickens is

- $0 < t < 6mm, b_{haz} = 20mm$
- $6mm < t < 12mm, b_{haz} = 30mm$
- $12mm < t < 25mm, b_{haz} = 35mm$
- $t > 25mm, b_{haz} = 40mm$

The reduction in strength depends on what type of alloy is treated as well. Annealed alloys, such as Alloy 5083, temper O does not have any reduction in HAZ at all, due to the heat treatment of annealed alloys give them the weakest strength possible, so that

further heat treatment does not reduce strength further. Table **??** below shows how the reduction in the HAZ for the different alloy effect each of them compared to base material, collected from Eurocode 9 part 1.1 [**?**]

	Mechanical properties of Aluminium Alloys in HAZ		
Physical Property	5083 O	5083 H12	6082 T6
Yield strength in base material $[N/mm^{-2}]$	125	250	260
Ultimate strength in base material $[N/mm^{-2}]$	275	305	310
Yield strength in HAZ $[N/mm^{-2}]$	125	155	125
Ultimate strength in HAZ $[N/mm^{-2}]$	275	275	185

Table 3.4: Properties of heat affected zone for aluminium alloys

Young's modulus, density is not affected by heat treatment as yield, and ultimate stress is. Alloy 6082 with temper T6 is most affected by heat affected zones. Alloy 5083 O is not affected at all, while temper H12 of the same alloy has quite the significant reduction.

3.4 Material model for finite element analysis

When using finite element software to solve a collision analysis, it is important to implement a correct representation of material behaviour into the model in the program. Using LS-DYNA3D, there are some different methods of how to describe a stress-strain curve for material. It was decided to try and implement a Ramberg-Osgood representation of a stress-strain curve in an LSDYNA model.

There are different options one can use to simplify a material model in LSDYNA. There are the linear elastic, elastoplastic and piecewise plastic models. The most accurate of them is piecewise linear plastic description, and the most computational cheap is elastic plastic. Linear elastic is of course not an option where it is assumed plastic utilisation in the elements of the model. Figure **??** shows how elastic-plastic compares to piecewise linear plastic simplification of Ramberg-Osgood law.

It was decided to choose a piecewise linear plastic model because it is much more accurate compared to the elastoplastic model. Also, there are possibilities to make advanced subroutines in LSDYNA3D where one can implement an analytical expression or law, such as the Ramberg -Osgood analytical expression. One can programme very detailed information for fracture and so on. This was not encouraged to do, as it would

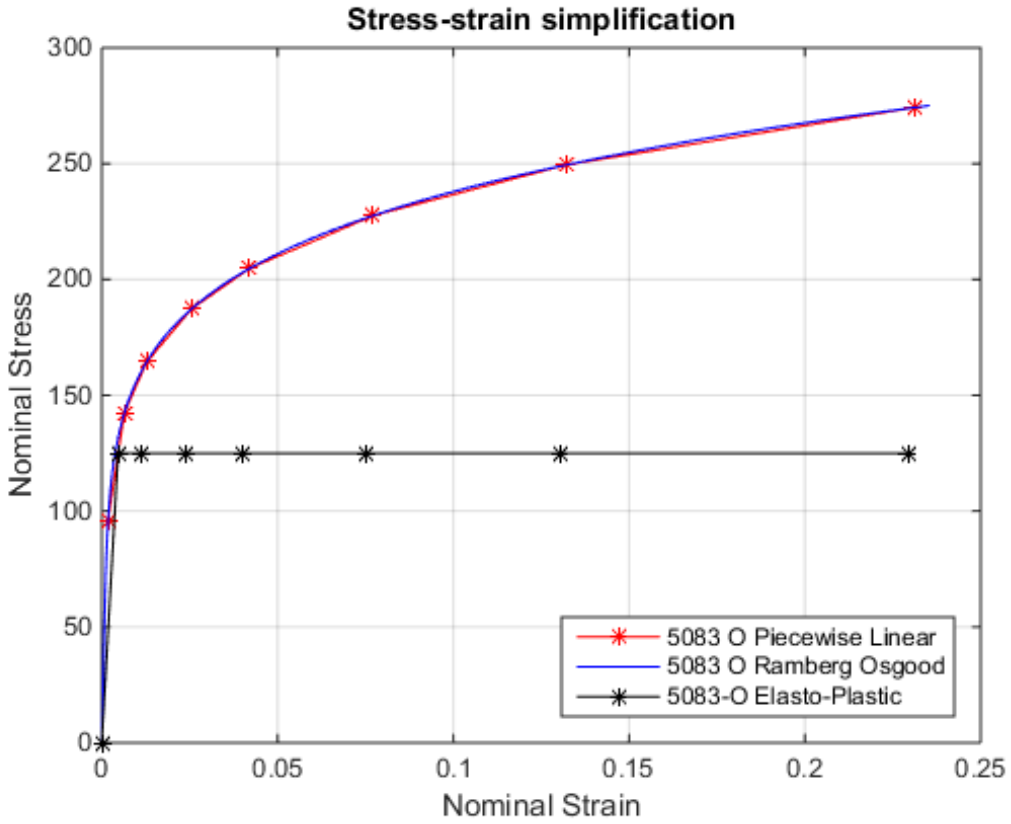

Figure 3.3: Ramberg-Osgood, Piecewise vs Elasto-plastic description. [Amdahl, 2005]

require more time and probably empirical testing to make it correct. It was decided that I be to use the piecewise linear plastic model in addition to the fracture criterion given in the Eurocode 9, described in chapter 2. It should be noted that this simplification is very simple and it gives reason to doubt the probability of correctness in the results. The fact that all of the alloys has an increase in ultimate strain because the yield is reduced in HAZ is not always true, and the Eurocode does not specify if the failure criteria are for both base material and in the heat affected part of the structure.

3.5 Fabrication process and aspects

To obtain aluminium one must purify the mineral bauxite. Alumina or aluminium oxide is transformed into aluminium and oxygen trough electrolysis at an aluminium fabrication facility. Liquid aluminium is then cast into pure metal or aluminium alloys by adding different metals such as magnesium or silicon. The aluminium can be made

into different shapes, such as rigid bodies or thin plates, by extrusion or casting. By use of cold working, the strength of the structure is increased and ductility decreased mazzolani1994aluminium. Thus when aluminium is welded ,the strength is decreased. The area or part of the aluminium structure where the strength decrease, is called the heat affected zone.

There are different fabrication aspects one should consider to try and avoid or reduce the total effect of reduction in the HAZ in the aluminium structure. Extrusion of parts such as stiffeners should be carried out as much as possible, to avoid welds, if one desire to avoid additional exposure to reduction in the HAZ. There are different procedures on how to design the strength in the heat affected zone and welds; some are given in [Mazzolani, 1994]. One should be mindful of the ratio of the width of HAZ and the plate thickness, when considering global strength of a structure [Mazzolani, 1994]

Chapter 4

Design

This chapter describes the design of the collision barrier. Both a local and a global perspective is used to argue for the final design. Different important functions of the barrier will be discussed, and various possible configurations will be presented. Stability of the barrier, with a ballasting system will be discussed. A comparison between the final choice of design will be compared to a design proposal provided in drawings by Reinertsen AS. Also, a description of the ship that is used in the collision analysis is provided.

4.1 Financial and safety considerations

The object of interest in this thesis is a barrier and a ship involved in a high energy impact collision. The purpose of the barrier is to protect the submerged floating tunnel from damage. The ship should also not be too damaged, as this may cause instability of the ship, which again turns to danger with regards to people's safety on the ship. When considering financial costs, damage to the ship is probably more costly than costs of damage to the barrier. When the ship is in repair, its income drops significantly, while the barrier itself can be replaced quite simple. Also, the design of the barrier is probably simpler than the design of the ship, resulting in lower repair costs. A desired outcome of the accident is that the ship is damaged minimal, while the barrier deforms a lot, but not too much so that the ship strikes the tunnel. Just before impact, the ship possesses high amount of kinetic energy. This must be partly or totally absorbed by the barrier to stop the ship. It is important that the barrier can absorb as much energy as strain energy as possible. It is true that if the bow of the ship is deformed, more

energy will be absorbed, but as said earlier, this damage is probably more expensive. In a financial perspective, a destroyed barrier is more attractive than a damaged ship. In a safety perspective, as long as the ship avoids damage beyond the collision bulkhead, the stability of the ship should not be compromised. The barrier should be able to absorb all the kinetic energy of the ship locally and globally to keep the tunnel safe.

4.2 Design values for ship

Design ship parameters used in the analysis is given by Reinertsen AS [**?**]. The design parameters are based on a probability study by Rambll AS. This study is based on a frequency analysis regarding ship traffic in the Sognefjord.

	Design ship parameters
Physical Property	Value
Mass [tonnes]	30000
Kinetic Energy [MJ]	1550
Impact Velocity [m/s]	9.3
Added mass coefficient in collision direction[-]	0.2

Table 4.1: Design ship parameters

The impact energy is calculated based on classical energy consideration

$$E = \frac{1}{2}mv^2 = \frac{1}{2}m_s(1+a_c)v_s^2 = \frac{1}{2}(30*10^6kg)*(1+0.2)(9.3m/s)^2 \approx 1556MJ \quad (4.1)$$

This is used as a design value of how much energy the barrier must absorb. The probability of occurrence of ship impact is 10^-4 . This information is gathered from rjan Konstalis master thesis. [**?**] This value is calculated from a probabilistic analysis, considering accidental actions limit states as a probability of occurrence of 10^-4

4.3 Bridge Concept

The bridge concept proposed by Reinertsen consist of five main parts. They are an artificial seabed, a floating bridge, a submerged floating tunnel, a collision barrier and an anchoring device consisting of chambers in the mountain of each side of the fjord.

4.3.1 Artificial Seabed

The artificial seabed is a 3600-meter long structure, composed of two main pipes spanning the fjord. The main pipes are pulled together by 13 cross beams, to give the main pipes a tension, equal to 40 percent of yield stress. Figure **??** illustrates the seabed

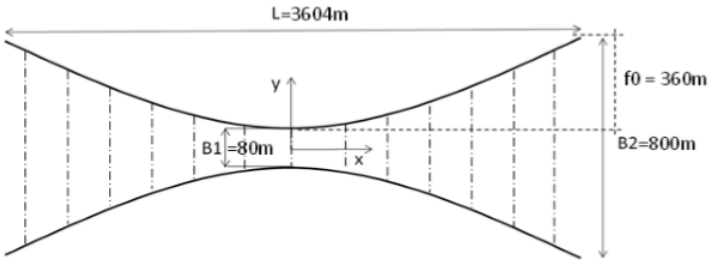

Figure 4.1: Design for artificial seabed ; provided by Reinertsen AS

4.3.2 Floating bridge

The floating bridge starts at the fjord shores and is connected at the centre of the fjord to the floating, submerged tunnel. The floating bridge is 1200 meter long on each side and is floating on pontoons. The bridge is made of a steel box of 16 by 5 meter. The cross section of the pipe is illustrated in figure **??**

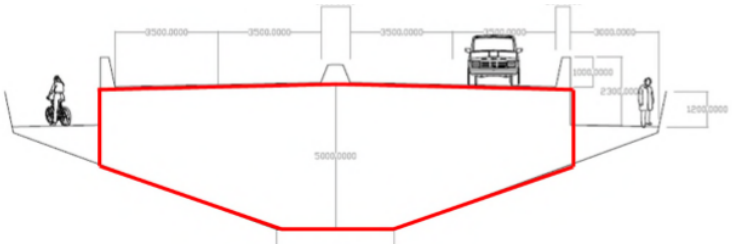

Figure 4.2: Cross section of floating bridge; provided by Reinertsen AS

The pontoons of which the bridge is floating on are circular with a diameter of 31 meters and height of 8.5 meters, with spacing every 100 meters.

4.3.3 Floating submerged tunnel

The floating submerged tunnel is connected to each of the floating bridges on both sides. The tunnel is of concrete and is 1600 meter long. Ballasting water is required to

submerge it. 6 pontoons support it.

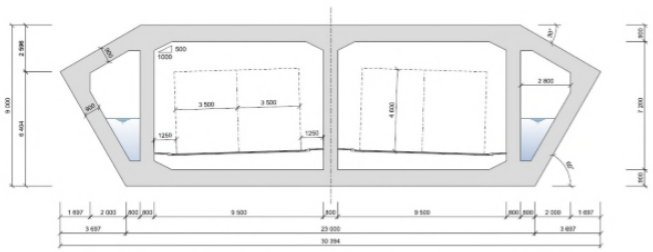

Figure 4.3: Cross section of submerged tunnel; provided by Reinertsen AS

4.4 Barrier configuration

Various configurations of the collision barrier are discussed with considerations on various aspects such as size, location and how to connect it to the bridge and seabed.

4.4.1 Straight vs Curved configuration

A drawing provided by Reinertsen AS shows a detailed layout of the barriers on both side of the bridge 3.1.1.

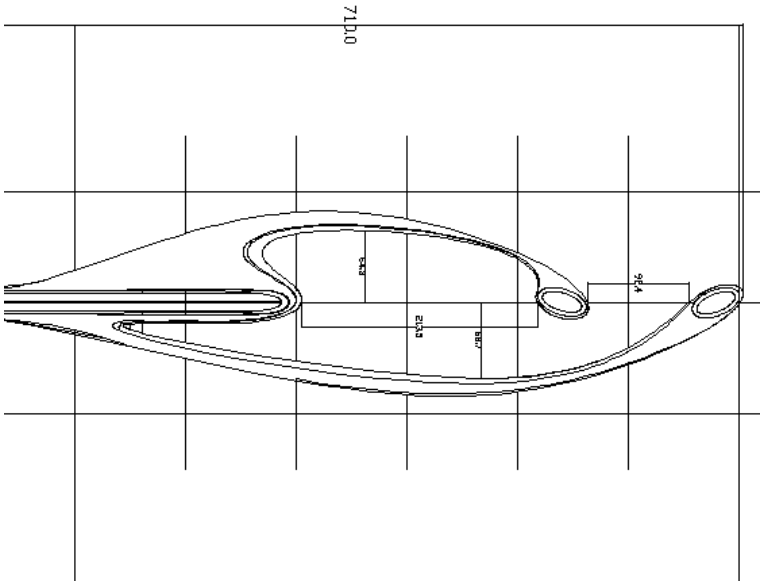

Figure 4.4: Overview of collision barriers on bridge; provided by Reinertsen AS

As can be seen, the barrier on both sides has a curved configuration. The barrier configuration on the other side of the tunnel is antisymmetric on the axis along the bridge, as can be seen in **??**.

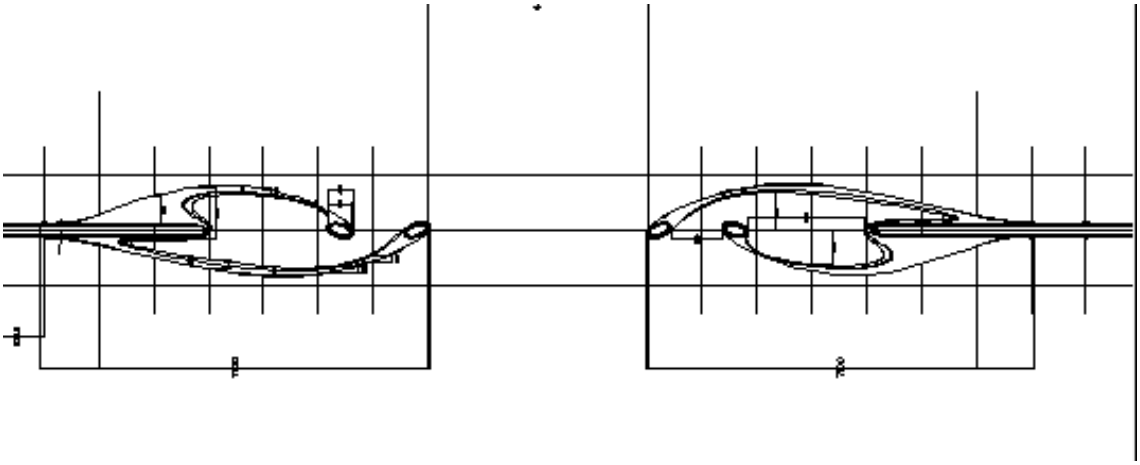

Figure 4.5: Overview of collision barriers on bridge 2; provided by Reinertsen AS

The barrier is connected to the floating bridge and on the submerged tunnels as can be seen in figure **??**

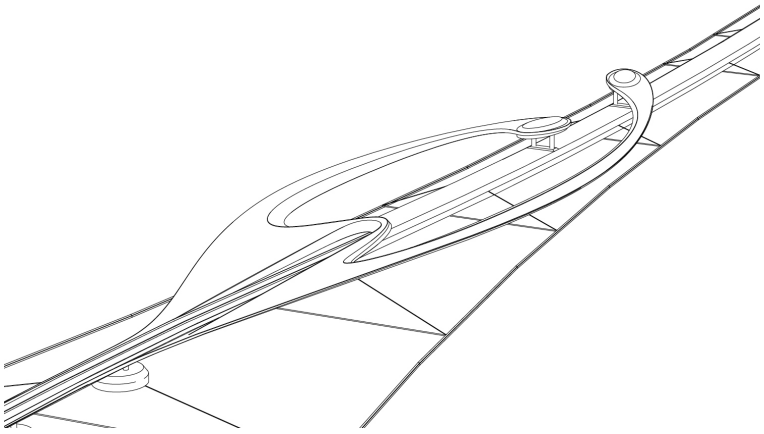

Figure 4.6: Overview of collision barriers on bridge 3; provided by Reinertsen AS

A straight floating beam could also be used. Jrgen Lima Hansen wrote a thesis on collision analysis on a straight beam instead of a curved beam. The year before rjan Konstali compared the two different configurations. rjan Konstali describes in 2014 the benefits of a curved barrier as opposed to a straight barrier in his master thesis

[Konstali, 2014]. He concluded that a straight barrier would fail with a plastic mechanism while the curved barrier would deform more locally. It was however decided by supervisor Professor Jrgen Amdahl, upon starting the thesis that a straight barrier configuration should be used in the collision analysis.

A conceptional drawing of a curved beam compared to a straight beam is given in figure **??**

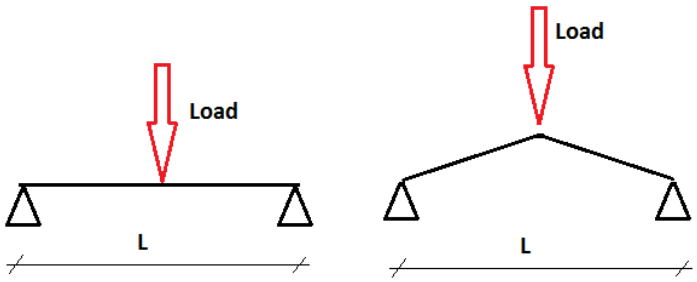

Figure 4.7: Global design by use of hinge theory

4.4.2 Size and location

The barrier needs to protect the submerged floating tunnel until it reaches a depth large enough for a ship to pass over. From the initial descent at the floating bridge, this distance the problem description states this to be 380 meters long. Figure **??** shows how the barrier protects the bridge. The red zone illustrates where the submerged tunnel is exposed to a collision, and must be protected. The length of this area is about 380 meter. The barrier must protect the entire length of this area.

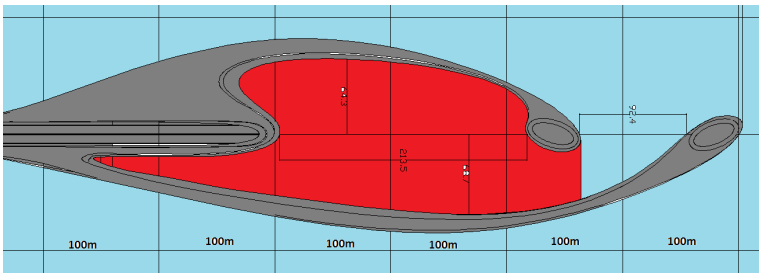

Figure 4.8: Picture of exposed area to collisions; Provided by Reinertsen

The width and height of the barrier are also of importance. The draught of the barrier must be deep enough to make sure the bulb does not slip under. This is to make sure

the bulb is somwhat deformed. This is beneficial when it comes to absorption of strain energy in the collision. The height of the barrier from the water surface and upwards should also be significantly large. If one decide the barrier need more ballast, some extra height is probably a good idea. I reckoned one-third of the entire height should be above water. The breadth of the barrier should not be too small. A slender barrier is more prone to breaking than a thick one. The higher the breadth of the barrier the more energy it can absorb locally. Looking at figures provided by Reinertsen , it seemed as though the thickest part of the barrier was around 18.5 meters. The final design is based on the reasoning here.

4.4.3 Boundary conditions and mooring lines

If the barrier is to be assumed pinned or clamped at the ends, the ending points must be much stiffer than the beam itself. Looking at fig **??** it is reasonable to think that the left connection to the barrier is stiff enough to make the assumption of clamped boundary condition there. The right connection, the connection to the tunnel trough the pontoon is more doubtful, however. A pinned connection could be more reasonable. A weak link is also a possible scenario. A weak link is thought of as a boundary condition that acts like rigid for all other loads except for accidental loads, with high enough energy. If a ship strikes the barrier the connection to the link is broken, and the only thing supporting it is drag forces, inertia forces and potentially mooring forces. This could be smart if one consider the damage to the connection points as dangerous or cost expensive.

Designing a weak link could be done by giving the connections a much lower stiffness than it would need to act as a rigid connection when the loading are of accidental nature. One could use a very simple beam model as described in Chapter 1. By finding the critical load by assuming a point load one could expect from the ship collision one can find a design of the strength of the weak link. The weak link would then break if the barrier was to be struck by a ship but act as rigid points otherwise.

One could potentially use mooring lines to use as additional protection. If the inertia forces and drag forces acting on the barrier is not enough to stop the ship from colliding with the tunnel, one could use mooring lines. They could be attached to the artificial sea floor. One would connect a certain amount of mooring lines along the barrier, to make sure enough energy is absorbed from the collision energy.

4.5 Global Design by plastic hinge theory

4.5.1 Global strength consideration

The barrier can be designed using a simplified approach. One can look at the barrier as a straight beam. One can use plastic hinge theory to find the required plastic moment capacity to find cross section dimensions to the barrier. A plastic hinge analysis is a good first approach to ensure that the barrier does not fail globally.

A beam that is clamped at both ends, and given a point load at the midspan of the beam will form plastic hinges at the middle as well as the two end points. The plastic moment capacity is found in a similar manner as the example in chapter 1 , but the force is twice as big.

$$M_p = \frac{P_I L}{8} \tag{4.2}$$

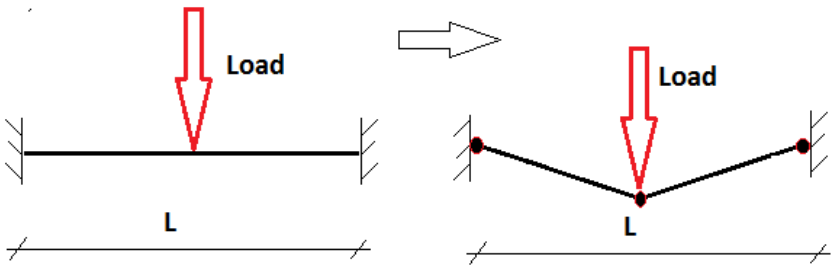

Figure 4.9: Global design by use of hinge theory 2

Where

P_{cr} - Critical load at beam

M_p-Plastic moment capacity

L-Length of barrier

The assumption of a clamped beam is as mentioned depending on the stiffness of the connections. The assumption of clamped ends is not conservative. It is more likely

that the right end might act as a pinned end. Therefore assuming clamped end makes the beam stronger than it probably is.

If the barrier is to be assumed freely floating,the critical loading is calculated somehow differently. If it is freely floating, only inertia and drag forces will support it. They will work as distributed loads along the length of the barrier. The ship can be modelled as a pin point see figure **??**

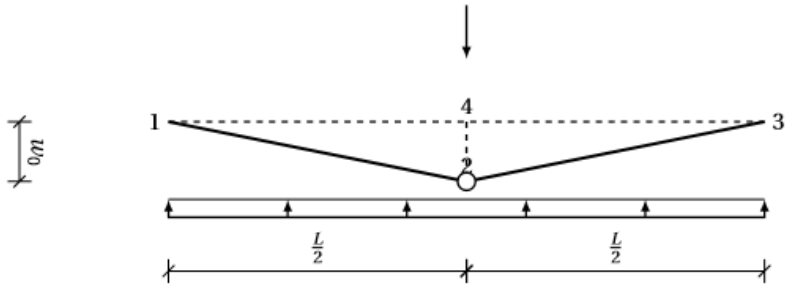

Figure 4.10: Global design by use of hinge theory 3; [Hansen, 2015]

Jrgen Lima Hansen preformed a design analysis with these conditions, [Hansen, 2015]. He showed that the plastic moment capacity would be if using these conditions

$$M_p = \frac{qL^2}{8} \tag{4.3}$$

q - Distributed load at beam

The distributed loading would, in this case, be the inertia forces, drag forces and added mass forces acting on the beam. If one assumes a freely floating beam or a weak link, this would be a good first approach to make an estimation for the dimensions of the cross section of the barrier. In both cases, the moment capacity is depending on the length of the barrier. One can see that the first case, the moment capacity is proportionally related to the length, while in the second case, it increases with the square of the length. It could be wise to shorten the span between supports along the beam by mooring forces. This would reduce the need for a high plastic moment capacity.

One of the assumptions of using plastic hinge theory is that the cross section is fully plastic deformed, as discussed in chapter 1. Aluminium does not fail the same way as steel. The global cross section is also not purely one material. It is built by two materials, alloy 5083 and 6082. Therefore the material properties are not the same everywhere in the cross section. One should choose the weakest yield value in order

to make a conservative assumption, or find an equivalent yield value for the two alloys in the cros section. With a constant cross section, the worst case scenario is when the load is at the centre of the beam. If the cross section is varying, one must find where the loading makes the worst impact, along the barrier, to make a design for the cross section.

4.6 Local Design by finite element analysis and stability consideration

4.6.1 Local strength consideration

Whereas the barrier must have a high enough stiffness globally to avoid plastic hinge formation, the barrier also must be able to absorb as much energy locally as possible. If the barrier is strong enough to crush the bow, there will be absorbed energy there as well. A detailed local design should prevent the ship from completely breaking trough the barrier and colliding with the tunnel. An obvious consideration is that the barrier is protecting something in the water, a submerged tunnel. Therefore it should be able to float in the water somehow. An enclosed cross section would be preferable. A circular cross section could be floating, but not very easy to walk on. A collision barrier could be used as a tourist attraction, and people could walk or even ride their bike on it. Therefore a flat top would be preferable. By all these considerations, a rectangular cross section would seem a simple and rational choice.

One could use plate thickness that is large and only design one hollow cross section. This would float well and could have the global strength required. However, instability could be a major concern for this section, due to the effect of the free liquid surface. I will later discuss more on the stability of the barrier. The thickness would have to be quite large for a single hollow barrier. This could make fabrication aspects more difficult and costly. A sectioned cross section as seen on the right-hand side of figure **??** is a preferred option as it can give the same stiffness as the hollow case, but dividing the barrier by use of decks and longitudinal bulkheads.

By stiffening the bulkheads with stiffeners, the barriers ability to resist local bending and buckling is increased. The more bulkheads and stiffeners, the more energy, is absorbed locally. A finite element analysis should be carried out to find how many bulkheads is needed and what stiffener spacing should be used. In a general point

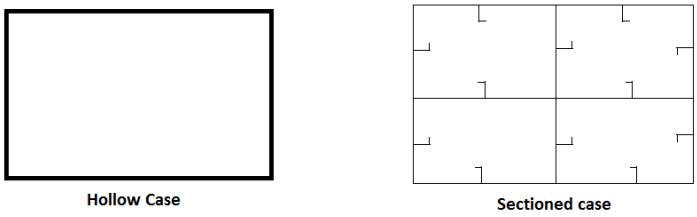

Figure 4.11: Hollow cross section vs Cross section with sections

of view, with more longitudinal bulkheads, comes higher section modulus about the vertical axis. The more amount of decks, the better local resistance to a collision. The more transverse bulkheads, the more rigid the barrier will be, and the instability effect of water in motion between sections will be reduced. The bulkheads and decks all contribute to the global stiffness and the local damage resistance, and so the more the better. The stiffener spacing will stiffen the plates locally. Buckling of transverse bulkheads is a possibility when accidental load occur, thus they should also be stiffened. A possible starting option could be a distance of 500 mm between each stiffener.

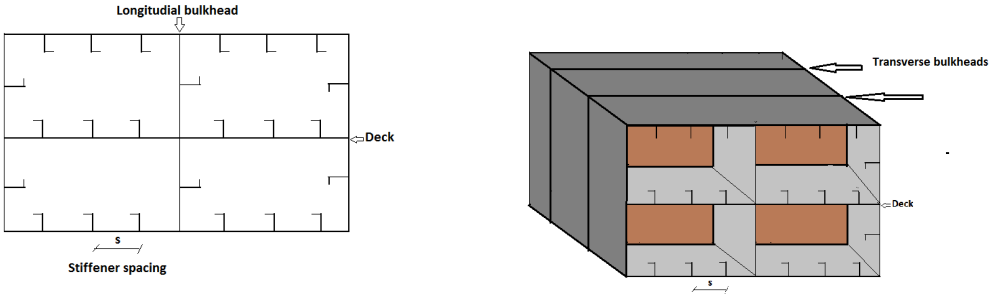

Decks, Lungidutinal and transverse bulkheads.

4.6.2 Stability consideration and ballasting

The stability of the barrier before and after impact is important to make sure the barrier does not capsize. If people are present on the barrier, this could be dangerous. The stability of a vessel is in traditional hydrostatics measured by the metacentric distance

The definition of positive stability is;

$$GM > 0 \tag{4.4}$$

Where the distance GM is defined as

$$GM = KB + BM - KG \tag{4.5}$$

$$BM = \frac{I}{\Delta} \tag{4.6}$$

Where

KG' - Distance from keel to center of gravity

KB' - Distance from keel to center of buoyancy

BM' - Distance from keel to center of gravity

GMG' - Distance from center of gravity to meta center. Stability measurement

Δ - Volume displacement of barrier

I - Second moment of area of water plane of barrier

The distance from keel to the centre of gravity and the centre of buoyancy are measurable. The value BM is a measure of the rotational stiffness ability of the barrier. See figure **??** for an illustration of the different geometrical values of the barrier.

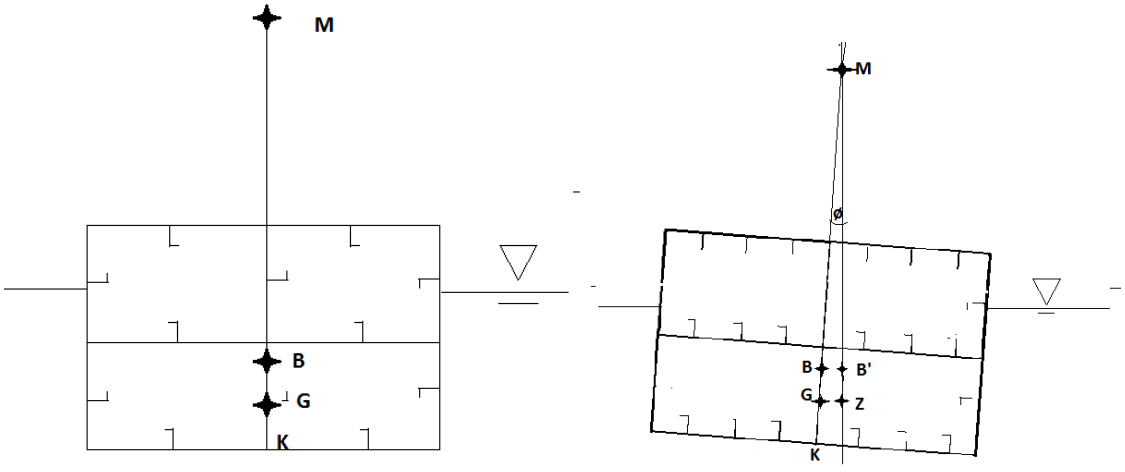

Stability of barrier

Stability after impact is not so easy to determine, however. It is dependent on the geometry of the barrier, which will change. It is possible to predict the shape after impact by using a finite element analysis. After impact, stability analysis could be based on the form after impact. One must consider that the ballast tanks that are deformed might leak the ballast water out, which also will shift the centre of gravity. In all likelihood, the stability will be worsened. It matters on how many sections are deformed. Thus the advantage of having many sections are increased.

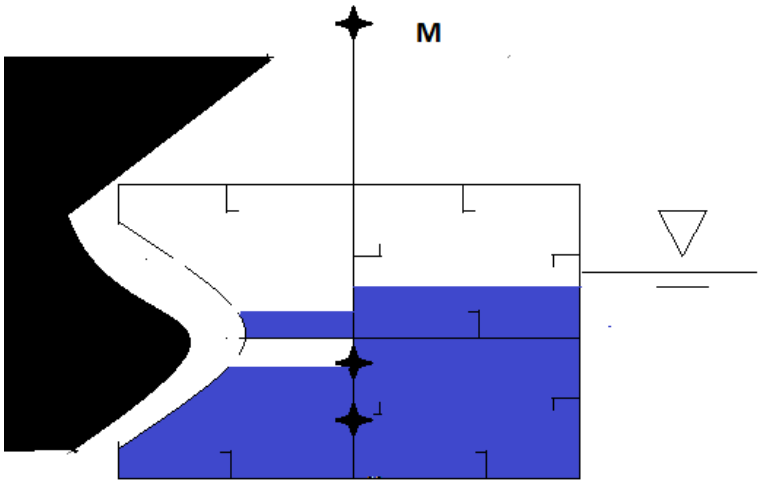

Figure 4.12: Stability after collision [Amdahl, 2005]

Ballast water is a good way to add inertia to the barrier. The barrier could be filled with only air, and be pulled down to its desired draught by cables, but it is beneficial to have a heavy barrier. The barrier could also be filled with stone or sand, but water is the simplest. It is assumed that the water used to fill the barrier is sea water. The required ballast water can be calculated based on simple equilibrium between gravitational forces and buoyancy forces.

$$F_b = F_g \tag{4.7}$$

$$LBdr\rho = m_{barrier} + m_{ballast} \tag{4.8}$$

$$m_{ballast} = LBdr\rho_{sw} - m_{barrier} + \tag{4.9}$$

Where

F_b - Bouncy forces on barrier

F_g - Gravity forces on barrier

L - Length of barrier

B - Width of barrier

dr - Draugth of barrier

rho_sw - density of sea water

$m_{barrier}$ - Self weight of barrier

$m_{barrier}$ -Weight of ballast

The self-weight of the barrier is the sum of the mass of all the decks, all the bulkheads and all the stiffeners. The higher this weight is, the less ballast water is needed to fill the barrier to reach its desired draught.

Ballast should be pumped in from the fjord into barrier trough a watering hole. The watering hole should be placed on the top of the barrier, where leakage is most unlikely to occur. There should be drilled a few holes in the decks for the water to flow to the lower levels of the barrier.

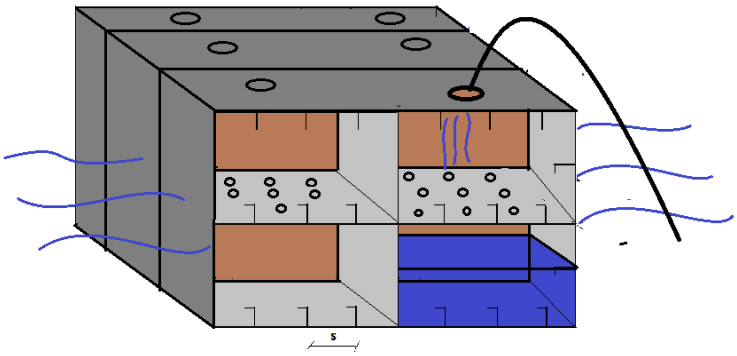

Figure 4.13: Filling ballast tanks

There filling holes does not need to be large, but one for each chamber as shown in figure **??**. The holes that transport water further to the lower levels can be even smaller. They should not be on the vertical plates, to avoid the effect of free surface effect. If water is restrained only to move upwards, the effect of free surface effects will be reduced, as it depends on the area of the free surface.

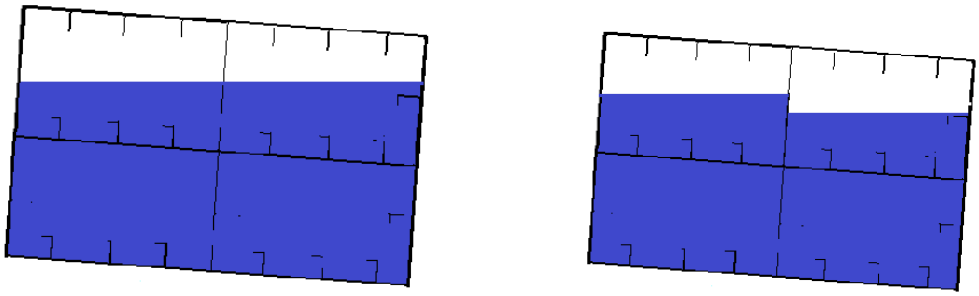

Effect of free liquid surface

The case on the left is where water is allowed to move sideways between each chamber. This is not preferable as the ballast water will make a larger overturning moment compared to if the barrier is divided into more sections. The effect of liquid with the free liquid surface can be written as a reduction in stability.

$$GG'' = \Sigma \frac{\rho'_{ballast} I_{tank}}{\rho_{sw} \Delta} \tag{4.10}$$

Where

GG'' - Bouncy forces on barrier

$\rho_{ballast}$ - Density of water in ballast tanks

$\rho_{ballast}$ - Density of sea water

$\rho_{ballast}$ - Volume displacement of barrier

This effect occurs when ballast tanks are not filled completely. A good design could be to figure out how much ballast water one need, and then design the ballast tanks dimensions from that. It could be possible to seal the holes after they are filled aswell. This would prevent water from moving from tank to tank, and the reduction in stability due to ballast tanks would disappear.

Another reason of why there should be a possibility for water to exit the tanks is that if the water is completely sealed inside the tanks, they will act as pressure on the inside of the tanks, due to the incompressibility ability of water. When the bow of the ship hits the barrier, it will deform. The instance this happens, the pressure inside the tanks will increase dramatically, and it will weaken the structure. Therefore there should be a hole where water can exit if a ship should collide so that the barrier does not fail where it is unexpected.

4.7 Final Design

In this chapter I will present the design of the barrier, what assumptions I have made, and why.

4.7.1 Global Design parameters.

The design of the barrier, on which the finite element model on, has the global design values below.

	Global barrier parameters
Design parameter Property	Value
Length [m]	380
Shape(Cross section)	Rectangular
Configuration (Curved/straigth)	Straight configuration
Breadh [m]	20
Draught [m]	8
Heigth [m]	12
Submerged Displacement [mˆ3]	60800 mˆ3
Mass of Barrier [mˆ3]	62320000 kg

Table 4.2: Global design parameters.

The barrier is modelled as a rectangular shaped straight barrier with a length of 380 meters. The length was specified in the problem description and is the main reason of why the barrier is straight and not curved. The global barrier is illustrated below in figure **??**

The draught was needed to be at least 8 meters to make sure that the bulb of the bow collides with the barrier.

4.7.2 Local Design parameters

A detailed overview of the local design of is in the the table below.

Figure **??** below shows how to cross section looks like.

It was decided to design a barrier with at least ten sections to reduce the effect of the free liquid surface . For local energy absorption, it was decided that at least three decks and four vertical bulkheads were needed. To have an even distance between each bulkhead

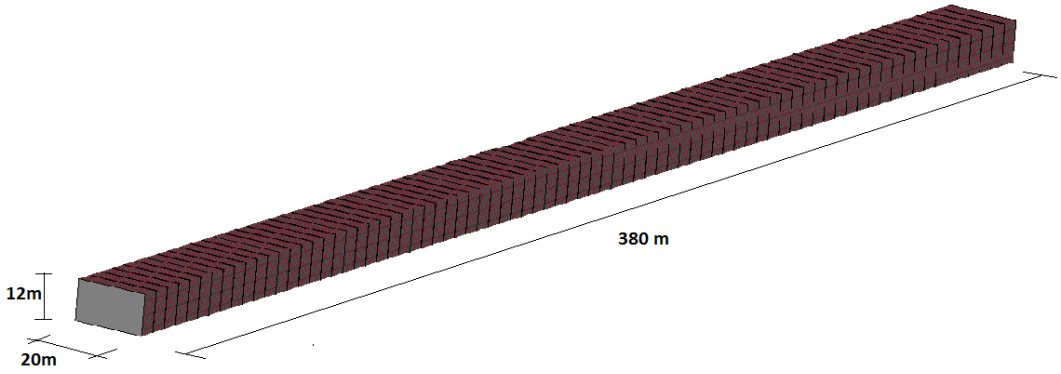

Figure 4.14: Global design of barrier

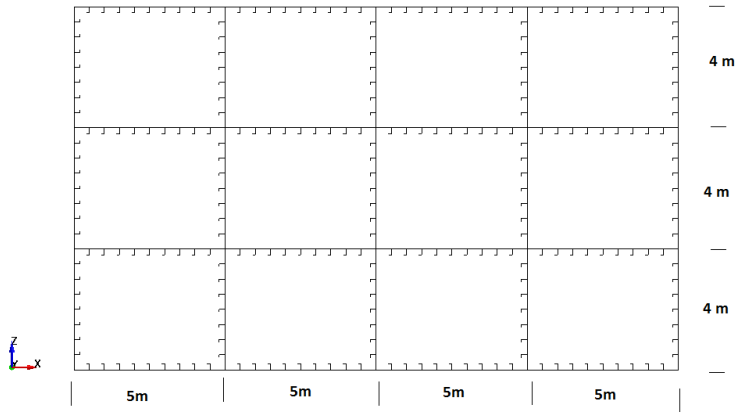

Figure 4.15: Local design of barrier

and deck, it was decided to use a distance of four meters between each deck, and five meters between each vertical bulkhead. This results in a total height of 12 meters and a total breadth of 20 meters. A distance of five meters between each transverse bulkhead was chosen as a preliminary design. The amount of bulkheads, decks and stiffeners are based only on typical stiffener in a ship and other slender floating structures. It is not based on any design standards for a ship or offshore design.

	Local Cross section Design
Design parameter Property	Value
Number of decks	4
Number of vertical bulkheads	5
Number of transverse bulkheads	77
Vertical Spacing between each decks	4m
Horisontal Spacing between each vertical bulkheads	5 m
Spacing between each transverse bulkheads	5 m
Plate thickness [m]	0.015
Stiffener type(Cross section)	L-shaped stiffener
Stiffener Spacing(Both in vertical, horizontal and transverse plate)	500 mm
Web heigth[mm]	200 mm
Web thickness[mm]	12 mm
Flange width[mm]	90 mm
Flange thickness heigth[mm]	15 mm
Weld type assumed	Fillet welds
Cross section area of barrier [mˆ2]	3.0337
Total weight of aluminium in barrier [mˆ2]	3.1126e+06
Moment of inertia z axis [kgmˆ2]	3.0862
Moment of inertia z axis [kgmˆ2]	3.0862
Second moment of area on y axis [kgmˆ2]	3.0862
Second moment of area on y axis [kgmˆ2]	3.0862

Table 4.3: Local design parameters of barrier.

4.7.3 Material in Barrier

The barrier is made in aluminium. Table **??** gives the design values of the material used in the finite element analysis . The values are collected from Eurocode 9, and the ultimate strain value is calculated based on formula E.19 in Eurocode 9. As mentioned, this failure criterion is questionable, but in discussion with supervisor Professor Amdahl, it was desided it was sufficient enough for this analysis.

4.7.4 Ballast consideration

In order to reach a depth of 8 meters, ballast water is required. The amount of ballast water and other ballast requirements are gathered in table below

This means that the ballast tanks are almost completely filled up, which is very good, when considering stability requirements.

	Material design values		
Physical Property	5083 O	5083 H12	6082 T6
Density	2700 kg/mˆ3	2700 kg/mˆ3	2700 kg/mˆ3
Youngs modulus	70000 GPa	70000 GPa	70000 GPa
Poisson's ratio	0.344	0.344	0.344
Ultimate strength in HAZ $[N/mm^{-2}]$	275	275	185
Yield strength in base material $[N/mm^{-2}]$	125	250	260
Ultimate strength in base material $[N/mm^{-2}]$	275	305	310
Yield strength in HAZ $[N/mm^{-2}]$	125	155	125
Ultimate strength in HAZ $[N/mm^{-2}]$	275	275	185
Ultimate strain in base material []	275	275	185

Table 4.4: Material design values

	Material design values
Physical Property	5083 O
Assumed ballast liquid	Sea water
Required ballast mass	5.9207e+07 kg
Required volume sea water	5.7763e+04 mˆ3
Depth of ballast water inside barrier	7.6004 m

Table 4.5: Ballasting design values

Chapter 5

Finite element analysis in LS DYNA3D

In this chapter, the modelling done in LS DYNA3D is discussed. LS-DYNA is a general purpose finite element analysis program. It is very suitable to use in complex non-linear dynamic problems such as collisions. The analysis of collision on the barrier is very time demanding and complex, involving a total of over 1.5 million elements. Thus it was necessary to use one of the supercomputers at NTNU, called Vilje.

The modelling is done in two parts. The first part regards an analysis of a stiffened plate. The first analysis was to model heat affected zone with its properties in a plate. The second part is a collision analysis of a bow model and a barrier model. The bow model already developed from before was given to the author of this thesis upon starting the analysis. The barrier model is made by using the design provided in chapter 4.

5.1 Modelling of stiffened panel

Two load conditions are applied to the stiffened panel. The first load condition is lateral loading using a colliding rigid sphere. The other load condition is by axial crushing. Those two load conditions are of interest since when the bow strikes the barrier, the outer plates will be loaded laterally, while the plates in the bulkheads will deform axially.

5.1.1 Geometry of panel

Table ?? gives information on the geometry of the plate and the stiffeners used in the stiffened panel.

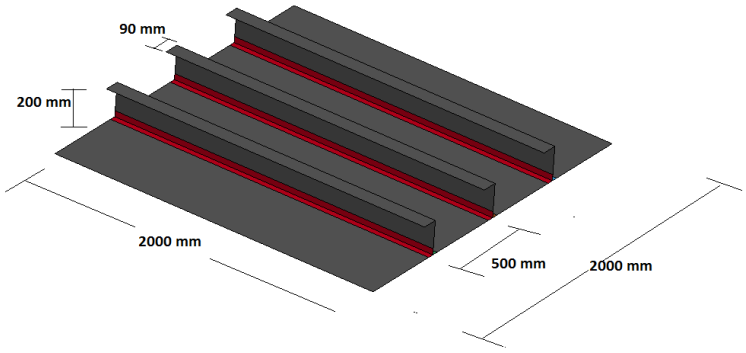

Figure 5.1: Stiffened panel

Geometry of stiffened panel				
Part	Length	Width	Height	Thickness
Plate	2000 mm	2000 mm	-	15 mm
Wedge	2000 mm	2000 mm	-	15 mm
Flange	2000 mm	2000 mm	-	15 mm

Table 5.1: Modelling of stiffened panel

The stiffened panel is modelled as a square plate with stiffeners going across one length. The stiffener spacing and dimensions are the same as in the barrier model. The stiffeners are L-shaped.

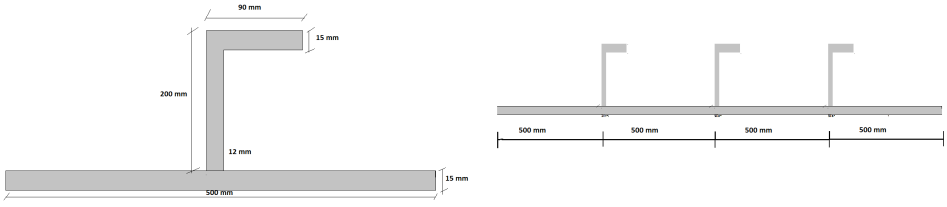

Stiffener in plate dimensions

5.1.2 Boundary conditions of panel

When the loading is lateral,the boundary conditions along all the edges of the plate is fully restrained. This simplification is not truly best describing how a plate in the

barrier will react when the ship strikes, but the main purpose of this analysis is to analyse the effect of heat affected zone when considering energy absorption , it is not very important how the panel is constrained. However, a correct boundary condition would perhaps be if the panel was free to translate in the plate plane. Figure **??** displays the boundary conditions

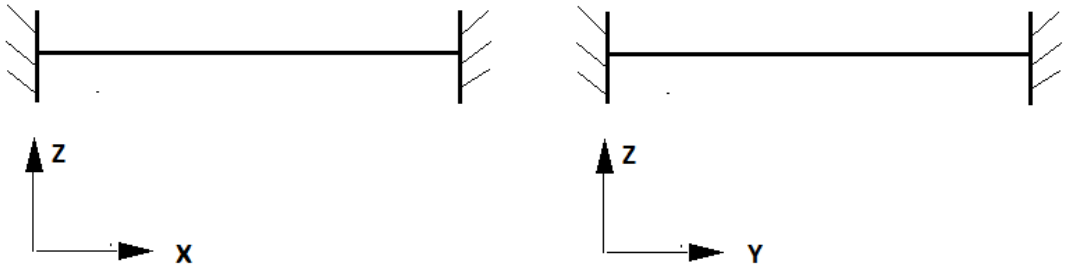

Figure 5.2: Boundary conditions in plate, seen from front side and left side

When the loading is axial,the panel is fully constrained at the edge opposite to the edge which is exposed to the loading. The edges parallel to the loading direction are allowed to translate in that direction. Otherwise, they are fully constrained.

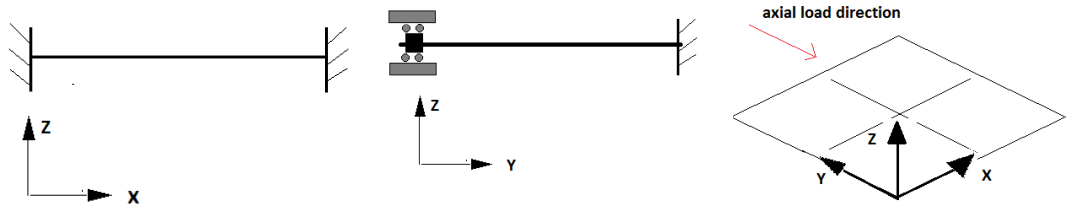

figureBoundary conditions in panel, when axial crushing.

5.1.3 Modelling of heat affected zones

Four models are made of the stiffened panel. Two panels with heat affected zones and two without. Of the models with HAZ, one panel has alloy 5083 O in plate and the other model has alloy 5083 H12 in the plate. Both are made with alloy 6082 T6 in the stiffeners.

The geometry of heat affected zone is displayed below. As prescribed by Eurocode 9, the extent of heat affected zone was 35 mm in all directions from the weld centre.

It is assumed that the reduction in the heat affected zone is constant across the extent of HAZ, as well as constant trough the plate thickness. The red zones in the figure

Model panels			
Panel nr	HAZ	Alloy in plate	Alloy in stiffeners
Panel 1	No	5083 H12	6082 T6
Panel 2	No	5083 O	6082 T6
Panel 3	Yes	5083 H12	6082 T6
Panel 4	Yes	5083 O	6082 T6

Table 5.2: HAZ in the different panel cases.

HAZ in stiffened panel			
HAZ in panel	extent of haz(b˙haz)	Depth of haz (across thickness)	
HAZ in Plate 15 mm	35 mm	35 mm	-
HAZ in Stiffeners 12 mm	35	35 mm	-

Table 5.3: Extent of HAZ in plate and stiffener.

below show how the heat affected zone is modelled as a rectangular area from the weld centre.

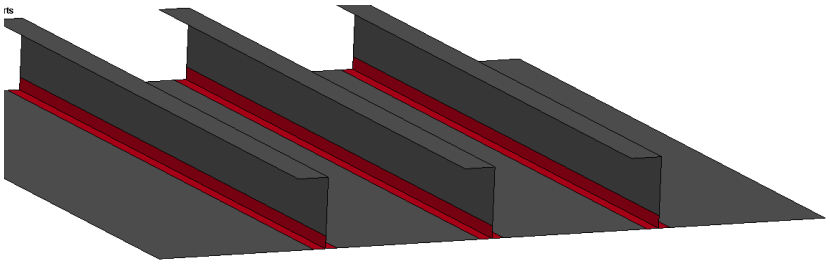

Figure 5.3: Heat affected zone in panel

5.1.4 Plate element model

In addition to the stiffened plate, a plate element model was analysed with lateral loading. The plate element model was just taken as a part of the stiffened plate between two stiffeners. This means a plate of 2000mm length and 500mm width, with the same thickness as the stiffened plate, and also with fully clamped ends at all edges. Figure **??** below shows how it was modelled with HAZ along the longer edges.

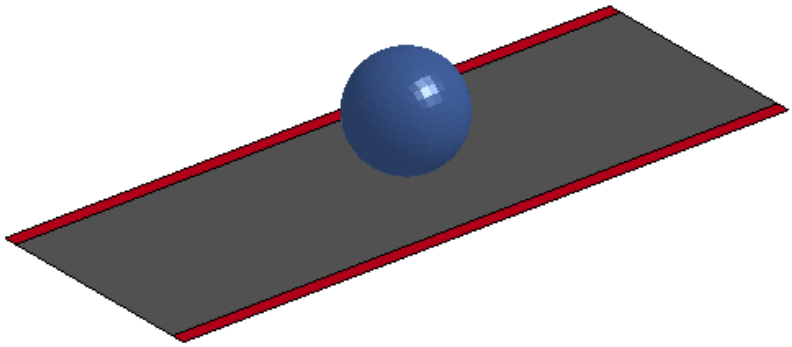

Figure 5.4: Plate element model [Amdahl, 2005]

This smaller modelled was subjected to loadings in a similar fashion as the stiffened plate, but with a smaller sphere. It was desired to use a sphere that did not have a direct contact on the welds. This was to see if transverse stress or contact forces was the main reason for failure.

5.1.5 Material modelling in panel

As mentioned, the Ramberg-Osgood model is used to describe material behaviour for the elements in the FEM analysis. As also mentioned, the way of describing the Ramberg-Osgood model is by a 8 point piecewise linear plasticity model. The stress and strain must be converted to true stress and strain to be correct description for use in LSDYNA. Figure **??** compares the Ramberg-Osgood representation for the three alloys, with corresponding curves for the heat affected zone.

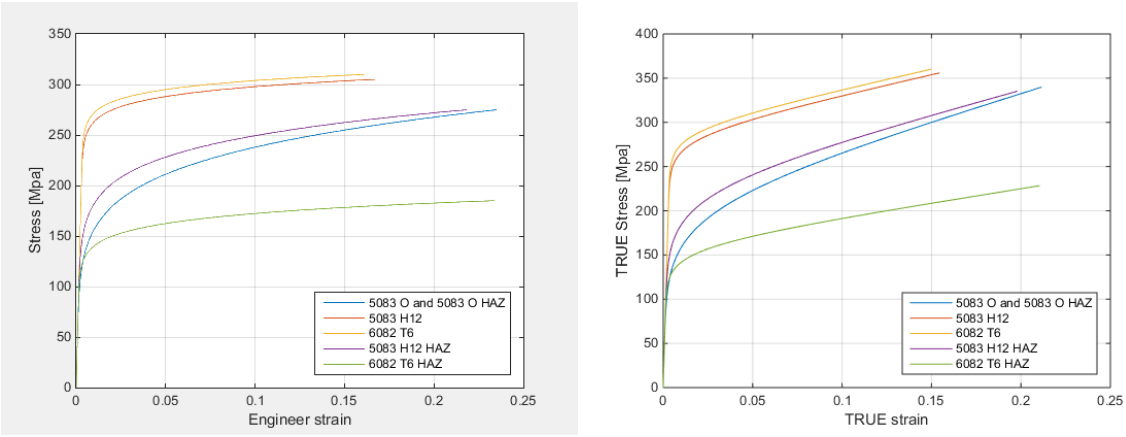

Stress-strain curves for the alloys. Left: engineering stress and strains, right: True stress and strains

As one can see, the material which describes the heat affected zone has a higher ultimate strain compared to the base material. This is because of the failure criteria discussed earlier.

The figure **??** below shows how the approximation curves fit the Ramberg-Osgood curves.

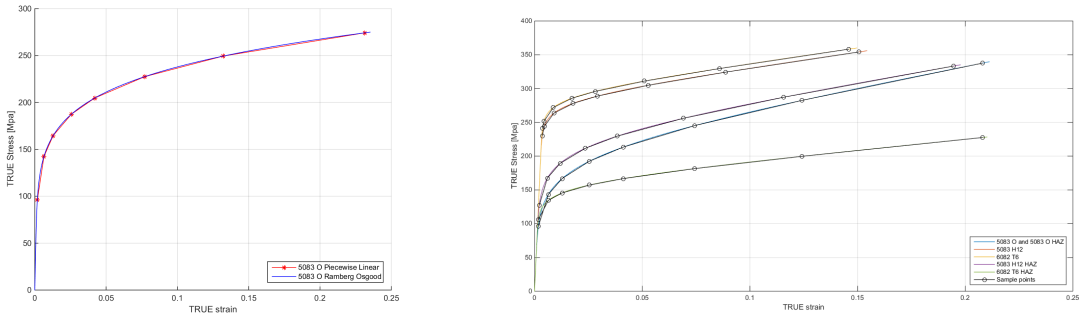

Curve fits by using piecewise linear plastic model.

A complete table showing the fracture strain and all Ramberg-Osgood parameters is shown in table **??** below

	Ramberg Osgood-Parameters			
	Yield Stress	Ultimate Stress	Ultimate Strain	Hardening Parameter
5083 O Base	125MPa	275MPa	0.2312	6.0249
5083 H12 Base	250MPa	305MPa	0.1625	22.1147
6082 T6 Base	260 MPa	310MPa	0.1570	24.8057
5083 O HAZ	125MPa	275MPa	0.2312	6.0249
5083 H12 HAZ	155 MPa	275MPa	0.2148	8.1562
6082 T6 HAZ	125 MPa	185 MPa	0.2312	12.1169

Table 5.4: Ramberg Osgood parameters for the different alloys

The stress-strain curve for alloy 5083 O has no difference between base material and heat affected zone. Alloy 5083 O is heat treated such that it has the lowest possible strength, and thus has no reduction in strength in heat affected zones. Welding causes no more reduction in strength since the material has the minimum strength, to begin with. It can be seen that alloy 6082 T6 has quite a significant reduction in HAZ. The ultimate stress is lower in HAZ compared to yield stress in the base material. The ultimate elongation is about 53 percent larger.

With the piecewise linear plasticity model, the user can prescribe 8 points to describe a stress -strain curve for a material component. The first point is the yield stress ,

with corresponding yield strain. The last point is the failure strain with corresponding stress. Figure **??** below shows how each of the alloys stress-strains is modelled and implemented into LS-DYNA.

5.1.6 Two load cases

As mentioned the panel is subjected to lateral and axial loads. These loads are modelled in LS-DYNA as a rigid sphere crashing into the plate on the flat side, and a rigid plate crashing into the plate on the left side. The former causing lateral deformation, the latter causing axial deformation. Figure **??** and **??** shows how the sphere and plate crush into the stiffened plate

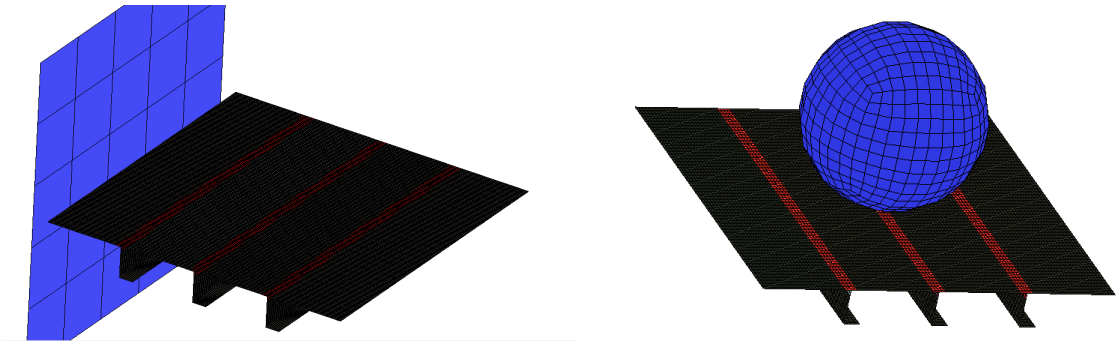

Load cases. Left: axial deformation. Right: Lateral deformation.

The plate element model is also subjected to lateral loading by a smaller sphere, it can be seen in figure **??**

The sphere and plate move in constant velocity, until the plate is pierced completely in the lateral loading case, or buckled completely in the axial loading case.

The panel is fully constrained as mentioned, at all outer edges, when subjected to lateral loading. When the plate is crushed axially, it can move in the axial direction, in the longitudinal direction(same direction as the motion of the moving plate), but is not able to move out of the plate plane.

5.1.7 Mesh and Elements

Trough discussion with supervisor Professor Amdahl we decided to use a mesh that would have four elements along the extent of the HAZ. The mesh of the plate is decided

based on how many was needed to describe what happened in the HAZ, in a satisfying way. A convergence test should have been applied to verify, but it was not enough time to do this. The elements are shell elements, of the Belytschko-Lin-Tsayformulation.

	Mesh size and Element amount		
	Coarse Mesh	Medium Mesh	Fine Mesh
Number of Elements along extent of HAZ	1	2	4
Element size	35mm*35.1mm	17.5mm*17.5mm	8.75mm*8.75mm
Total number of elements in stiffened plate	4824	19296	77184

Table 5.5: Mesh size parameters

Belytschko-Lin-Tsay elements

The elements used in the plate are four node quadrilateral Belytschko-Lin-Tsay elements with five integration points along the thickness. The kinematic relation of the element comes from a combined formulation. It is combined on a Co-rotational and a velocity strain formulation. The Belytchenko -Tsay elements are usually preferred because they are computational effective, compared to other element formulations such as the Hughes-Liu shell elements. The elements are based on Mindlin plate theory and use it to calculate the velocity at any point in the elements and the co-rotational formulation to find corresponding velocity strain. The elements use a penalty parameter to enforce Kirchoff normality condition when the shells are thin. The elements, which use one point quadrature in the plane of the elements, adds hourglass viscosity stresses to suppress hourglass deformation modes that accompany one-point quadrature form [**?**]. This makes the elements quite computational effective, please see [**?**] for more information.

5.2 Barrier modelling

The modelling of the barrier is done in two parts. A local model that will describe local damage from the bow, and a global model that will describe the response of the barrier in a global sense. The reason behind dividing the barrier by two models, one very detailed and one not so detailed is because the computational time for having a complete detailed barrier would be too long.

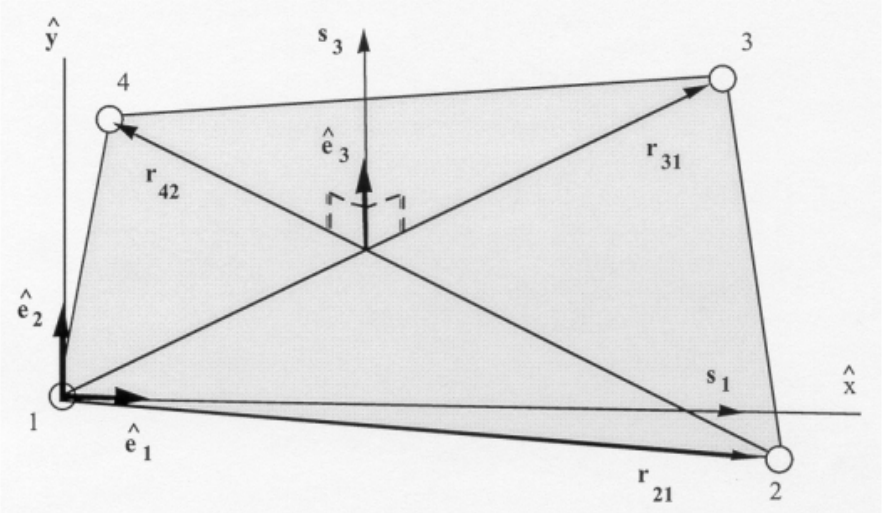

Figure 5.5: Belytchenko -Tsay Elements [Hallquist et al., 2006]

5.2.1 Local model

Main body

This model is based on the design of the barrier in chapter 4 . The longitudinal distance between each transverse bulkheads is five meters, **??**. The vertical distance between each deck is four meters and the horizontal distance between each vertical bulkhead is also five meters. The model is built by six sections of five-meter length, that are connected in between each bulkhead to build the main body of the model **??**

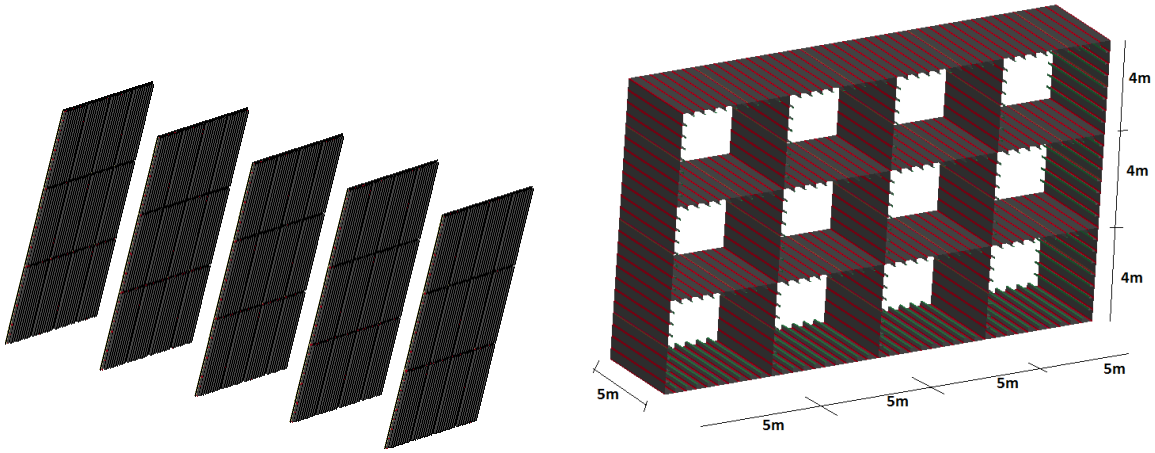

figureTransverse bulkheads(left); sections(right)

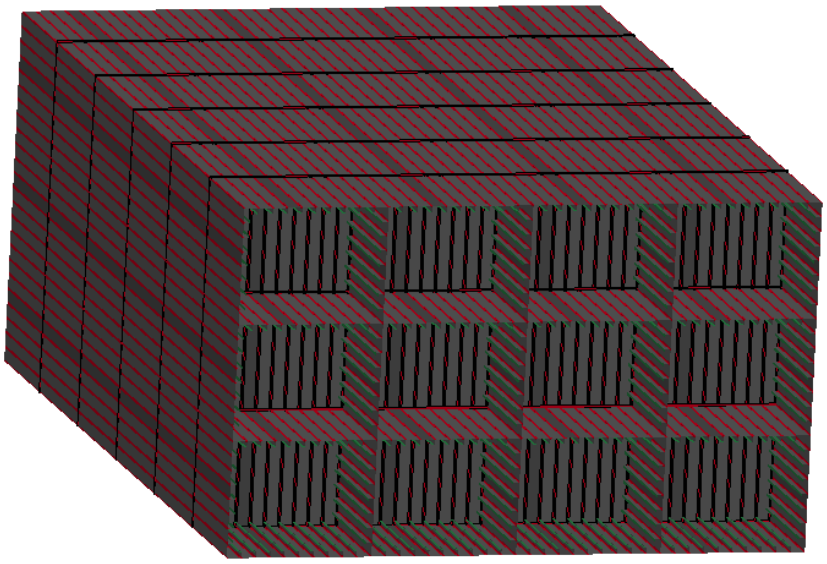

Figure 5.6: Built local model [Amdahl, 2005]

Connection points

The local section is then connected to a rigid plate at both ends. This rigid plate is the connection to the global model. The connection plate is rigid, to avoid deformation across the border between local and global model. This rigid plate caused some errors in the first attempts of analysing the collision. Because of the rigid plate, the local model started to fracture very early at the boundary to the rigid plate , see fig **??**

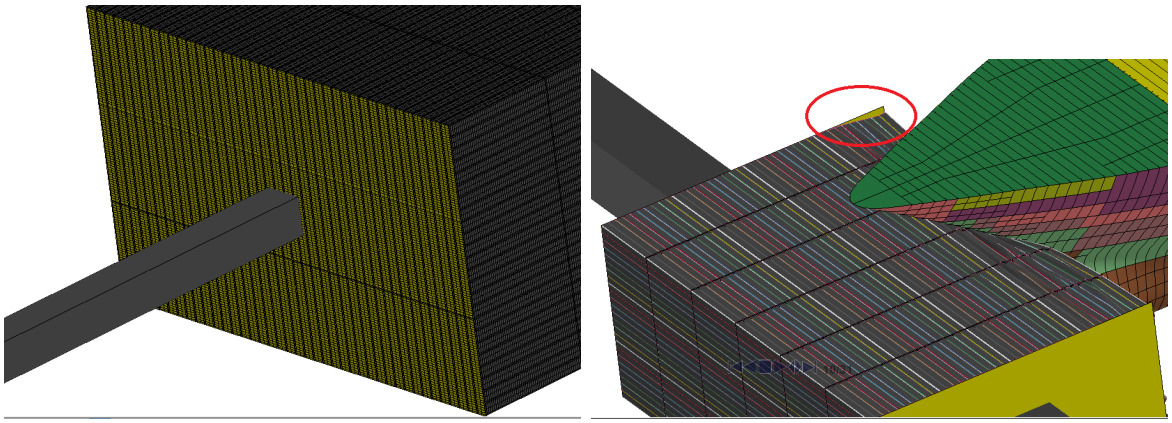

figureRigid plate, yellow colour. (left); Rupture at boundary between rigid plate and local barrier.

To fix this, there was made a modification of the model. This modification was to make

the material at the ends of the barrier more ductile to prevent early rupture near to the rigid plate and to instead try to capture the rupture at the centre of the model. The modification is described in the table below. Trough discussion with supervisor Jørgen Amdahl , it was advised to use a strain failure of 6. The length of this zone is 450 mm from the rigid plate, see figure. The new stress-strain curve for this zone is plotted in figure **??**. The stress value corresponding to the extended strain failure is not changed from the origional strain failure.

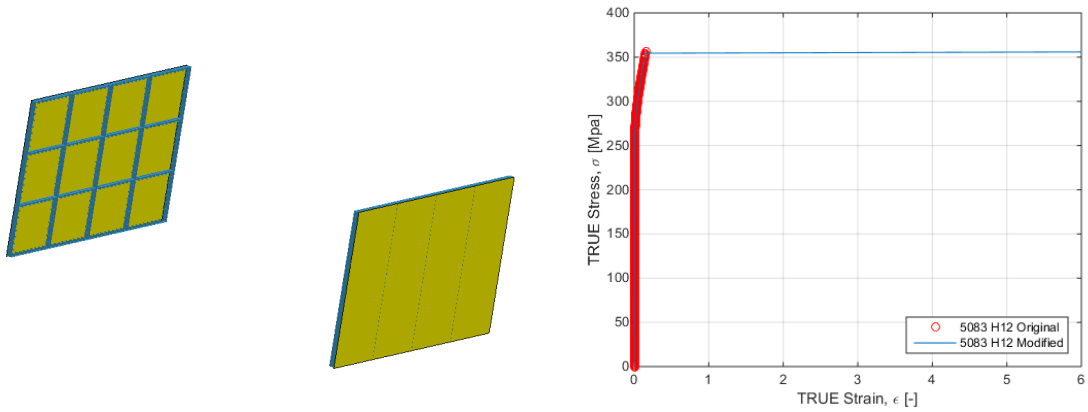

figureSection with extended ultimate strain(left); Material curve; original stress-strain vs updated stress strain curve. (right)

With this modification, it was hoped to avoid early fracture along the rigid plate, although it is a very bold simplification to give material along the edges this high ductility.

Material in local model

The material used in the main body for the local model is the same as for the stiffened panel explained above, using the Ramberg-Osgood law. The rigid plate has a rigid material type, which means that it does not deform whatsoever. Table **??** below summarise the material for the local model.

	Mesh size and Element amount		
	Main body	Ductile end zones	Rigid plate at end
Material model	piecewise linear plastic	modified piecewise linear plastic	rigid material

Table 5.6: Material model in local model

HAZ modelling in local model

There is modelled a heat affected zone in all welds in the local model. This means the welds between all stiffeners in decks and bulkheads and between all plates. The extent of the HAZ is increased in the local barrier model compared to the stiffened panel. Since the thickness of the plate is 15 mm for the barrier, the extent of heat affected zone should be 35 mm, but it is increased to 50 mm. This was done in order to reduce the computational time. This simplification is assumed to be conservative since the reduction in strength is increased over a larger zone than actually is true. The elements used in the local model is the Belytschko-Lin-Tsayelements. Fgure **??** below shows how the heat affected zone is modelled in all welds, (between stiffener and plate and between bulkheads and decks so on).

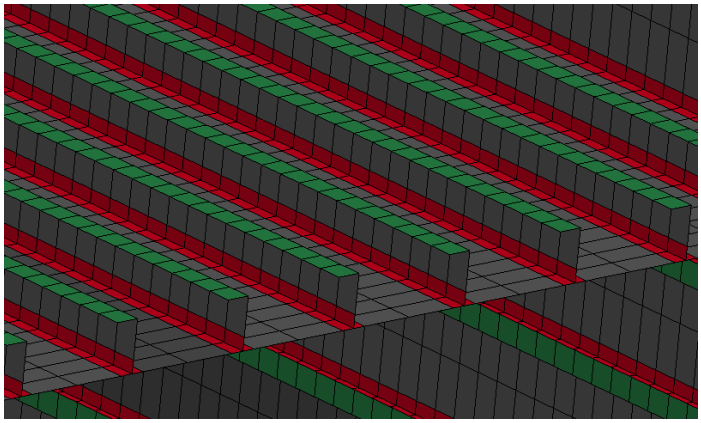

HAZ in local model.

5.2.2 Barrier modelled as beam

The barrier is modelled using beam elements elsewhere than the impact area.Using beam elements is very computational cheap, and this was the main motivation to why it was decided to use beam elements.

Since bending deformation is of highest interest, due to the colliding ship from the side, the bending stiffness of the beam elements had to be the same as the local cross section. The beam elements are of Belytschko-Schwer formulation. This is the default option in LS DYNA3D. The cross section is a hollow square beam.

Figure below shows how the cross-section parameters are given in LS-DYNA and a conceptional drawing of the global cross section of the barrier

	Global barrier parameters
Design parameter Property	Value
Length [m]	380
Shape(Cross section)	Hollow rectangular
Configuration (Curved/straigth)	Straight configuration
External Width [m]	20
Internal Width [m]	19.9480
External Heigth [m]	12
Internal Heigth [m]	11.8800
Second moment of area strong axis I˙zz [mˆ4]	141.7011
Cross sectional area [mˆ4]	3.01776

Table 5.7: Global model parameters

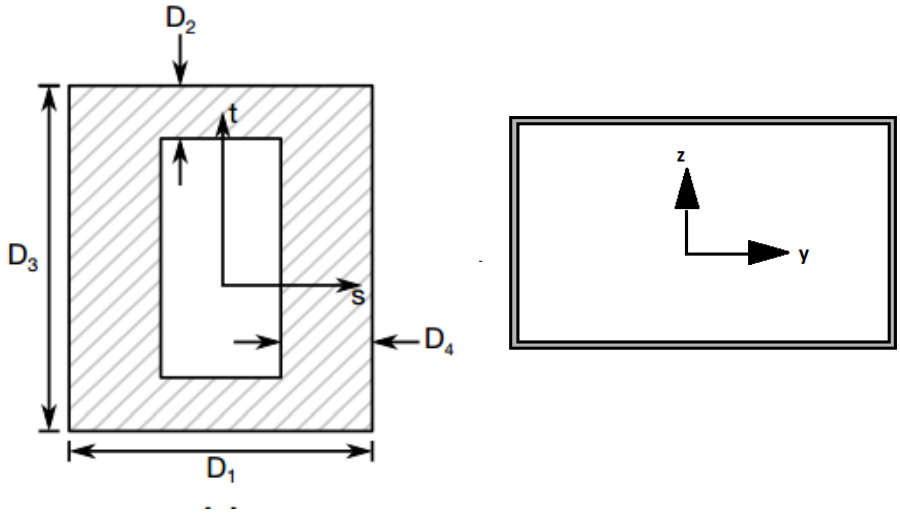

Conceptional drawing of cross section of beam elements. Left, hollow cross section in LS DYNA[Hallquist et al., 2006]. Rigth : Cross section of beam elements in barrier.

Iteration finds the thickness of the hollow rectangular tube until the moment of inertia on the strong axis and the cross-sectional area is the same as in the local model.

5.2.3 Inertia forces: Ballast and added mass

Added mass forces acting on the barrier is modelled by increasing the density of the material in the global beam model. The total inertia force acting on the model can be calculated as

$$F_{inertia} = m_t ota_{barrier} \tag{5.1}$$

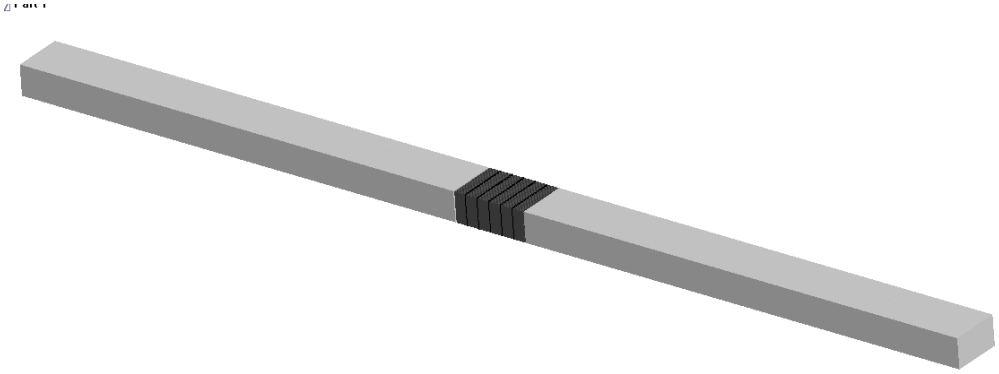

Figure 5.7: Global model of barrier, with local model in the centre.

And

$$m_{tot} = LBd\rho_{sw} * (1 + C_a) \tag{5.2}$$

The resulting density of the material to be used in the modelling is

$$\rho_tot = \frac{m_{tot}}{V_{barrier}} \tag{5.3}$$

Where

F_b - Bouncy forces on barrier

F_g - Gravity forces on barrier

L - Length of barrier

B - Width of barrier

dr - Draugth of barrier

rho_sw - density of sea water

$m_{barrier}$ - Self weight of barrier

$m_{barrier}$ -Weight of ballast

This approach by scaling the density up to account for the mass of ballast water and inertia forces is a very simplified approach. In reality, the ballast water will slosh around in the tanks, and the added mass will act as pressure on the side of the barrier. When increasing the density, it will take about the same amount of force to accelerate the barrier, which is of most importance. The coefficient of added mass is dependent on the shape of the barrier and the frequency of oscillation. Trough discussion with supervisor Amdahl, it was decided to model the added mass as 80 percent of the weigth of submerged volume displacement of the barrier.

5.2.4 Drag and mooring forces

Drag forces acting on the barrier will most likely be small. The barrier has a large mass compared to the ship, and the velocity of the barrier will most likely be small after impact. This will result in a small drag force acting on the barrier, compared to inertia forces. Thus they where negelected in the analysis. It would be possible to model the drag forces based on a typical drag force equation:

$$F_{drag} = \frac{1}{2} C_D \rho A v(x)^2 \tag{5.4}$$

Where

F_b - Bouncy forces on barrier

F_g - Gravity forces on barrier

L - Length of barrier

B - Width of barrier

dr - Draugth of barrier

$rho_s w$ - density of sea water

$m_{barrier}$ - Self weight of barrier

$m_{barrier}$ -Weight of ballast

Since the barrier is clamped at the ends, the velocity will not be constant along the length of the barrier. The barrier will form a mode shape, and the velocity will vary along the length. This should be accounted for if the drag force should be implemented in the analysis.

Mooring forces would be possible to model in LS-Dyna by assuming a non-linear relation between restoring force acting on the barrier, and the displacement of the barrier from its initial position. By using catenary equations, found in [Faltinsen, 1993], one can find this relation. It is typical that the mooring force gives a small force at the beginning, and then increase rapidly as the displacement gets large **??**. Due to time limitations, this was not included.

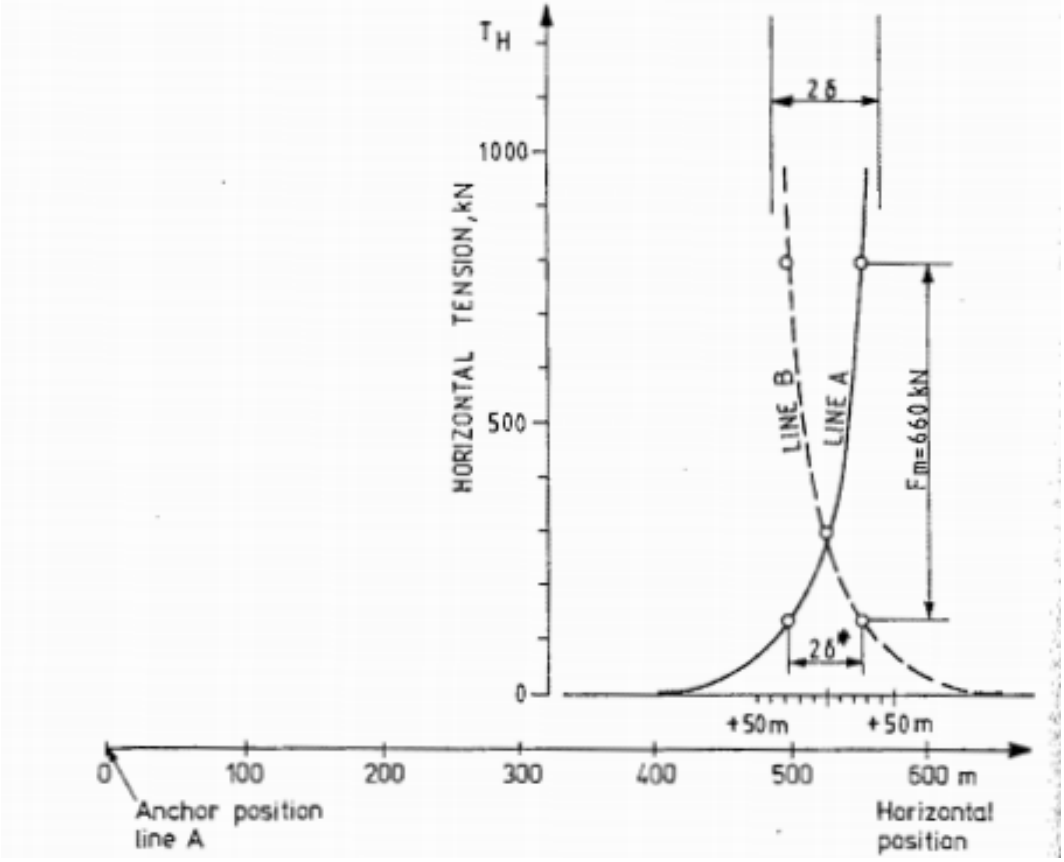

Mooring characteristics [Faltinsen, 1993]

5.2.5 Ship modelling

The ship model used in the analysis was given to me upon starting the thesis . ørjan Konstali developed the analysis in 2014, see [øK]. I will briefly discuss its material and geometrical modelling properties. The bow model is shown below in figure **??**

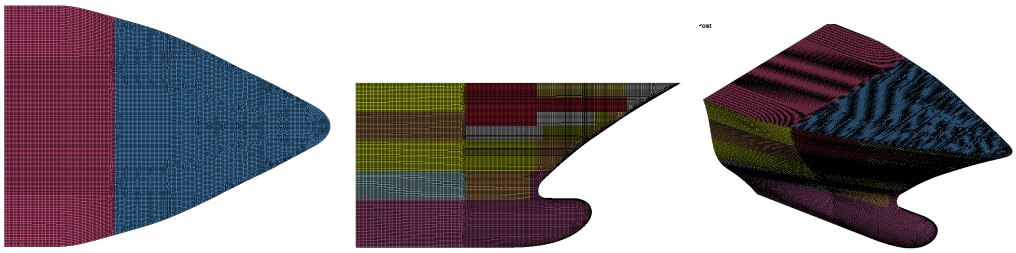

View of ship model. Top, left and panorama

The bow model is based on a cruise ship called MS Balmoral [øK]. Ship parameters are given below.

	Ship model parameters
Design parameter Property	Value
Length Ship	195 m
Breadth Ship	25 m
Displacement Ship	11000
Gross tonnage	24000
Moving Velocity of Ship	17 knots
Draught of Ship	5.5 m

Table 5.8: Design values for model of bow

The bow model is not including the entire ship, only the front part. It includes the collision bulkhead, which is of importance when considering the stability of the ship. The model is elsewhere modelled on the geometry of MS Balmoral [øK].

Further, the material modelling in the bow model is based on failure criteria developed by [**?**]. This is implemented by using a user defined material in USFOS. The material model is developed at the Department of Marine technology, at NTNU by [**?**]. Please see [**?**] and [**?**]

5.2.6 Collision analysis

The collision analysis is preformed by moving the bow model with a constant velocity, trough the barrier, in the local model. The collision is centric. The analysis is of a shared energy design, meaning both the model of the barrier and the model of the bow is allowed to deform. This is very time-demanding, and in hindsight, I believe the analysis should be carried out somewhat differently, which I discuss in chapter 8.

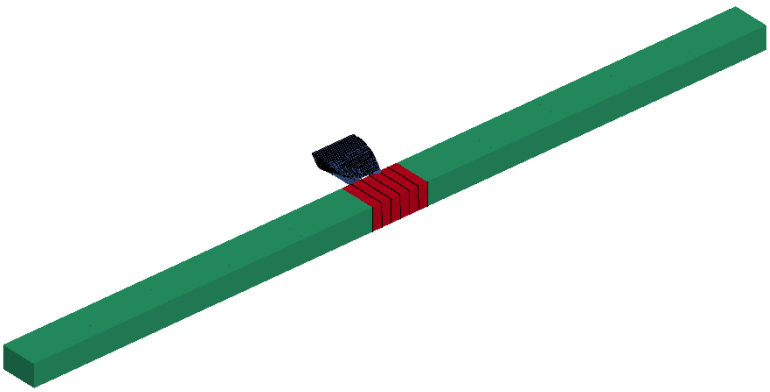

Collision between bow and barrier

Chapter 6

Modelling in USFOS

In this chapter, I will describe the modelling done in USFOS GUI. A beam element model of the artificial seabed, floating bridge and submerged floating tunnel was developed. .

The model is made in USFOS, a computer program for nonlinear static and dynamic analysis of frame structures. USFOS is a cost effective simulation program that describes collapse mechanisms well.

6.1 Overview of model

The crossing concept consists of five main parts. Namely, artificial seabed, pontoons, two floating bridges, a floating tunnel and collision barrier. The model parts are shown in the figures below

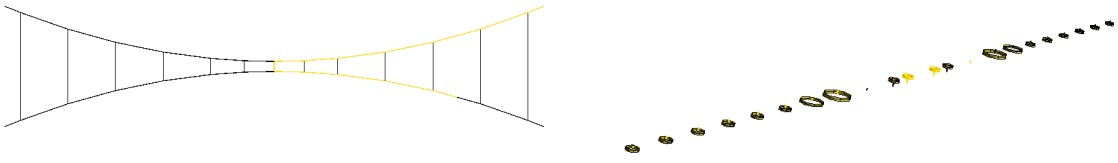

Model of bridge concept: left: artificial seabed. Right : pontoons

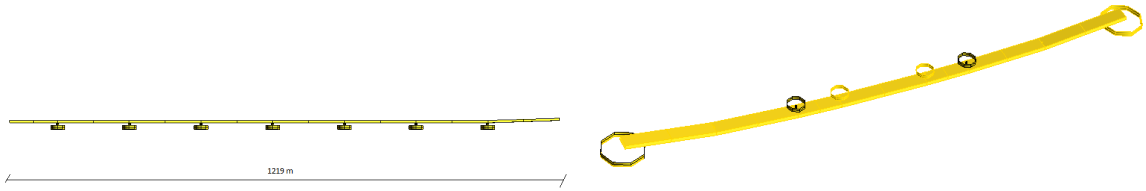

Model of bridge concept: left: floating bridge. Right : submerged tunnel

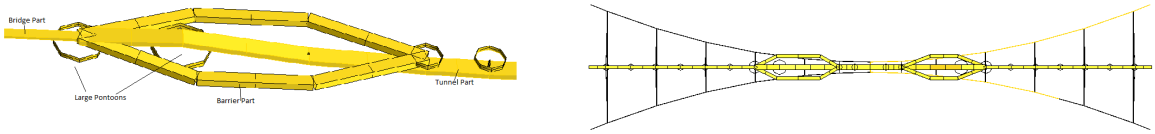

Model of bridge concept: left: Collision barrier . Right : Overview

The upper left figure illustrates the artificial seabed, consisting of main pipes and cross beams. The upper right illustrates all the pontoons that are used to support the floating bridge and submerged tunnel. The middle pictures illustrate the floating bridge(left) and the submerged tunnel(right). The lower two figures display the total collision barrier and the total model. These parts will now be described all in detail. And lastly, I will describe the analysis that was to be preformed.

6.2 Geometry of model

6.2.1 Artificial seabed

The artificial seabed is defined by two pipes crossing the fjord, as seen in figure 4.3.1 The main pipes are connected to the land side by drilling into the mountain, and pulling the end of the pipes into a chamber, supporting with wires and a chamber. The main pipes are then pulled together by cross beams, making it stable by the tension resulting in the main pipes. This will make the crossing concept stable in the fjord. There are 13 cross beams in total.

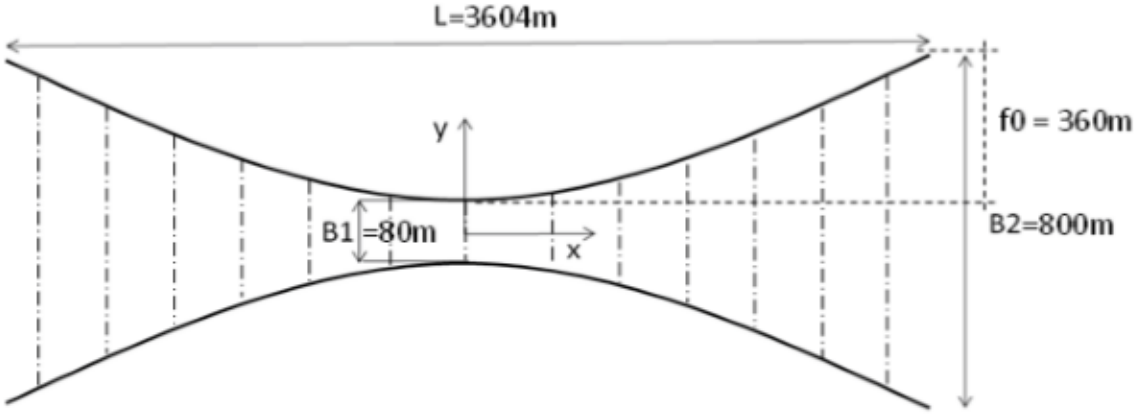

Model of bridge concept: artificial seabed1

Upon starting the work on the thesis, I was provided with data on coordinates of the connection points between main pipes, and the 13 cross beams, hereby referred to as nodes. The coordinates were the position of all the nodes, before and after pre tension is applied. The coordinates are given below in table **??**

	Coordinates of nodes between crossbeam and main pipes			
Node ID	X [m]	Y [m]	Y [m]	$\delta Y[m]$
1,9	0.000	40.000	33.279	6.722
2,10	200.000	44.444	37.806	6.639
3,11	424.000	59.975	53.627	6.349
4,12	742.000	101.174	95.594	5.579
5,13	1060.000	164.844	160.454	4.391
6,14	1378.000	250.987	248.205	2.782
7,15	1696.000	359.602	358.848	0.754
8,16	1802.000	400.800	400.815	-0.015

Table 6.1: Coordinates of sea bed before and after pre tension

The table only shows the coordinates for the left-hand side of the seabed. Since the seabed is symmetrical, the coordinates on the right-hand side are the same, just with opposing values.

In USFOS, the coordinates that were chosen was the X-positions, and the new Y positions, meaning the coordinates after the pipes are pulled together by the cross beams. Later discussed, USFOS has a function suitable to add tension in a structure suitable for this model. The node numbering is shown below in figure **??**

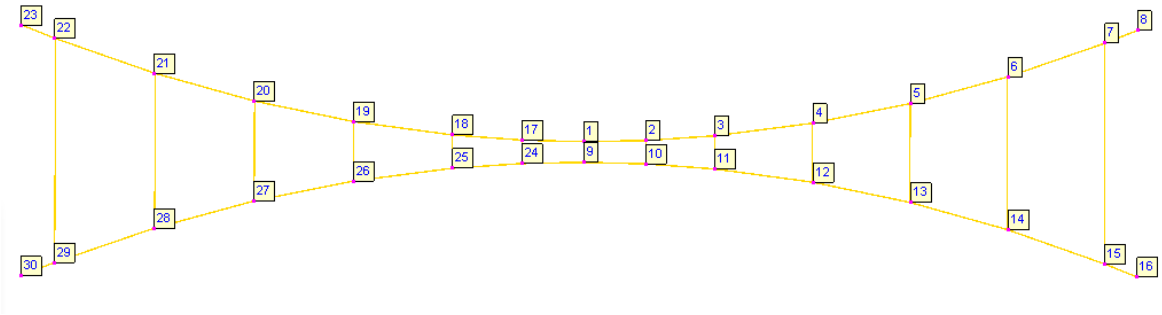

Model of bridge concept: artificial seabed 2

The floating bridge is connected to the seabed by anchor lines. This is to relieve the bridge from having just a single moments at the end sides of the bridge. By having mooring lines across the floating bridge, the ending moment at the end of the bridge does not need to be as large as it would be if there were no anchor lines.

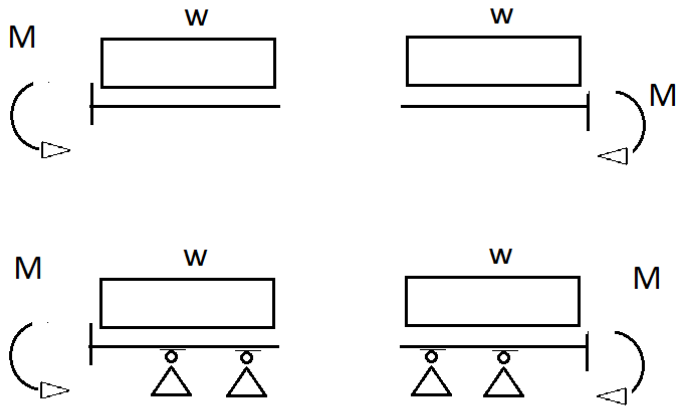

Model of bridge concept: Help from mooring lines

The anchor lines are modelled as non-linear spring forces in USFOS. Mooring lines work with a non-linear restoring force on a moored structure. The values of the mooring force-deformation relation is based on supervisor professor Amdahls suggestion of a total of 1000 N/m. There will act a force on the bridge and seabed where the anchor lines are attached, and the force will follow the force-deformation pattern in figure 4.3.2

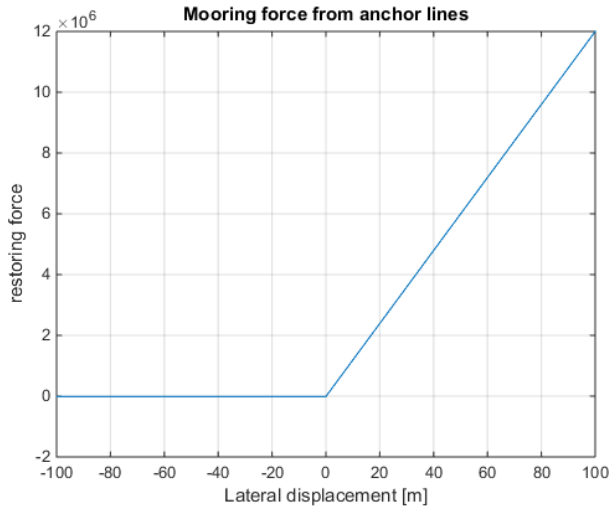

Mooring lines characteristic

As can be seen, the non-linear spring works in tension, but not in compression. It is assumed that the anchor lines work as traditional anchor lines and they will restore only in tension. The pipes and crossbeams are made of beam elements in USFOS. The elements are of pipe types, meaning circular cross sections with a specified thickness and diameter. There is only one beam between each node.

The cross section of the beams, used in the seabed and anchor lines is gathered below.

Coordinates of nodes between crossbeam and main pipes

Part name	Pipe Diameter [m]	Pipe thickness [m]
Main Pipes	1.5592	0.1057
Cross Beams	0.640	0.0308

Table 6.2: Cross sectional properties of sea bed.

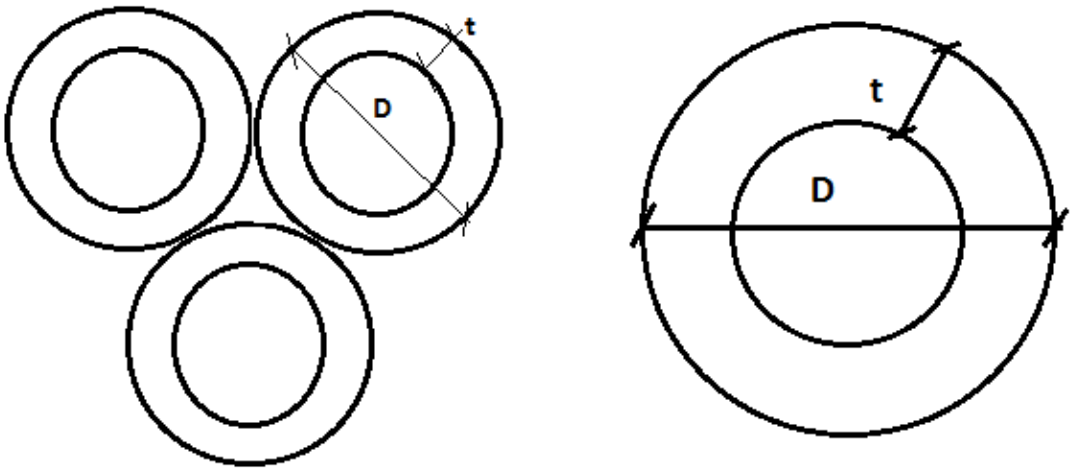

Crosss section of pipeline: Pipes in bundle or single pipe

The cross section of the main pipes was not specified by Reinertsen. The information they provided me regarding the cross-sectional properties was in general form, meaning only the value of the cross section area was given, but not the dimensions of the cross section. Thus i calculated the diameter and thickness of the main pipes so that its properties matched the ones provided by Reinertsen. The cross sectional area had to be 0.25 m^2. This was the most important parameter since the seabed will be dominated by axial forces. The other important thing was that Reinertsen provided information that the seabed was in equilibrium between buoyancy and gravity forces. The diameter and thickness are calculated based on this assumption.

6.2.2 Pontoons

The floating bridge and submerged tunnel are connected to pontoons, for buoyancy. The pontoons, made of concrete and filled with ballast water has a total mass of 1786,6 tonnes. In USFOS the pontoons are modelled as circular beam elements.

There is used three types of pontoons in the USFOS model. They are all cylindrical elements, but with a different diameter. The pontoons are modelled as beam elements, using draught and height from documents by Reinertsen [**?**]. Large pontoons are used where the barrier and tunnel is connected to bridge, to make more stability and buoyancy in this region. Documents provided by Reinertsen stated that the pontoons in this region have a rectangular cross-section, however, it was decided to use circular cross section for all pontoons for simplicity. The rectangular cross section for pontoons gave

some trouble in calculations because when using rectangular elements the elements intersected each other, and this caused some problems for USFOS. Instead, a circular cross section was used. The density of the pontoons is calculated based on the mass and the total volume of the elements

	Coordinates of nodes between crossbeam and main pipes			
Pontoons ID Position X[m]	Diameter [m]	Height [m]	Draugth [m]	Density [kg/mˆ3]
1,9	40	8.5	5.0	3.65
2,10	40	8.5	5.0	3.65
3,11	40	8.5	5.0	3.65
4,12	40	8.5	5.0	3.65
5,13	40	8.5	5.0	3.65
6,14	40	8.5	5.0	3.65
7,15	40	8.5	5.0	3.65
8,16	85	8.5	5.0	3.65
17,18	60.000	8.5	5.0	3.65
19,20	60.000	8.5	5.0	3.655

Table 6.3: Geometrical properties of pontoons

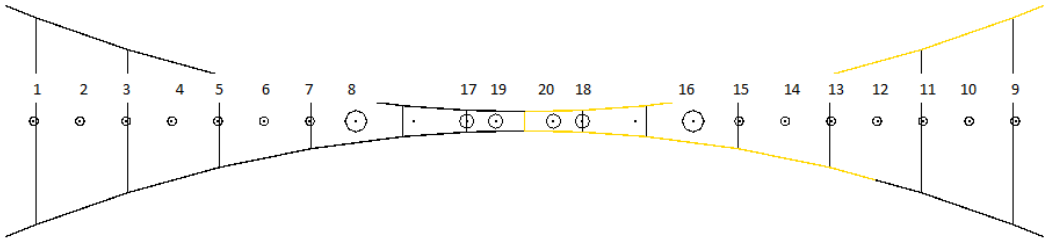

x

Pontoons distributed along bridge and tunnel

The pontoons are positioned all along the floating bridge and over the submerged tunnel, to give them buoyancy. Documents provided by Reinertsen stated that there was a total of 6 pontoons on the submerged tunnel, wherein two of them included the part where the collision barrier is attached. I have used a slightly different way of modelling the part of the bridge where the tunnel connects to the bridge.I did not model the platform as it is in the drawings provided by Reinertsen. I made two larger pontoons where the connection between bridge and tunnel is , see **??**

I also use a total of 8 pontoons on floating bridge with a distance of 159 meters between each. Looking at documents from Reinertsen it seemed as there was one pontoon directly above each cross beam, and also one in between. Figure **??**

6.2.3 Floating bridge and submerged tunnel.

The floating bridge is modelled with Box shaped beams. The bridge is floating on top of cylindrical pontoons described above. The bridge model has a length of 1219 meters if including the part where the barrier is connected.

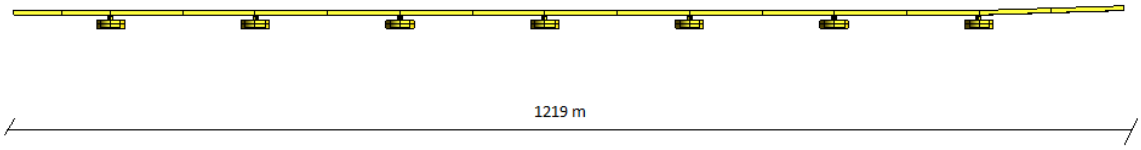

Model of bridge concept: floating bridge

The ridge lane is a 16m by 5 m box. A comparison between the cross section shape of the model and the design proposed by Reinertsen AS is shown below

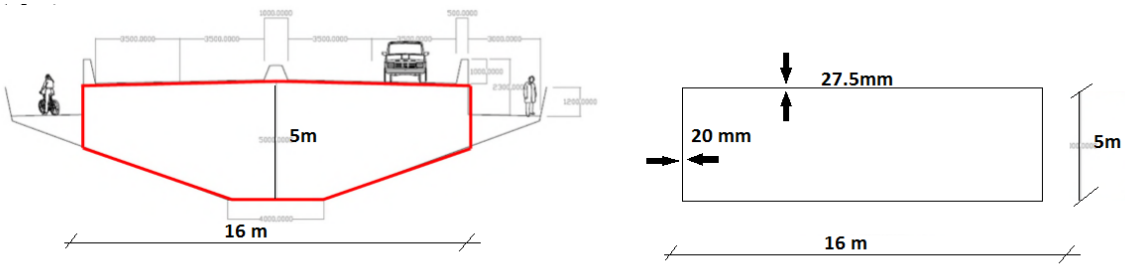

Cross section of floating bridge in USFOS. Left: design by Reinertsen , right design in USFOS

The tunnel is connected to each side by the floating bridges.The span and depth of the tunnel is 1166 meter and -30.5 meter. The total length of the tunnel model is 1374 meter. The ending points have a height of 16.82 meters . The additional elevation of the bridge prior to the tunnel connection is to make sure that the bridge slope is steep enough to give the tunnel a desired depth. The same principle was applied for the submerged tunnel, regarding cross-sectional properties. The drawing in figure **??** displays a comparison between the design proposed by Reinertsen AS and what I have used in my model in USFOS.

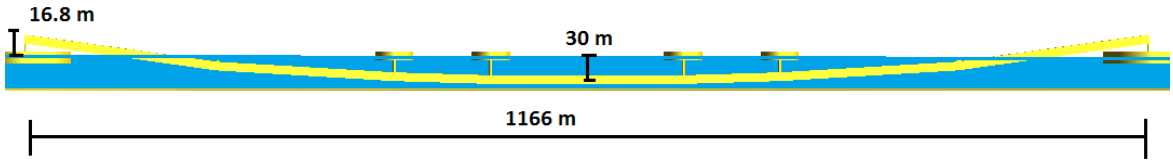

Model of bridge concept: floating tunnel

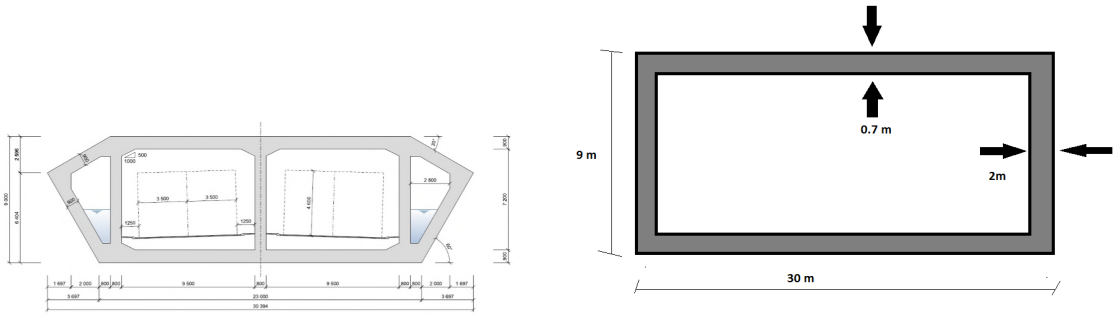

Cross section of floating tunnel in USFOS. Left: design by Reinertsen , right design in USFOS

The table below data for the cross section of the bridge and tunnel. The cross-sectional data is calculated to give the same cross section area and bending stiffness on strong axis ,as the design in documents from Reinertsen. This will give a correct mass and stiffness properties of the bridge.

The table and figure below describes the bridge elevation and tunnel depth at equilibrium, along the bridge path way.

Submerged tunnel parameters				
Part	Width [m]	Height [m]	Plate thickness sides [m]	Thickness top and bottom
Floating bridge	16	5	5	.02
Submerged floating tunnel	30	9	0.7	0.0275

Table 6.4: Number of turns and distance between top and bottom.

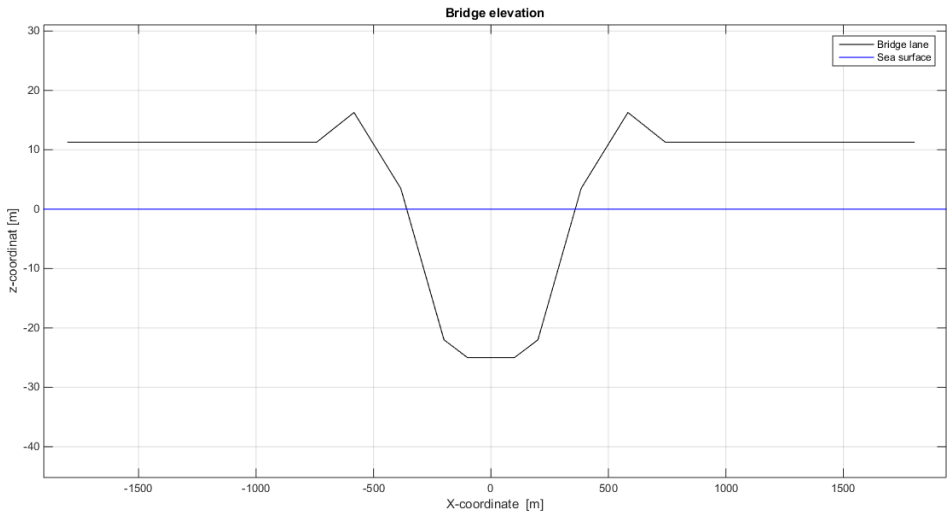

Bridge elevation

6.2.4 Collision barriers

The collision barrier is modelled with 3 beams in a wide u-shape. See figure below. They are modelled with motivation from figures given from Reinertsen, see figure **??** The figure below shows the geometry of the barrier. The cross section is the same as the global model described in chapter 6.

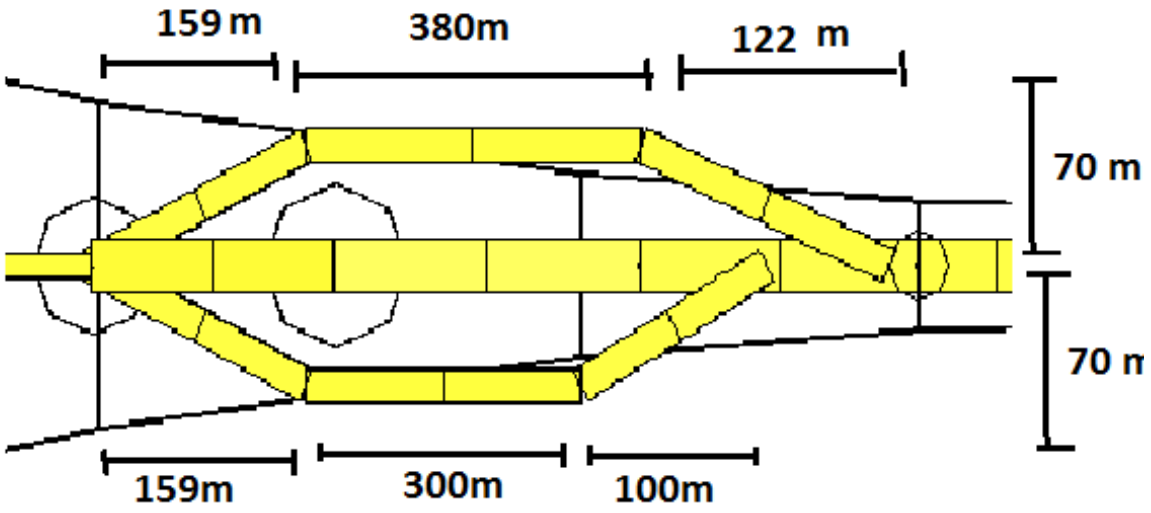

Global Design of barriers

6.3 Material properties of main parts

Submerged tunnel parameters				
Part name	Yield stress [m]	Youngs modulus [m]	Density [m]	Poissons ratio
Artificial seabed, steel	480 MPa	210 GPa	7800	.3
Floating bridge, steel	480 MPa	210 GPa	7800	.3
Submerged floating tunnel, concrete	30 MPa	40 GPa	2240	0.25
Pontoons , concrete	30 MPa	40 GPa	2240	0.25
Collision barrier, Aluminium	230	70GPA	2700	0.34

Table 6.5: Material parameters for crossing model.

The aluminium in the barrier is in detail described in chapter **??**. The effect of welds and heat-affected zones will not be able to be modelled in USFOS. The collision analysis in USFOS will be more of a global analysis looking at the response of the entire bridge concept.

The density of the different parts had to be scaled a little to make the bridge stable and in equilibrium between the buoyancy forces and the gravitational forces. Also, the density of the pontoons is quite low. This is because the elements are not filled with air, as the real pontoons are, and the density stated is only based on equivalent density, which means the total mass of the pontoons, included ballast water, divided by the total volume.

6.4 Bouncy and Gravity

The gravity acts as proportional to the constant of gravity 9.81 m/s. This force acts on all elements, of all the main parts. The buoyancy was a little trickier. In USFOS one can either add buoyancy forces by a built-in function called BUOYANCY, or one can add loads on the elements which has the same quantity as the buoyancy force. I choose the latter option, after trying for a long time to add buoyancy forces the conventional method. Later discussed in chapter 8 this caused many problems, which led to not being able to do the desired analysis. In addition to the loads, which act on the submerged parts, pontoons and seabed, the water plane stiffness is added by spring elements.

6.5 Boundary conditions

The bridge has boundary conditions at each side of the artificial seabed, as well as at the bridge ends. The figure and table below describe the boundary conditions of the bridge.

Boundary condition parameters

Boundary condition type Poissons ratio	Type Blue	Type Red [m]	Type Green [m]
X-Trans-Restriction [N/m] seabed,	0(inf)	0	inf
Y-Trans-Restriction [N/m] seabed,	0(inf)	inf	inf
Z-Trans-Restriction [N/m] seabed,	inf	inf	inf
X-Rotational-Restriction [Nm/rad] seabed,	inf	inf	inf
Y-Rotational-Restriction [Nm/rad] seabed,	inf	inf	inf
Z-Rotational-Restriction [Nm/rad] seabed,	inf	inf	inf

Table 6.6: Boundary conditions of bridge model

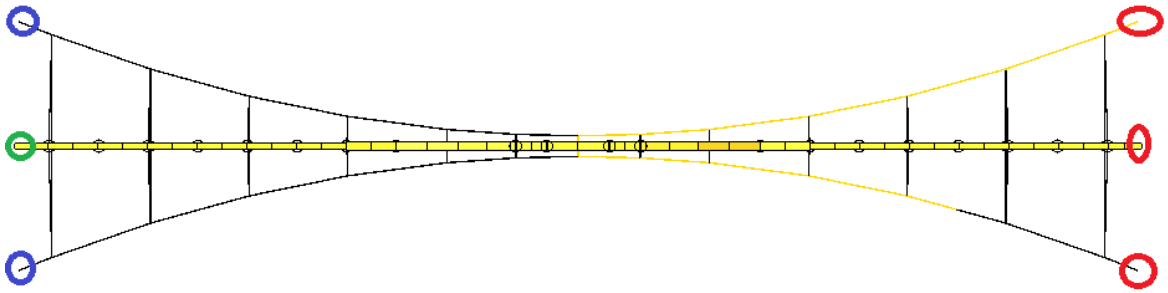

figurePlate with HAZ modelled in welds(left); Axial Crushing: Force-deformation plot (right)

The boundary conditions marked as blue is where the pre tension is applied by node loads. Therefore the model must be able to move in the plane of the seabed. After the pretension is set, the boundary conditions are fastened completely, as the red boundary condition. This is possible to do in the USFOS analysis, by the use of the function ACTIVELM. The last boundary condition is the one marked green. This is boundary allows the bridge to axially translate along the x-axis. It is likely that the bridge can move axially because the rest of the bridge is in reality connected there. The value is set equal the axial stiffness of the bridge box.

Chapter 7

Results

This chapter deals with the results of the analysis carried out in this thesis. The results will be presented in three parts, the stiffened panel analysis, collision analysis of the barrier and bow model, and last analysis carried out in USFOS. I did not obtain all the desired results I had hoped. This will be explained in the relevant sections of this chapter.The files used in the thesis work is uploaded trough the DAIM portal trough NTNU, one should be able to access the files there.

7.1 Analysis of stiffened panel

The purpose of this analysis was to look at the effect the reduction in the heat affected zone for Aluminium. By loading a simple structure in two different ways, axial loading, and lateral loading I hoped to obtain enough data to make an opinion on the matter. The analysis is focusing on the plates ability to absorb energy as strain energy, as well as the reaction force between the loading and the plate itself. The strain calculated displayed in the results is the strain calculated at the middle integration point over the cross section. The strain in the results is the effective plastic strain.

7.1.1 Plate element model analysis

The plate element model has been analysed with five different material compositions. They are explained in table 7.1 and figure 7.1 below, also see table **??** on page 75.

As one can see, the material in the first case is for alloy 5083. There is as explained, no material reduction in the heat affected zone for this temper class. Therefore I

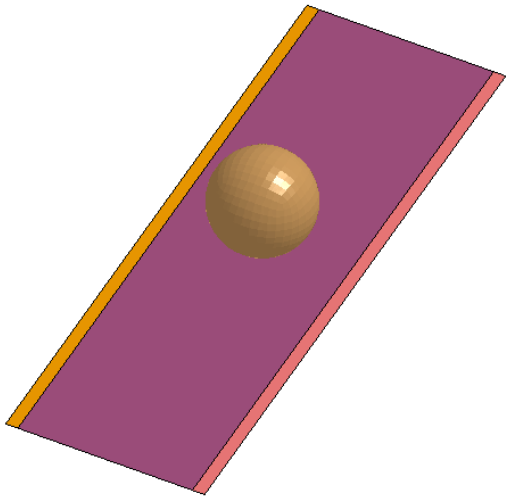

Figure 7.1: plate element model

	Material composition of plate element model		
Case number	left HAZ(colored orange)	rigth HAZ(colored pink)	base material(colored pur
1	5083 O Base	5083 O Base/HAZ	5083 O Base/HAZ
2	5083 H12 Base	5083 H12 Base	5083 H12 Base
3	6082 T6 Base	6082 T6 Base	6082 T6 Base
4	5083 H12 Base	5083 H12 HAZ	5083 H12 HAZ
5	6082 T6 Base	6082 T6 HAZ	6082 T6 HAZ

Table 7.1: Plate cases

have written both base and HAZ for the material composition. Otherwise, there is a comparison between a plate with and without HAZ at the weld zones at the ends, and one without for both alloy 5083 H12, and 6082 T6.

Energy and resistance force plots

Figure 7.2 is displaying the force-deformation and energy absorption curve for the five cases described above. The reaction force is taken as the force acting on the sphere by the plate. The energy is the internal energy in the plate occurring because of the impact. This energy is the sum of the product of incremental volume, stress and incremental strain of all the elements in the plate.

The sphere colliding with the plate element model moves with a velocity of 1 $\frac{m}{s}$. Case 1, which is alloy 5083 with temper O, has the highest overall ability to absorb strain

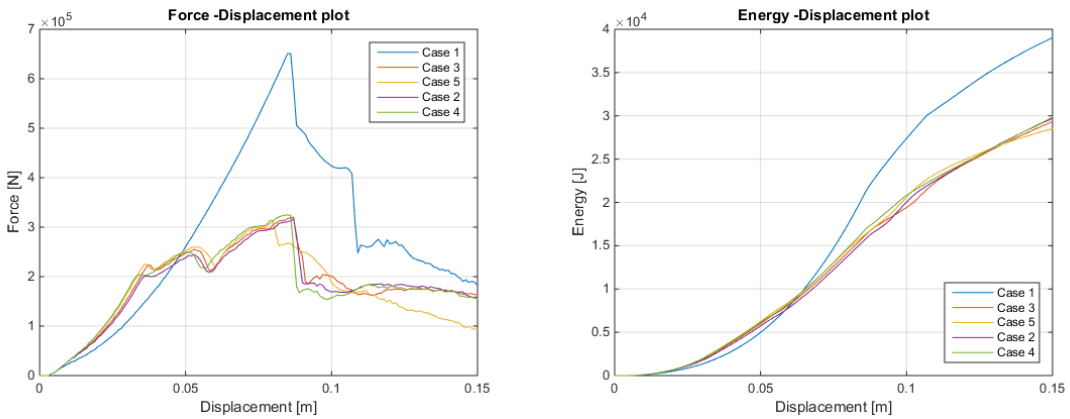

Figure 7.2: plate element model

Figure 7.3: Panel resistance plot. Left: Force-deformation. Right: Strain energy-deformation

energy. Because it has the highest ultimate strain value, it is able to deform more compared to the others. It is believed that the softness in alloy 5083 with temper O is making it deform more easily than the others and thus being able to distribute the forces arising in the plate better compared to the other cases. This way, more elements are activated, distributing the stresses in a larger area, and the plate is able to resist more. The work hardening properties of alloy 5083 O are also beneficial it seems. The stress-strain curves for the base materialof the other two alloys has a more flat work hardening compared to that of alloy 5083 O. Afther the elements yields, the transition to ultimate failure is not as quick as for the other alloys . One can see that all the cases except case 1 have a minor peak at about 0.35 seconds. It was verified that this is where the first elements start to fail. Case 1 does not fail until about 0.8 seconds, which one can see the peak in figure 7.2

The importance of velocity was also analysed. The impact velocity was reduced to 0.1 m/s to see if a slow impact would change the results in any way, especially the strain development in HAZ.

As can be seen in figure 7.4, there is a drop resulting in zero resisting force for all the cases except case 1. It is comparable with the left figure in fig 7.2, as case 1 here also has a larger resistance peak. What was different in this case is that the internal energy absorbed in the plate is higher in case 3. This is believed to be because of the curve of case 3 has a peak at about 0.15 s (displacement of 0.15 m). This might explain why case 3 has a larger energy absorption than case 1. The reason behind the drop in the resistance force, resulting in the part where there is no acting force (from about 0.4

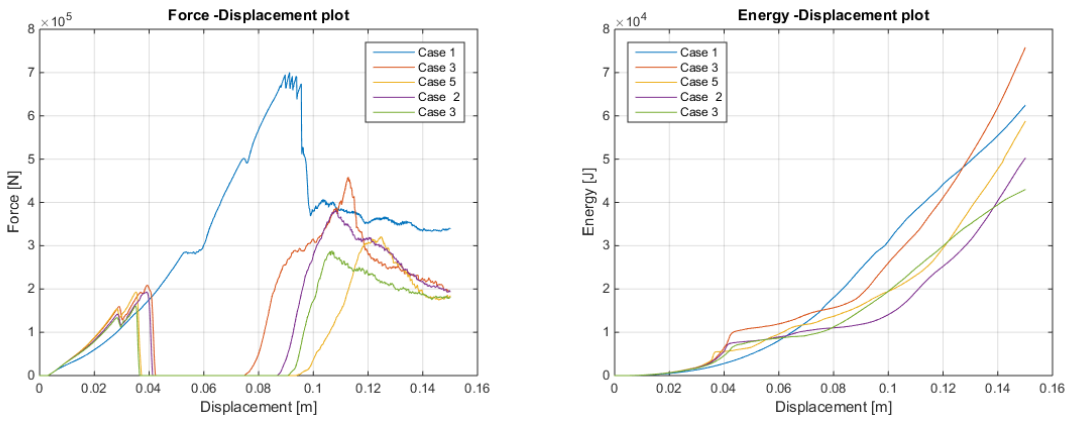

Figure 7.4: plate element model

Figure 7.5: Panel resistance plot 2. Left: Force-deformation. Right: Strain energy-deformation

seconds to 0.7 seconds) is that there is a fracture at the shorter edges for all the cases except case 1 at this moment. Moreover, even though there is no force resulting here, the plate is still being deformed, which is why the internal energy is slightly increasing in this time. Internal energy is not the same as external work. External work is the work done in the system by all applied pressures and forces, but internal energy is the work done resulting in permanent deformation. It is believed that the fracture crack is getting larger in this time span, but without resulting in a resistance force and that this is the reason of why internal energy is increasing, but resistance force is zero.

Fracture pattern

Below in figure 7.6 is a comparison between fracture pattern for the plates when the sphere was moving with velocity 1 $\frac{m}{s}$. . First element failure is displayed in figure 7.6. This applies for all the results presented in this report. Table 7.2 describes where and when the first fracture occurs in the plate element model.

As can be seen, the strains are not fully developed at the welds for any of the cases, except case 1. What is believed to happen is that the impact from the sphere causes the strains due to contact stresses to rise and quickly reach the failure strain. Except for case 1, which has a higher failure strain in the entire plate. The heat affected zone has a ultimate strain(even though questionable) that is large, but only at the sides, where the sphere does not impact. It might seem that the impact strain is not large enough to quickly penetrate the plate element model for the alloy 5083 temper O. Therefore

First fracture for the different plate element model		
Case number	Position of fracture)	Time at first fracture
1	About at center of platestrip,	0.089 s
2	Completely at center of platestrip	0.039 s
3	Completely at center of platestrip	0.039 s
4	Completely at center of platestrip	0.039 s
5	Completely at center of platestrip	0.039 s

Table 7.2: First failure values.

this plate has a later fracture, as can be seen in the force-deformation plots. The cases 2, 3, 4 and 5 all have a dip in the force-deformation curve after about 0.4 seconds. The case 1, however, does not get a drop until bout 0.9 seconds. This corresponds well with the fracture pattern. The reason of why the fracture line is not symmetrical for case 1 is most likely because the area in which is in high strain(coloured red in figure 7.6 top left) is much larger compared to the other fracture patterns. Therefore it is more likely to be anti-symmetrical, e.g., a little to the side of the centre of the plate.

Below in figure 7.1.1 describing further fracture pattern for the plate element model, when the sphere was also moving with $\frac{m}{s}$

The maximum strains in the plots correspond well with the ultimate strain given in the model, see table **??**. The capacity to endure a higher strain is greater for the case with the heat affected zone compared to the ones without. The development of plastic strain in the heat affected zone is not as dominant as perhaps one might think beforehand. The reason for this is believed to be because the plate element model develop quickly a fracture due to impact. One can see that for the plate cases 2-5 there is a second peak at about 0.09 seconds, see figure 7.2, and for case 1 a drop at about 0.12 seconds. The reason behind this is because this is when the plate element model develops horizontal cracks as seen in figure 7.1.1. The first crack is vertical, and then the horizontal cracks form. After this, the sphere is just pressed trough the plate, and the resistance force is not changing much.

Below in figure 7.8 fracture development for the plate element model is described, here the sphere is moving with 0.1 $\frac{m}{s}$

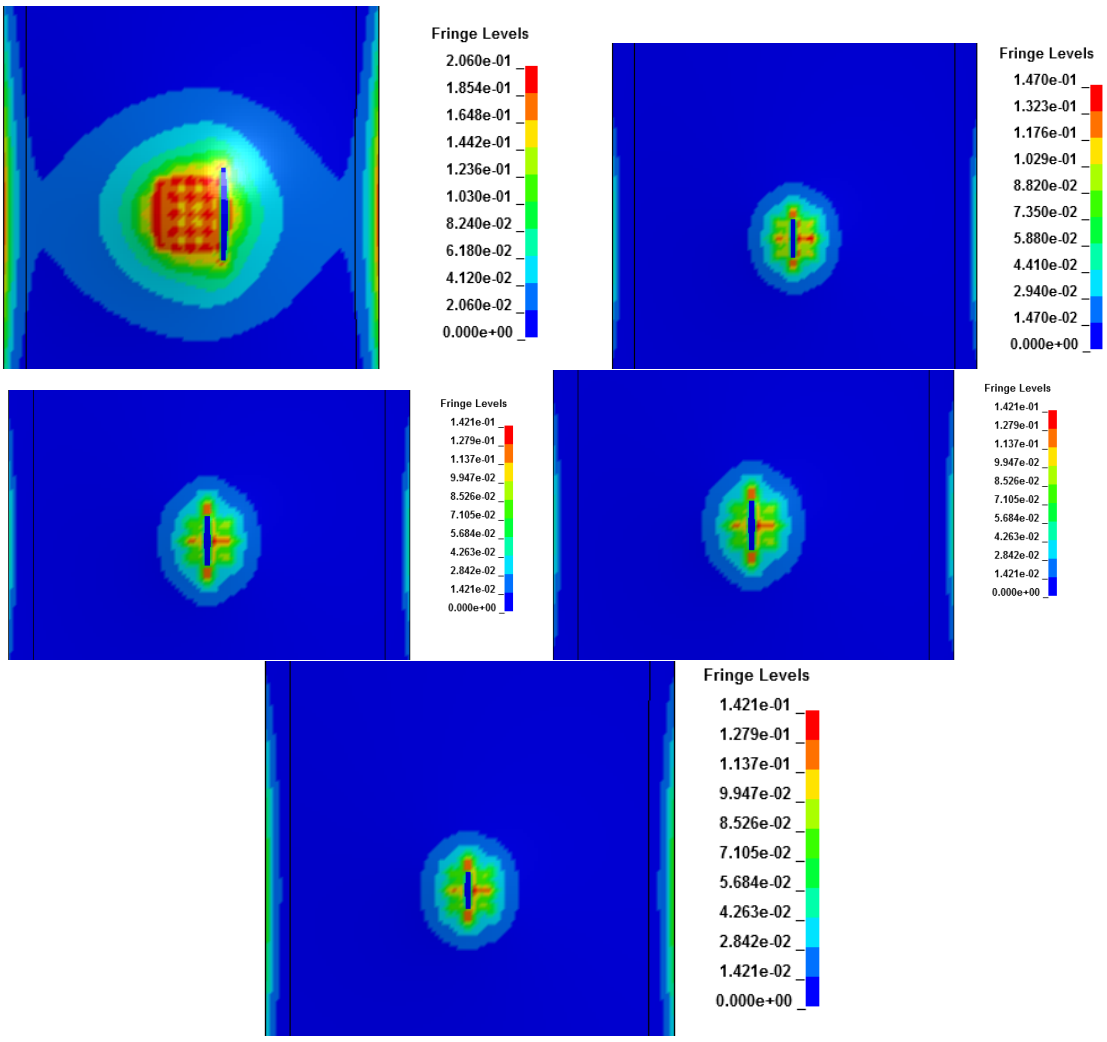

Figure 7.6: Development of strain and fracture pattern. From top to bottom; Case 1 left, case 2 right, Case 3 left, Case 4 right, Case 5 centre

The development of plastic strain in HAZ is much more prominent when the impact velocity was reduced. One can clearly see the difference between the strain in the models for alloy 6083 T6, with and without HAZ. The strains have more time to develop trough the whole plate, as 0.1 m/s is a very low velocity, It is believed that the reason of why the latter 4 cases, has a drop in resistance force is because the shorter edges of the plates develop a sudden failure crack, unlike the plate case 1 where there is an even development of crack at the side. This is believed to be because the low strain capacities in the base material, except for alloy 5083 O. The longitudial stresses in the plate element model does have a impact on the fracture pattern it seems, and it

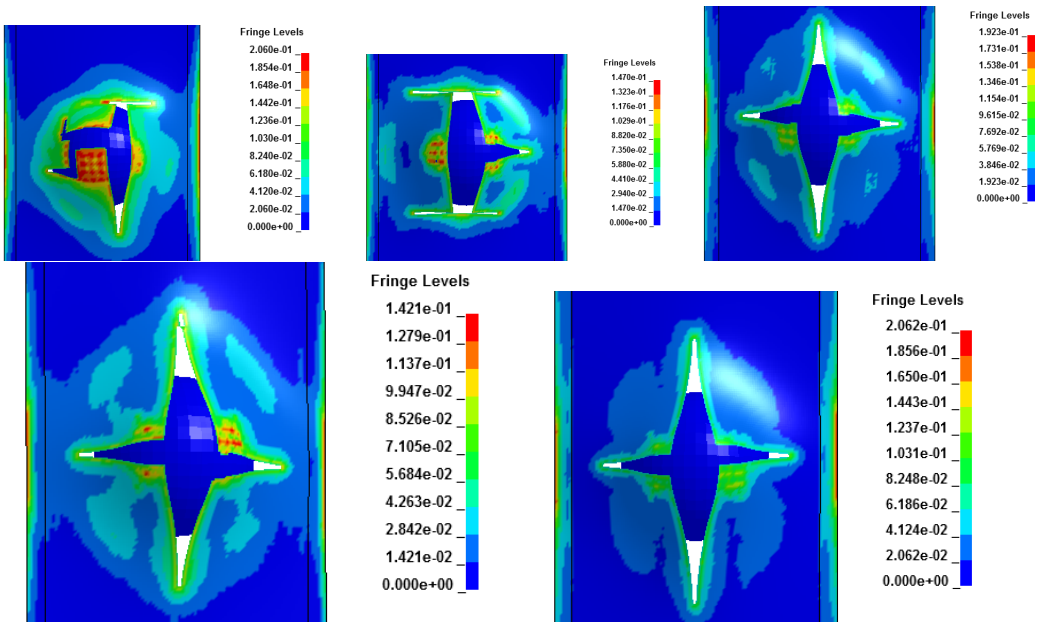

Figure 7.7: Development of strain and fracture pattern 2 .Top,(Case1),Middle left (Case2),Middle rigth (Case4),Lower left (Case3),Lower right (Case5)

is what cause the fracture at the shorter edges.

7.1.2 Lateral loading of stiffened panel

As mentioned before, the purpose of this analysis is to compare a stiffened panel with two different materials in the plate and also look at the effect of reduction in HAZ. The purpose of lateral loading in the form of a rigid sphere is to see how the plates in the barrier react to this type of loading, since the bow will act as a lateral load on the longitudinal bulkheads. Below in table 7.3and figure 7.9 a description of different cases that was analysed are compared.

	Material composition of stiffened pannel			
Case number	1)	2	3	4
Plate material(blue)	5083 O	5083 O	5083 H12	5083 H12
Stiffener material(green)	6082 T6	6082 T6	6082 T6	6082 T6
HAZ Plate material(red)	5083 O	5083 O HAZHAZ	5083 H12	5083 H12 HAZ
HAZ Stiffener material(black)	6082 T6	6082 T6 HAZ	6082 T6	6082 T6 HAZ

Table 7.3: Stiffened panel cases.

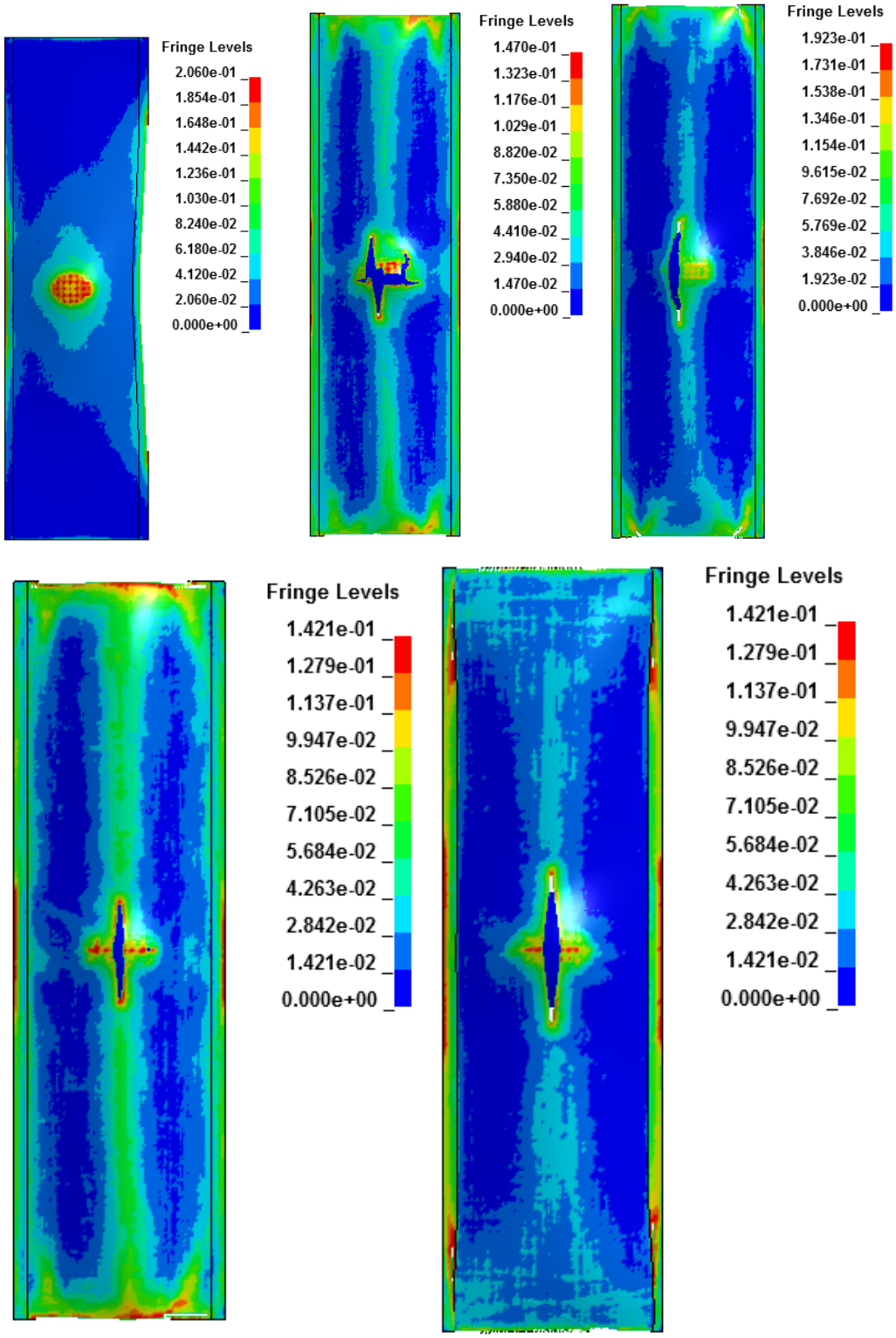

Figure 7.8: Development of strain and fracture pattern 2 .Top,(Case1),Middle left (Case2),Middle rigth (Case4),Lower left (Case3),Lower right (Case5)

As can be seen, of the table, case 1 and 2 are modelled without the effect of HAZ, while the other two are modelled with the reduction in HAZ.

Figure 7.10 is displaying the force-deformation and energy absorption curve for the separate cases.

The reaction force capacity is larger for the panel when alloy 5083 O is used in the plate , compared to if the plate is modelled with alloy 5083 H12. The cases where modelling includes the reduction in the HAZ, the energy absorption is less compared to the models without. Of the cases where reduction in the HAZ is included, the panel where alloy 5083 is the strongest.

Fracture patterns

Below are figures and tables describing first fracture for the stiffened panel case. The sphere is moving with constant velocity of 1m/s.

The first failure is differing by where and when. The cases where HAZ is not included, the failure strains tend to localise in the middle stiffener, just under the sphere impact (the two top pictures in 7.11) while in the cases where HAZ is included, the strains tend

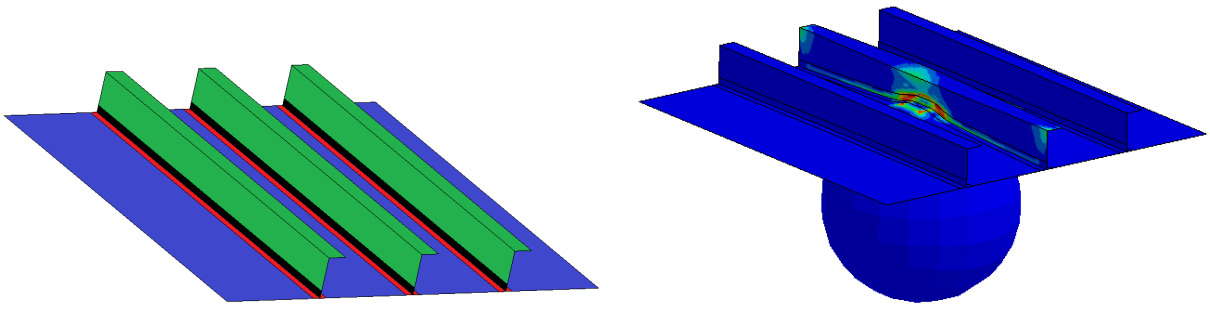

Figure 7.9: Lateral loading on stiffened panel; Color description of panel(left), Loading by sphere(right)

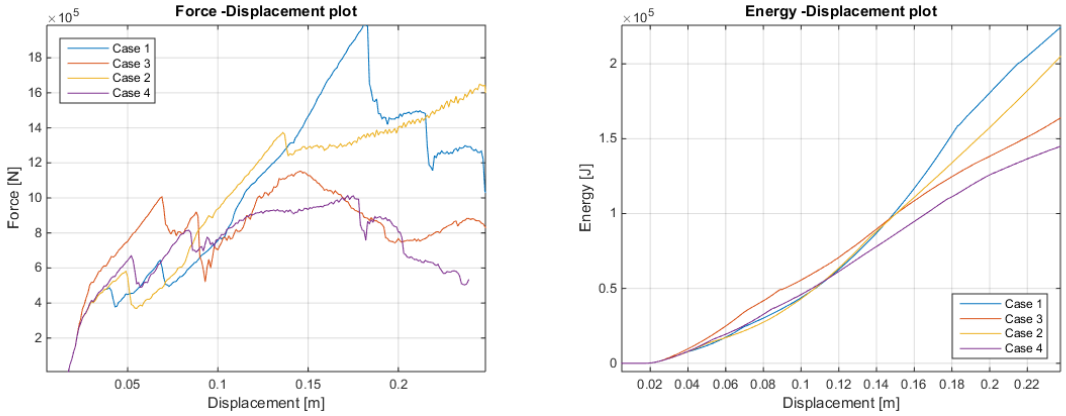

Figure 7.10: Panel resistance plot 3. Left: Force-deformation. Right: Strain energy-deformation

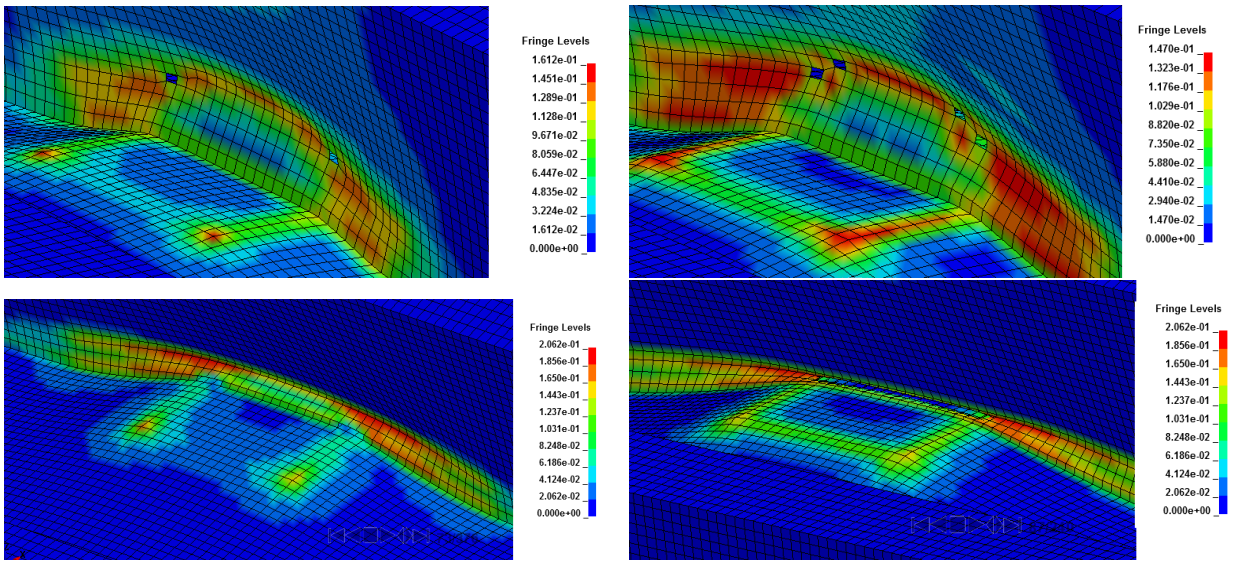

Figure 7.11: *Lateral loading on stiffened panel;Deformation in panel case 1(upper left),Deformation in panel case 2(upper rigth),Deformation in panel case 3(lower left),Deformation in panel case 4(lower rigth)*

First fracture for the different plate element models		
Case number	Position of fracture)	Time at first fracture
1	In stiffener, approx 35 mm upwards from weld line	0.071 s
2	In stiffener, approx 35 mm upwards fro	0.083 s
3	In stiffener, at bottom , exactly at weld line	0.071 s
4	In stiffener, at bottom , exactly at weld line	0.085 s

Table 7.4: First failure in stiffened panel.

to go higher along the HAZ in the stiffener. The cases where alloy 5083 H12 is used, the strain form a square U-shape outwards from the stiffener, (fig 7.11 right pictures, upper and lower). The strains in the plate develop closer to the ultimate strain, in a larger area in the plate in these cases, compared to the cases where the plate material is 5083 O.The effect of the HAZ is mostly apparent in the stiffener, and not so much on the plate. It is believed that the contact force acting directly under the stiffener from the rigid sphere is causing the stiffener to react this way. The stiffener will absorb much more of this contact force, than bending forces or membrane forces in the plate. If the sphere was not rigid and could deform, it is possible that more forces would be distributed more evenly trough the plate.

Further is shown the fracture pattern and strain development in the stiffened panel, the pictures are taken at 0.1 s.

As the figures show, the panels with Alloy 5083 H12 in the plate, breaks before the plate with the alloy 5083 O. In figure 7.10, on can see that the cases where alloy 5083 H12 is used in the plate has a more steep curve in the beginning before it peaks and drops(red and purple curve). What happens is that a larger part of the plate in the panel under the sphere is failing. The panel where alloy 5083 O is used, this does not happen. It has a larger failure strain and can deform more before it breaks. It is believed that this makes the alloy 5083 O better at resisting lateral collision forces, compared to alloy 5083 H12.

7.1.3 Axial loading of stiffened panel

The same plate configurations as in the lateral loading were used in axial loading case, see figure 7.13

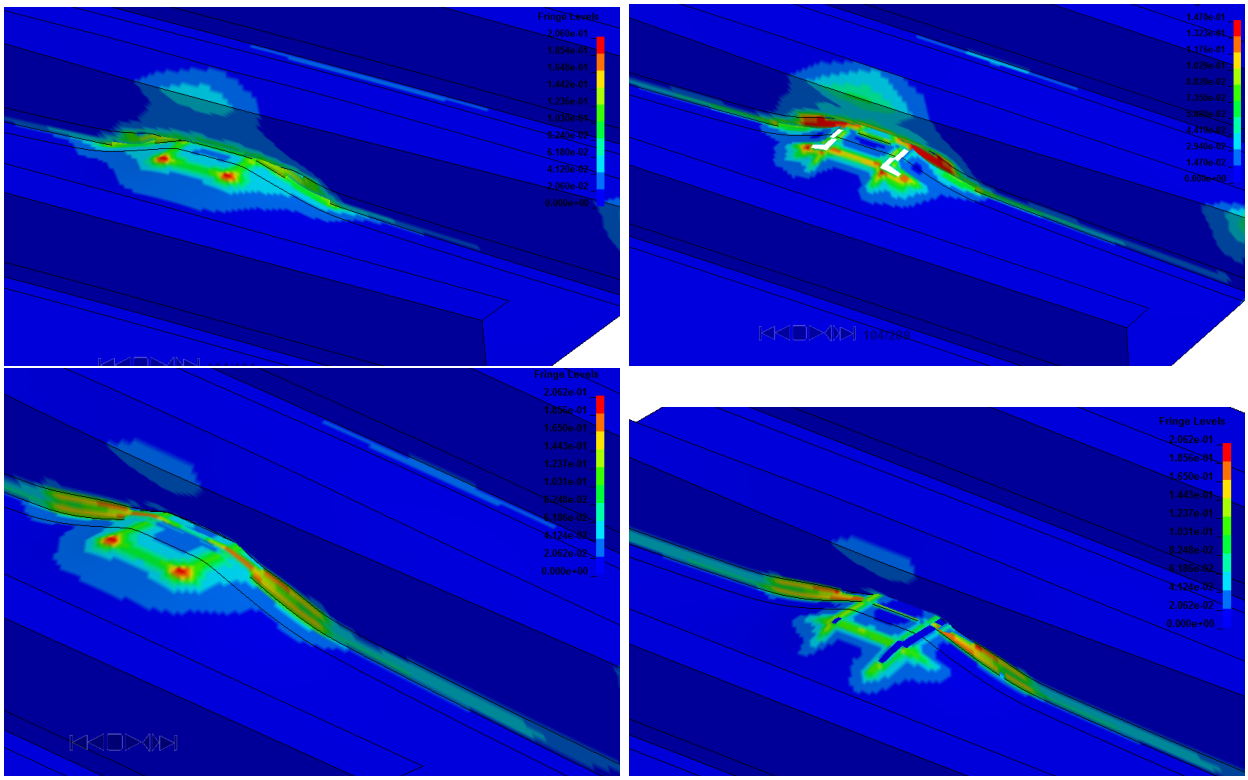

Figure 7.12: *Lateral loading on stiffened panel;Deformation in panel case 1(upper left),Deformation in panel case 2(upper rigth),Deformation in panel case 3(lower left),Deformation in panel case 4(lower rigth)*

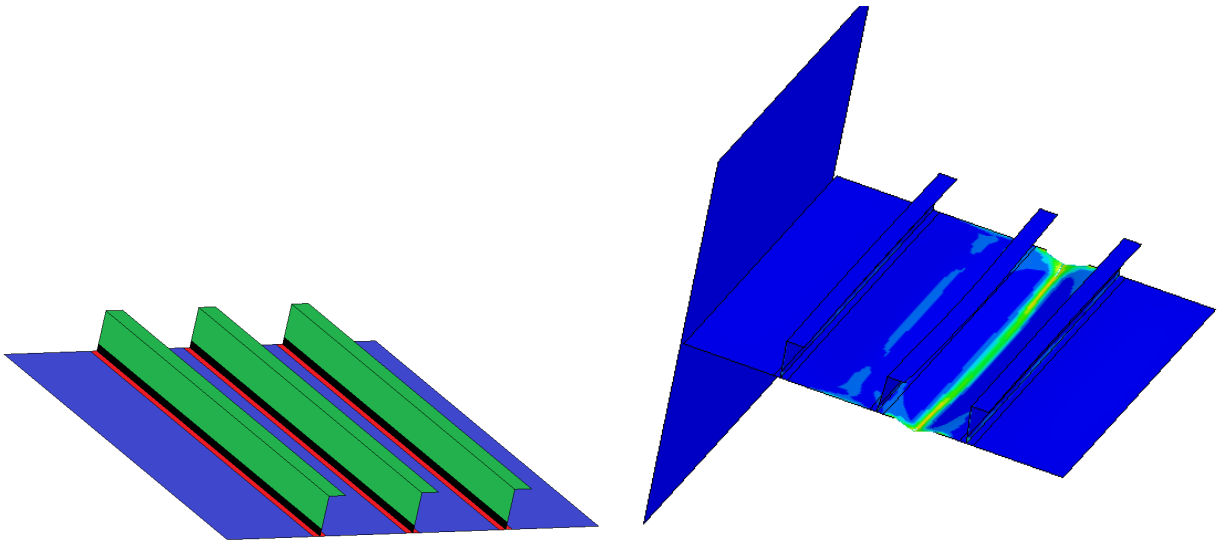

Figure 7.13: Axial loading on stiffened panel; Color description of panel(left), Axial Loading by rigid plate (right)

The purpose of this analysis was to look at how the panel react to axial crushing because the decks and the transverse bulkheads will be deforming axially when the barrier is deformed. Below is gathered energy absorption and reaction force plots, in figure 7.14 similar to the earlier. The rigid plate is moving with 1m/s.

As one can see, the panel with temper H12 in the plates has the largest peak in resistance force. This differs from which plate was the strongest in the lateral loading case. The first peak is just before the plate starts to buckle. The plate will buckle and form a buckling mode between the stiffeners as seen in figure 7.15.

The plates with Alloy 5083 O in the plate buckles as seen in the upper two cases in figure 7.15, while the panels with Alloy 5083 H12 in the plates buckle as the latter. It is believed this has to do with the softness of the plates. In figure 7.14 there is a second peak for the cases. This peak is because the plate breaks between the middle and the right stiffener in figure 7.15 and then the two severed plates make contact again. The

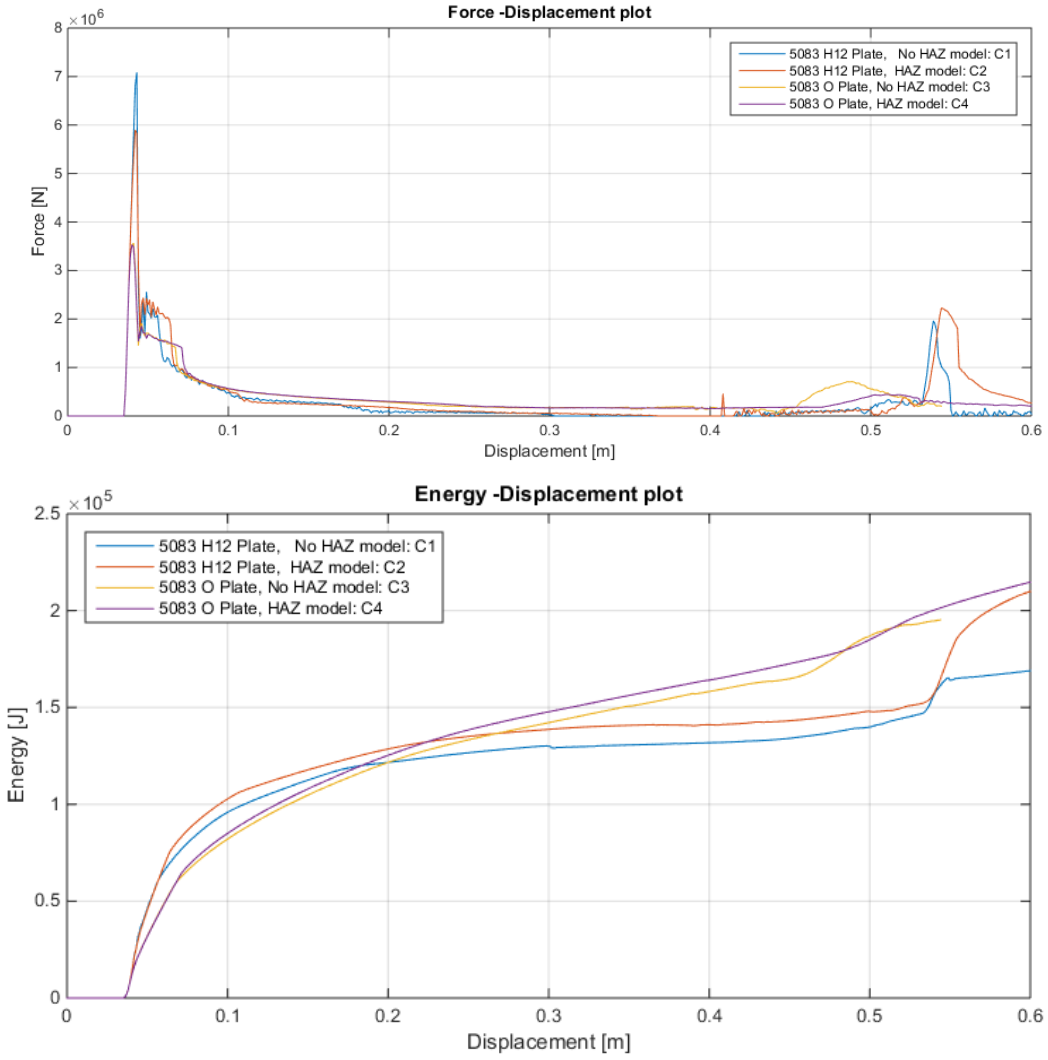

Figure 7.14: Panel resistance plot. Axial loading. Top: Force-deformation. Bottom: Strain energy-deformation

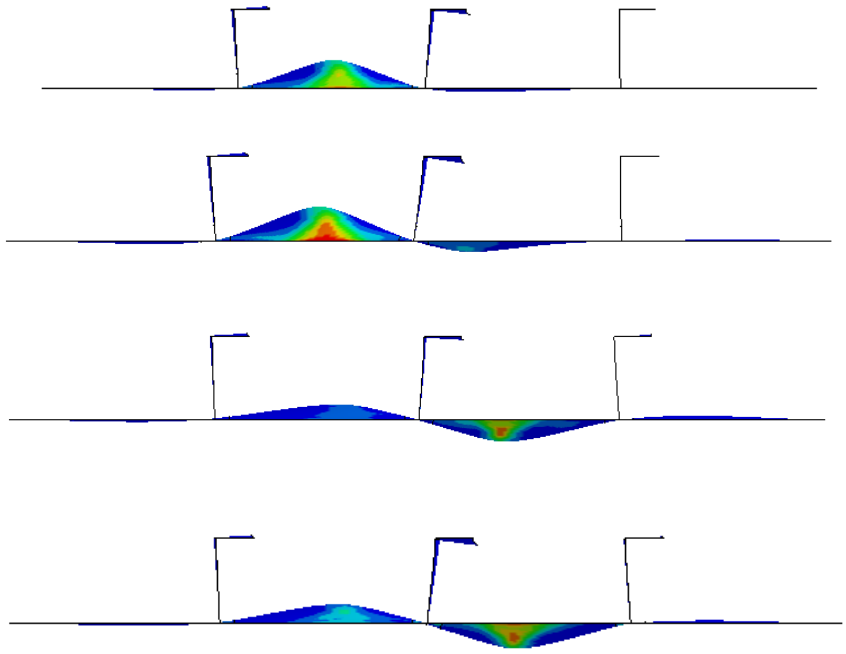

Figure 7.15: *Axial loading on stiffened panel;Deformation in panel case 3(upper),Deformation in panel case 4(second upper),Deformation in panel case 1(second lower),Deformation in panel case 2(lower)*

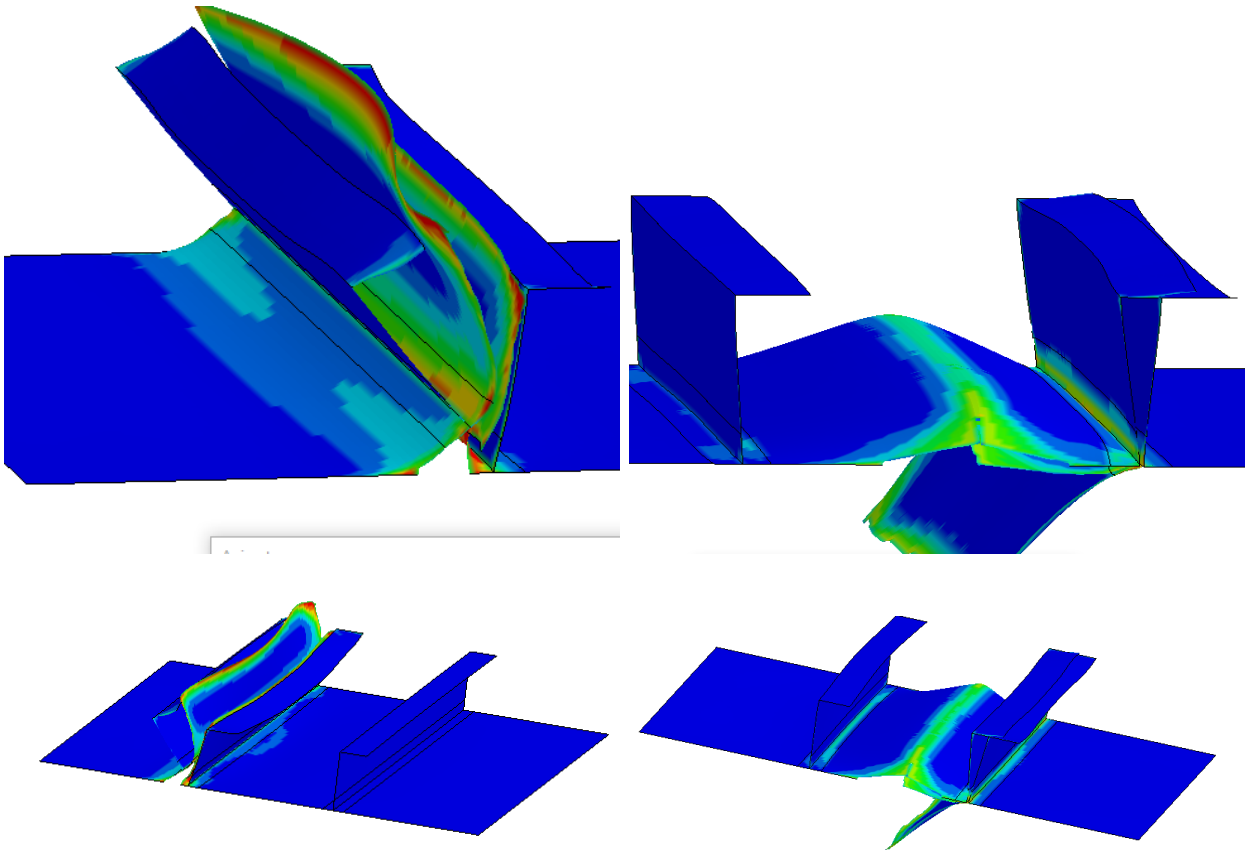

Figure 7.16: *Lateral loading on stiffened panel;Deformation in panel case 1(upper left),Deformation in panel case 2(upper rigth),Deformation in panel case 3(lower left),Deformation in panel case 4(lower rigth)*

peak is small for case 1 and 2, because the plate is pressed upwards when the severed parts make second contact. For case 3 and 4 this does not happen, and the remaining part of the plate starts to buckle again,see figure 7.16.

7.2 Analysis of collision barrier in LS DYNA3D

The purpose of this analysis was to see how the barrier configuration and design responded to a simulation of a ship collision. The analysis done is of a shared energy design, meaning both the ship and the barrier can be deformed. This analysis is the most time-consuming option, compared to strength or ductile design, wherein one of

the objects are of rigid material. The results are compared to simplified methods in the discussion, Chapter 8.

The intention of the analysis was to run the bow model trough the local part of the barrier, and then look at how much energy was absorbed in the entire collision. This energy would be a measure of how much energy could be assumed to be absorbed as strain energy in the collision.

The analysis was not complete; I am disappointed to say. The final analysis was too time demanding, and I could not get enough computational power that I needed to run it completely. I only got a part of the result, not all. If the analysis were completely run, the displacement of the bow model would be 25 meters, enough to crush the barrier the whole way trough. I only got to run it 9 meters, about half the width of the barrier. I will present energy absorption plots, as well as force-deformation plots of the collision, and I will describe the deformation of the barrier as well as the ship.

7.2.1 Force and energy absorption

Below is a figure displaying the resultant resisting force from the barrier acting on the bow, as well as the energy absorbed as strain energy in the collision. The amount of energy absorbed is about 150 MJ when the bow has travelled 10 meters into the bow. The resultant resistance force acting on the bow is also quite low, at about 20 MN. It is hard to predict how the resultant resistance would behave later, but it will most likely increase. How much is not certain and require a longer analysis. The energy absorbed is also going to increase , but how much is not certain.

7.2.2 Deformation pattern

The bow only receives minor damage. The barrier is deformed the most. The bow hits the barrier between deck two and three, and is crushing trough them. Since the analysis is not completely finished its hard to see, but the transverse bulkheads will deform more when the ship gets further. The extra ductility at the ends will affect the results however, and the validity of the results are indeed questionable. The extra

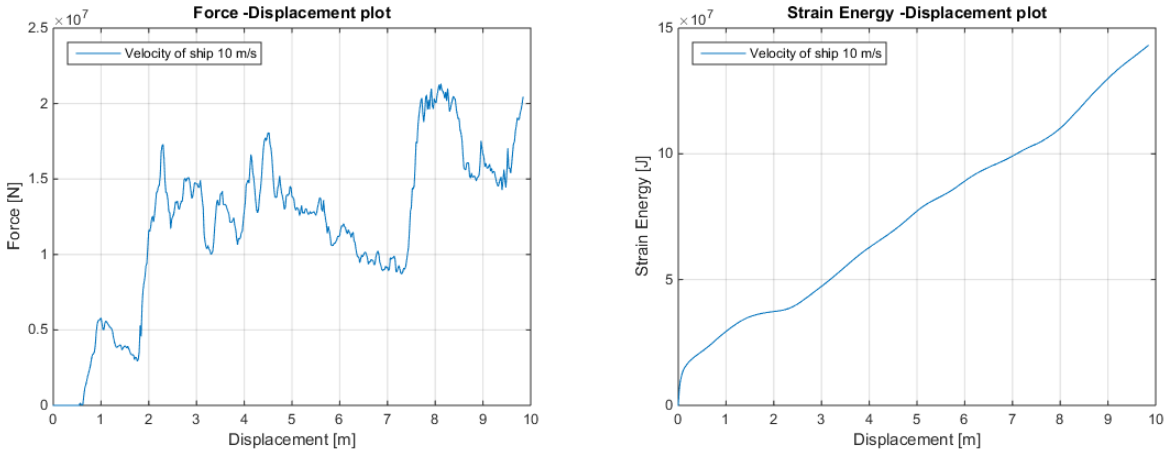

Figure 7.17: Lateral loading on stiffened panel; Color description of panel(left), Loading by sphere(right)

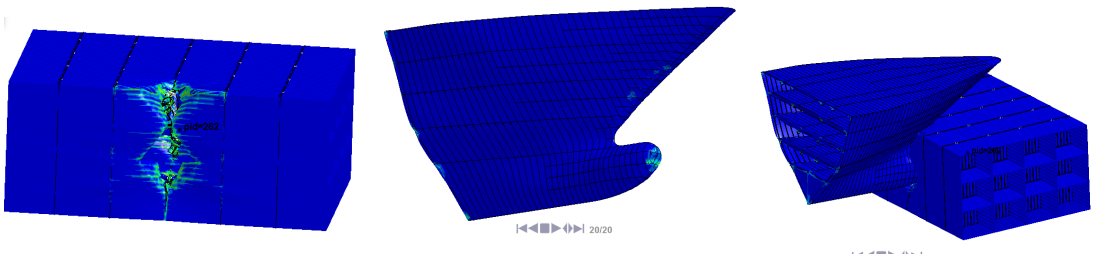

Figure 7.18: Lateral loading on stiffened panel; Color description of panel(left), Loading by sphere(right)

Figure 7.19: Lateral loading on stiffened panel; Color description of panel(left), Loading by sphere(right)

ductility at the ends could affect the resultant resistance force on the barrier in a negative way. In reality the bow will probably deform the barrier in a wider section than the local model. The local model should probably be twice as long, at about 60 meter to capture the collision forces more accurately. More on this in chapter 8.

7.3 Analysis of Bridge concept

In this section, i will describe the analysis preformed and results obtained in USFOS. There was intended to do three types of analysis in USFOS. Only one was succeeded in being carried out. In chapter 8 i discuss why it was so. The main reason was due a lot of time went with trying to solve a bug problem in USFOS.

7.4 Pre tension Analysis

In order to put set the pre tension in the sea bed, I used a function called HJHANSEN combined with applying node loads at the ends of the seabed, seen in figure **??**

The results obtained was somewhat similar to those obtained by Reinertsen AS. There are uncertainties in the fact that there seperate analysis has been carried out with different software, but also the methods of how the tension is modelled is different. The results from Aquasim(by Reinertsen AS) is based on

	First fracture for the different plate element models	
Cross beam number	Stress in cross bem(USFOS)	Stress in cross bem(Aquasim/Reinert
1	2.93e07 Pa	2.72e07 Pa 2
5.5e07 Pa	4.08e07 Pa 3	5.53e07 Pa
4.08e07 Pa 4	5.453e07 Pa	4.07e07 Pa 5
4.7e07 Pa	3.47e07 Pa 6	3.753e07 Pa
2.71e07 Pa 7	3.56e07 Pa	2.56e07 Pa height

Table 7.5: Pre tension in seabed. Results from USFOS vs Aquasim

Chapter 8

Discussions

In this chapter, I will discuss what I have learnt in the master thesis. I will discuss my results and look how they compare with previous work similar to my thesis. I will also discuss how it was to work with the thesis and the difficulties I experienced during the work.

8.1 Difficulties in modelling

One of the major problems I met while working on the thesis was a computational delay. As mentioned before, the analysis of the collision in LS-DYNA was very time-consuming. One analysis would take about 100 hours of computational time. Also, to be able to use the supercomputer at NTNU (called Vilje), which was necessary to run the analysis, one needs to wait in queue. This could take anywhere from a day to a week. The average waiting time between each analysis was about one nine days, and it was difficult to make fast progress as I would like.

Another difficulty I met was while modelling in USFOS. The software code in USFOS has difficulties calculating bouncy for elements positioned in the water plane surface if the elements are parallel to the surface plane.

It was very difficult and very time-consuming to try and find this problem/bug in the program, and it was alas not solved. This was disappointing for me, as I would like to understand how the global response of the bridge would be when a ship collided with it. It was decided to try and instead of using the built-in function Buoyancy, to try too hard code the buoyancy by adding springs and loads on the submerged elements of the bridge, that would act as buoyancy forces. This could have worked, but in the

end, it was not enough time to do this. Therefore, eigenfrequency analysis and collision analysis in USFOS was not done.

8.2 On assumptions

The first assumption I would like to address is the simplified fracture model I used in the material modelling. The strain failure model presented by the euro code is based on extensive experimental results, however, it does not mention if the model is valid for both base material and heat affected zones. It is only dependent on the yield stress, wherein reality it is very difficult to make a general law for fracture for all aluminium alloys, since a lot of them act differently, due to their different composition. To make a fracture model only based on yield stress of the alloy is also very simple. In reality, some alloys can have the same yield stress, but have different ultimate strain values. Different alloys can have different fracture mechanisms on a particle level. Some alloys will form pores around particles, which will eventually merge with other small pores/holes and form larger holes, which in turn will lead to fracture.It would be desired to make a material model for each alloy, accounting for different particle level behaviour, but this would take much time, and would not be feasible for this thesis. Using the Eurocode 9 fracture model I would say is not a conservative assumption, since it increases the ultimate strain capacity in the heat affected zone, which may not always be true, see **??**.

On added mass assumptions. The added mass was modelled by using mass scaling by increasing the density of the material. This way of trying to model the added mass forces is not exactly physically correct. In reality, the added mass forces act as pressure on the outer sides of the barrier. The same applies to the ballast water. Also, ballast water might slosh inside the ballast tanks, which in turn might affect the stability of the barrier. The simplification of not to include the drag forces is a conservative assumption because, it would let the barrier move further, compared to if the barrier was modelled with drag forces.

On element size. Regarding the model of the barrier, it became clear after some time that the element size is too small. The effective length of minimum 50 mm makes the analysis very time-consuming. Running 100 hours of computational time, the bow was only about 10 meters into the barrier. The barrier needed to be fully penetrated to give a foundation for the analysis in USFOS. The reason of why 50 mm was used was because of the heat affected zone. The heat affected zone was for a 15 mm plate only 35

mm. This information, given by the Eurocodes, are in fact a conservative design value. In reality, the HAZ is usually only extended to about perhaps half of that value. Thus an extent of HAZ of 50 mm is potentially a four times too large assumption. This was to reduce computational cost. To reduce the computational cost, even more, it would be a good idea to increase the mesh even further, but then it would compromise the mechanical behaviour of the material. If the smallest mesh increased to for example 100 mm, this would not be a good representation for HAZ. If one could find a way to model the weakness due to HAZ, but still be able to increase the minimum mesh size, it would be very beneficial for further work. This problem, the smallest needed element size, is perhaps what caused the most time-delay in the thesis work.

8.3 Discussion on the results

In the plate element model analysis, the obvious difference in the results was alloy 5083 O, which was strongest in the resistance force capacity. This was not too surprising, since this model had the highest fracture strain, and it is modelled without the reduction in the HAZ. The plate element models for alloy 6083 T6 and 5083 H12 behaved more similar than the alloy 5083 O. It is believed that the material properties of the base material are dominating the results, especially when the sphere is moving with 1 m/s. The impact stresses pierce trough the plate before strains develop significantly in the HAZ. When the velocity is reduced to 0.1 m/s the strains develop more in the HAZ and there is more separation in the resistance-deformation plots for the five cases.

Regarding the stiffened panel, it seems that the panel is strongest with Alloy 5083 O in lateral deformation, but stronger with Alloy 5083 H12 in axial deformation. It is believed that the ultimate strain is dominating the lateral deformation, while the yield and ultimate stress dominate the axial deformation. This explains why alloy 5083 O is better to resist lateral loading, while alloy 5083 H12 is better at resisting axial loading. This can be argued by the fact that it is beneficial to distribute the loads on as much of the panel as possible, where alloy 5083 is good because it has a high strain failure capacity. When the panel buckles, however, the strain swill localise in the plate where it buckles, and the effect of yield stress and ultimate stress become more important.

The collision analysis was not finished. By the results I have obtained, it seems as the barrier will deform the most. This is not surprising, since the bow is made of steel, and is about three times harder. The Barrier does not seem to absorb much energy, 150 MJ was absorbed when the bulb had moved about 9 meters into the barrier. It would

probably rise to a higher level when the bow moves further into the barrier, but it is unlikely that the value will get close to the design value of the kinetic energy of 1565 MJ. Thus it is with all probability need for a stronger design. The Norsok standards provide design criteria to how much a structure should absorb as strain energy in a collision [Norsok, 2004]

For fixed installations([Norsok, 2004]);

$$E_s = \frac{1}{2}(m_s + a_s)\vec{v_s}^2 \tag{8.1}$$

For compliant installations

$$E_s = \frac{1}{2}(m_s + a_s)\vec{v_s}^2 \frac{(1 - \frac{v_i}{v_s})^2}{1 + \frac{m_s + a_s}{m_i + a_i}} \tag{8.2}$$

If the barrier is assumed fixed, this means that the barrier must absorb all the kinetic energy of the ship as strain energy. Some energy might go to the acceleration of the bridge as well since the barrier is connected to the bridge, but it depends on if the connection is a weak link or not. It would seem that the energy absorbed as strain energy due to deformation in the barrier is not enough to stop the ship.

Chapter 9

Conclusions and recommendations for further work

9.1 Conclusive arguments

1. A stiffened panel with Alloy 5083 O has a better resistance against lateral loading than a similar panel , but with alloy 5083 H12. Regarding axial crushing, it is the other way around.
2. Results in the analysis makes it reasonable to state that the design used for the barrier is to weak, and that a stronger design is necessary.
3. The bow is not significantly damaged by the collision. Most of the damage is taken up in the barrier. It could be beneficial to crush more of the bow in order to dissipate more energy. The bow is far from being damaged beyond collision bulkhead.
4. The effect of reduction in heat affected zone is significant , but it seems that the velocity of impact has a role in determining fracture patterns, perhaps even more than the reduction in strength in the HAZ.
5. The failure criterion gives reason to question the conclusions regarding the analysis of the effect of reduction in HAZ. A more advanced failure criterion should be developed.
6. The pre tension in the artificial seabed differs somewhat from the results provided by Reinertsen AS. This may be due to the fact that two different analysis programs has been used, and two different methods has been used.

9.2 Conclusions

To protect the submerged tunnel from ship collisions a design of a stronger barrier must be analysed. This could be done by increasing the number of decks, stiffeners and bulkheads in the barrier. Increasing the plate thickness and stiffener dimensions is also a possible option to increase the barrier strength. A finite element model of the barrier with a larger part being a detailed local model would be beneficial to find a more correct resistance force acting on the ship from the barrier. It could be beneficial to increase the strength of the barrier so that it crushes the bulb of the bow in order to dissipate more strain energy.

Aluminium is a much softer material than steel and it also has a reduction in strength in heat affected zones. One alloy that does not have a reduction in heat affected zones is alloy 5083 with temper O. It would be advisable to use this alloy to avoid the reduction in HAZ.

The stability of the barrier is sound before collision. After collision stability is possibly dangerous, and definitely altered. A more thorough stability analysis should be carried out.

9.3 Recommendations for further work

1. Preform the strength design and ductility design simulations. Run the bow trough the barrier, but give the bow a rigid material. This would be less computational expensive compared to the shared energy simulation I have been running in this thesis. Run the ship bow against a rigid wall to look at how much potential energy the bow can absorb trough strain energy. This is not a scenario likely to occur in a real collision.
2. Extend the length of the local model of the barrier to avoid the need of a section with extended ductility at the border between global and local model of barrier. If necessary one should make the local model twice as large as the one presented in this thesis. However, this wold be more computational expensive.
3. Instead of running analysis with only constant velocity of the bow, run analysis that better describe real conditions. By adding the mass of the whole ship to the model and running the bow against the barrier with an initial velocity would be a more realistic simulation.

4. Look at different impact locations in the barrier. It was only simulated collision at the centre of the barrier. Simulating collisions at the ends of the barrier should also be carried out.
5. Design a barrier that is better at absorbing local damage. By the analysis carried out, the barrier design seemed too weak. Increasing stiffener dimensions and plate thickness should be carried out.
6. Do experimental tests on the respective alloys in the barrier. Develop a fracture criterion that is specific for each of the alloys used in the thesis. This should be verified with experimental results.
7. Include the drag forces and potential mooring forces in the analysis.
8. Make a model with a more realistic extent of heat affected zone. 35 mm is more correct.
9. Preform a collision analysis on the bridge model in USFOS.
10. Preform eigenfrequency analysis on the bridge model in USFOS.
11. Make an estimation on how much costs different outcomes of the collision. Look at costs at various damage scenarios on the bridge and bow.
12. Make a model of the submerged tunnel as well. Do an integrated analysis with the model of the barrier and tunnel as well. This could be computational expensive however, but very interesting.
13. Preform weather loads simulations on the bridge in USFOS, such as Wave and wind loads.

Bibliography

[Amdahl, 2005] Amdahl, J. (2005). *TMR 4205 Buckling and Ultimate Strength of Marine Structures*.

[Eurocode, 2004] Eurocode, A.Vrouwenvelder, U. G. (2004). Eurocode part 1.7 accidental actions background document. Gathered from : http://eurocodes.fi/1991/1991-1-7/background1991-1-7/Background˙document˙to˙EN˙1991-1-7.pdf.

[Eurocode, 2006] Eurocode, A.Vrouwenvelder, U. G. (2006). Eurocode 9 : Design of aluminium structures - part 1-1 : General structural rules. Gathered from : https://law.resource.org/pub/eu/eurocode/en.1999.1.1.2007.pdf.

[Faltinsen, 1993] Faltinsen, O. M. (1993). *Sea loads on ships and offshore structures*, volume 1. Cambridge university press.

[Hallquist et al., 2006] Hallquist, J. O. et al. (2006). Ls-dyna theory manual. *Livermore software Technology corporation*, 3:25–31.

[Hansen, 2015] Hansen, J. L. (2015). Analysis and design of ship collision barriers on a submerged floating tunnel subjected to large ship collisions. *Master thesis NTNU ,Trondheim ,Norway*.

[Konstali, 2014] Konstali, . (2014). Analysis and design of ship collision barriers on a submerged floating tunnel subjected to large ship collisions. *Master thesis NTNU ,Trondheim ,Norway*.

[Mazzolani, 1994] Mazzolani, F. (1994). *Aluminium alloy structures*. CRC Press.

[Moan, 2003] Moan, T. (2003). *Finite Element Modeling and Analysis of Marine Structures*. Department of Marine Technology, NTNU.

[Norsok, 2004] Norsok (2004). Design of steel structures. *Standards Norway*, Gathered from : http://www.standard.no/pagefiles/1145/n-004.pdf.